



ARL-TR-8486 • SEP 2018



Recent Advances in Catalytic Materials for Water Sustainability

by Luther Mahoney, Dat T Tran, and Ivan C Lee

Approved for public release; distribution is unlimited.

NOTICES

Disclaimers

The findings in this report are not to be construed as an official Department of the Army position unless so designated by other authorized documents.

Citation of manufacturer's or trade names does not constitute an official endorsement or approval of the use thereof.

Destroy this report when it is no longer needed. Do not return it to the originator.



Recent Advances in Catalytic Materials for Water Sustainability

by Luther Mahoney

Oak Ridge Association of Universities, Belcamp, MD

Dat T Tran and Ivan C Lee

Sensors and Electron Devices Directorate, ARL

REPORT DOCUMENTATION PAGE

*Form Approved
OMB No. 0704-0188*

Public reporting burden for this collection of information is estimated to average 1 hour per response, including the time for reviewing instructions, searching existing data sources, gathering and maintaining the data needed, and completing and reviewing the collection information. Send comments regarding this burden estimate or any other aspect of this collection of information, including suggestions for reducing the burden, to Department of Defense, Washington Headquarters Services, Directorate for Information Operations and Reports (0704-0188), 1215 Jefferson Davis Highway, Suite 1204, Arlington, VA 22202-4302. Respondents should be aware that notwithstanding any other provision of law, no person shall be subject to any penalty for failing to comply with a collection of information if it does not display a currently valid OMB control number.

PLEASE DO NOT RETURN YOUR FORM TO THE ABOVE ADDRESS.

1. REPORT DATE (DD-MM-YYYY) September 2018		2. REPORT TYPE Technical Report		3. DATES COVERED (From - To) 1982–2016	
4. TITLE AND SUBTITLE Recent Advances in Catalytic Materials for Water Sustainability				5a. CONTRACT NUMBER W911NF-16-2-0085	
				5b. GRANT NUMBER	
				5c. PROGRAM ELEMENT NUMBER	
6. AUTHOR(S) Luther Mahoney, Dat T Tran, and Ivan C Lee				5d. PROJECT NUMBER	
				5e. TASK NUMBER	
				5f. WORK UNIT NUMBER	
7. PERFORMING ORGANIZATION NAME(S) AND ADDRESS(ES) US Army Research Laboratory ATTN: RDRL-SED-E 2800 Powder Mill Road Adelphi, MD 20783-1138				8. PERFORMING ORGANIZATION REPORT NUMBER ARL-TR-8486	
9. SPONSORING/MONITORING AGENCY NAME(S) AND ADDRESS(ES)				10. SPONSOR/MONITOR'S ACRONYM(S)	
				11. SPONSOR/MONITOR'S REPORT NUMBER(S)	
12. DISTRIBUTION/AVAILABILITY STATEMENT Approved for public release; distribution is unlimited.					
13. SUPPLEMENTARY NOTES					
14. ABSTRACT This comprehensive review summarizes the current knowledge of homogeneous, modified, and supported materials, and provides insights into water sustainability by increasing water availability through the use of catalytic materials. Metal cations, disinfectants, and hydroxyl radical-producing species are investigated in the homogeneous treatment of wastewater, such as organics, micro-pollutants, and heavy metals. Iron and manganese oxides are primarily demonstrated to accomplish many oxidation treatments of polluted water, albeit under limited conditions. Meanwhile, modified materials in wastewater treatment have become an active field despite the many limitations imposed in homogenous reactions. Carbon materials with periodic and aperiodic structures continue to evolve rapidly in water treatment, due to the ability to modify these materials under relatively simple treatments. Applying metal oxides onto polymers continues to increase, primarily in the arena of heavy metal removal because of the ability to use the functional groups and metal oxides in capturing heavy metal contaminants. This review reveals that advanced materials with supported high-valence metal oxides and high regenerability have a promising future toward water sustainability.					
15. SUBJECT TERMS periodic, aperiodic, micro-pollutants, metal oxides, oxidants					
16. SECURITY CLASSIFICATION OF:			17. LIMITATION OF ABSTRACT UU	18. NUMBER OF PAGES 111	19a. NAME OF RESPONSIBLE PERSON Ivan C Lee
a. REPORT Unclassified	b. ABSTRACT Unclassified	c. THIS PAGE Unclassified			19b. TELEPHONE NUMBER (Include area code) (301) 394-0292

Contents

List of Figures	v
List of Tables	vi
1. Introduction	1
1.1 Importance of Water Availability	1
1.2 Immediate Requirement to Develop Advanced Materials in Conversion of Aqueous Pollutants	3
2. Homogeneous Water Treatment	4
2.1 Synthesis	4
2.2 Characterization	9
2.3 Reactions	11
2.3.1 Organics	11
2.3.2 Micro-Pollutants	18
2.3.3 Heavy Metals	31
3. Classification of Materials	36
3.1 Synthetic Methods for Support Materials	38
3.2 Modified Water Treatment	46
3.2.1 Synthesis-Modification	46
3.2.2 Modified Characterization	48
3.2.3 Modified Reactions	48
4. Inorganic Supports Water Treatment	56
4.1 Synthesis of Inorganic Supports	56
4.2 Inorganic Supports Characterization	57
4.3 Inorganic Supports Reactions	59
4.3.1 Organics	59
4.3.2 Micro-Pollutants	61
4.3.3 Heavy Metals	62

5. Conclusions	67
6. Future Outlook and Perspectives	67
7. References	69
List of Symbols, Abbreviations, and Acronyms	99
Distribution List	103

List of Figures

Fig. 1	An image of the upcoming water crisis.	3
Fig. 2	Kinetics of breakdown as function of (top) micro-pollutant 17 α -ethinylestradiol (EE2) and oxidant. EE2 structure shown to the right where oxidant attack will initially take place.	28
Fig. 3	Kinetics of breakdown as function of micro-pollutant sulfamethoxazole (SMX) and oxidant. SMX structure shown to the right where oxidant attack will initially take place.	28
Fig. 4	Kinetics of breakdown as function of micro-pollutant carbamazepine (CBZ) and oxidant. CBZ structure shown to the right where oxidant attack will initially take place.	28
Fig. 5	Kinetics of breakdown as function of micro-pollutant atenolol (ATL) and oxidant. ATL structure shown to the right where oxidant attack will initially take place.	29
Fig. 6	Kinetics of breakdown as function of micro-pollutant ibuprofen (IBP) and oxidant. IBP structure shown to the right where oxidant attack will initially take place.	29
Fig. 7	Kinetics of breakdown as function of micro-pollutant <i>p</i> -chlorobenzoate (pCBA) and oxidant. pCBA structure shown to the right where oxidant attack will initially take place.	29
Fig. 8	Kinetics of breakdown as function of secondary wastewater pollutant and oxidant. Few secondary wastewater contaminants structures shown in center respective oxidant initial attack on organic functional group.	30
Fig. 9	Periodic mesoporous silica materials: (A) 1-D hexagonal MCM-41 pore arrangement and (B) Bi-continuous pattern in MCM-48 structure. Cubic cage pores assigned to SBA mesoporous materials: (C) SBA-6, (D) SBA-16 material, and (E) and (F) FDA-2 and FDU-1, respectively, part of class of materials from Fudan University. The symmetry of these six materials are as follows: (A) p6mm, (B) Ia3d, (C) Pm3n, (D) Im3m, (E) Fd3m, and (F) Fm3m. Other less predominant mesoporous materials can be classified into these six symmetry elements.	38
Fig. 10	Periodic Al ₂ O ₃ using PMMA spheres in soft-template synthesis. HR-SEM and TEM with insets of selected area (electron) diffraction (SAED) patterns show the different structures depending on the Al source used holding the PMMA and nonionic F127 surfactant constant. (a–f) Using aluminum nitrate in 95% ethanol; (g–l) using aluminum isopropoxide in 95% ethanol-HNO ₃ solution; and the (m–o) without Al precursor of only 95% ethanol-HCl solution.	44
Fig. 11	TEM image of Fe-KIT-6 at 10 wt%. loading with cartoon images of the cubic structure with and without iron(III) oxide nanoparticles: far	

	left (a), center (b), and far right (c). Consistent with the bi-continuous gyridol cubic space group Ia3d in the family of MCM-48 structures; the KIT-6 structure has larger pores than the MCM-48 structure, but it shares the same Ia3d space group.	45
Fig. 12	HR-SEM image of periodic macroporous MgO. (a) only PMMA; (b) PMMA with 95% ethanol solution; (c) and (d) PMMA with F127 in an aqueous solution; (f) and (g) PMMA with F127 contained in 40% ethanol media; (h) PMMA with F127 in 50% ethanol; and (i) PMMA and F127 contained within a 95% ethanol solution.	45
Fig. 13	TEM image of Fe ₂ O ₃ in CMK-3 carbon pore channels. (a, b, e, f) TEM images; (c and e) SAED patterns; (c and d) HR-TEM images, and (g) DF-STEM image. (a–d) pyrolysis at 300 °C, (e) 500 °C, and (f, g) 600 °C.	46
Fig. 14	Ozone mechanism of oxidation that occurs with MnO _x /SBA-15 with the probe molecule oxalic acid.	61
Fig. 15	Adsorption isotherms of As(V) and Cr(VI) using three materials: (a) the amount adsorbed at equilibrium (q _e) of As (V) comparing γ-Al ₂ O ₃ /Fe(OH) ₃ with γ-Al ₂ O ₃ and γ-AlOOH; (b) the Cr(VI) uptake with γ-Al ₂ O ₃ /Fe(OH) ₃ , γ-Al ₂ O ₃ , and γ-AlOOH; (c) and (d) the ratio of concentration equilibrium by adsorbed heavy metal equilibrium concentration.	63
Fig. 16	Adsorption isotherms using two different adsorption models with As(V) as the model heavy metal cation. The bold lines are Langmuir monolayer adsorption model, and the dotted lines are the Freundlich model that takes into the account the heterogeneity of the active sites on a support.	64

List of Tables

Table 1	Review publications on water remediation (homogeneous, modified, and supported).....	5
Table 2	Analytical characterization employed in wastewater/water treatment	10
Table 3	Aqueous organic pollutants removal with high-valence Fe, Mn, and Fe ₂ O ₃	13
Table 4	Aqueous pharmaceutical pollutants removal with high-valence Fe, Mn, and metal oxides	20
Table 5	Heavy metal removal using Mn, Fe, and supported metal oxides in water treatment.....	33
Table 6	Properties of supports employed as adsorbents	37
Table 7	Synthesis of ordered porous supports containing metal oxides in catalysis.....	40
Table 8	Mn, Fe, and metal oxides in aqueous organics water treatment	51

1. Introduction

Water sustainability is necessary not only for modern societies throughout the world, but also mandatory for military personnel deployed to various operations around the globe.¹⁻² Water composes a major portion of the mass of living organisms.³⁻⁵ Water also acts as a catalyst in various physical processes and as a medium to permit the transfer of electrons in numerous biochemical reactions that pertain to sustaining life on Earth. Therefore, clean water is a must. In the endeavor to obtain potable water, many water treatment processes are necessary to increase water availability by reducing the amount of toxic agents.⁶⁻⁷

1.1 Importance of Water Availability

Availability of potable water is a necessity for humans, animals, and other species in the environment because water functions as a catalyst in energy conversion for various organisms throughout nature.⁸ Aqueous pollutants in water affect the ability of organisms to function catalytically and remove waste products generated in energy conversion and storage. Aqueous pollutants have different effects on organisms depending on their concentration in water and their properties. Common aqueous pollutants in water bodies include biological, chemical, and heavy metals. In developing countries, bacteria in water is a major concern because of the public health concerns about water-borne illnesses. Water-borne illnesses and diseases kill 5 million people or more a year,⁹ with children being the most vulnerable.¹⁰ Therefore, availability of water that is safe to drink and free of microbes continues to be a challenge in many parts of the world, such as Africa.¹¹ Potable water reduces the cases of various bacterial infections and parasites, such as hookworm.¹² Likewise, graywater that has been used in washing items will be a major avenue for developing water sustainability throughout the world and within military organizations.¹³⁻¹⁶

Low concentrations of aqueous chemical pollutants and heavy metals have dramatic effects on species that consume or live within it, such as humans and fish. The health effects of organic contaminants in water, like dichlorodiphenyltrichloroethane, dichlorodiphenyldichloroethylene, and dichlorodiphenyldichloroethane, include increased occurrence of liver cancer.¹⁷ These are only a few of the organic pollutants found in drinking water.

Other common organic pollutants include micro-pollutants, such as pharmaceuticals. Antibiotics are heavily used in treating livestock, and also humans, with world consumption in the range of 100,000 tons or more.¹⁸ Complete removal of these antibiotics from wastewater is challenging due to the

size and recalcitrant nature of organic contaminants.¹⁹ Bacteria-resistant species continue to be of great concern because of the incomplete breakdown of antibiotics, which permits these microorganisms to evolve a resistance against medications. Micro-pollutants of equally great concern include drugs used to treat various medical conditions. Examples include endocrine-disrupting compounds (EDCs) and personal care products (PCPs), organic compounds that are widely present in bodies of water. EDCs of special emphasis include materials known to mimic hormones in humans and other animal species, such as bisphenol A (BPA), nonylphenol, benzophenone, and benzotriazole (BT).²⁰ Aquatic species, including fish and mollusks, have experienced changes in their reproductive organs due to various EDCs.²¹ In addition, PCPs are of emerging concern given their widespread use in various products, such as toothpaste.²² Examples of PCPs used as disinfectants includes triclosan and chloroprene.^{6,23} With triclosan, it is difficult to break down all of the antiseptic into innocuous products using conventional water treatments, so it accumulates in water bodies throughout the world.²⁴ The result of triclosan present with light forms toxic dioxins. Also, PCPs, such as triclosan, have been found in vegetables including lettuce and radishes. Therefore, pharmaceuticals, in addition to PCPs, are having profound effects on plants, animals, and humans. In addition, opiate usage has led to its continued rise in wastewater.²⁵ Moreover, the amount of opiates consumed is greater than national estimates from evaluation of wastewater by a factor of two and half times, such as in Italy.²⁶ The effects of opiates and metabolites may have direct negative outcomes on aquatic organisms, as has been seen with the zebra mussel.²⁷⁻³¹ Therefore, opiates and related drugs are difficult to remove and continue to increase in aqueous bodies with potentially adverse effects on the environment.

Heavy metals are also a major threat to public health throughout much of the world. Examples of arsenic (As) abound in Vietnam, Bangladesh, Taiwan, and other countries.³²⁻³⁴ As exposure has been shown to increase the occurrence of cardiovascular health issues³⁴ and cancer.³⁵ In addition to coronary disease, blackfoot disease is prevalent with As exposure. Groundwater containing As used to grow rice further increases the probability for stomach cancer, making As-contaminated groundwater a large public health challenge in many parts of the world. Also, other toxic heavy metals are of special concern, including cadmium (Cd), lead (Pb), and mercury (Hg). These toxic metal cations cause neurological damage and cancer. High concentrations of heavy metals abound in many areas used in Pakistan, yet there is little concern even though the impact of consuming these heavy metals been evaluated extensively.⁹ Other parts of the world, such as the United States, have had challenges with heavy metal pollution in the past; therefore, more research and public policy continue to be needed for obtaining potable water for all individuals throughout the world, considering the large

projected future population growth.^{36–42} Figure 1 shows the future global water crisis that is probable without needed intervention.⁴³

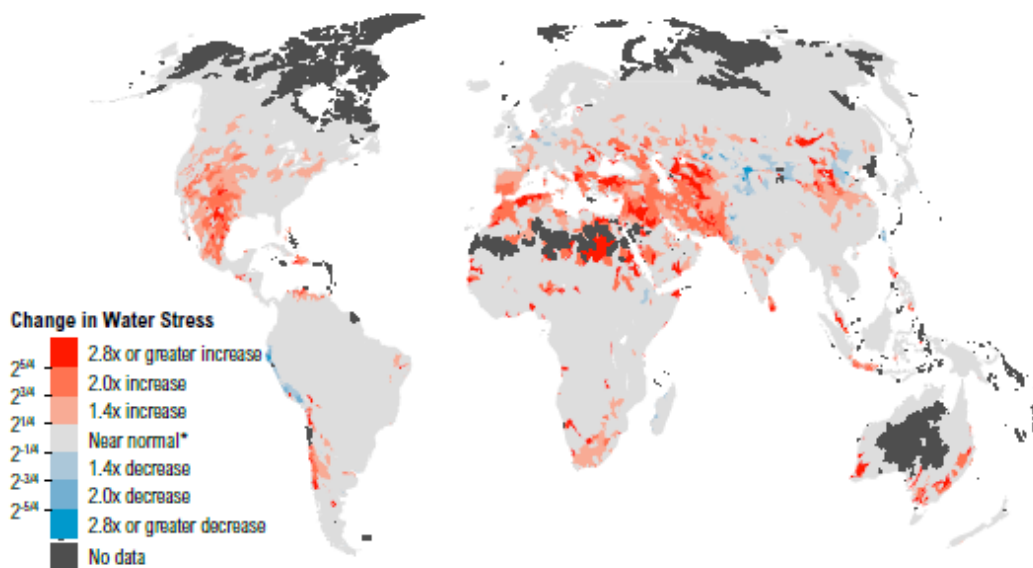


Fig. 1 An image of the upcoming water crisis.⁴³ Image credit: Gassert et al.;⁴⁴ permission granted via Creative Commons.

1.2 Immediate Requirement to Develop Advanced Materials in Conversion of Aqueous Pollutants

This review combines knowledge gleaned from studies in homogeneous, modified, and supported materials. These previous reviews focused in homogeneous water treatment, such as potassium ferrate(VI) (K_2FeO_4) or online large-scale electrochemical ferrate(VI) production,^{5,45–53} polymers,^{41,54–57} membranes,^{42,58–63} carbon materials,^{1,64–70} metal oxides,^{4,36,38,71–79} and clays.⁸⁰ Few studies combine knowledge of homogeneous reactions with supported materials. Advanced materials in water treatment have been slow to arrive because of the belief that current water treatments methods could be modified. This has not occurred, especially for micro-pollutants, which are accumulating in drinking water because large-scale treatment methods cannot convert these aqueous pollutants to innocuous products without negative consequences.^{74,78,81–89} Simple filtration and membranes can remove mainly larger aqueous contaminants, such as bacteria, but these filtration methods are lacking with regard to micro-pollutant removal. Reverse-phase osmosis removes many aqueous pollutants, but requires large energy input to remove pollutants, which is not sustainable. Finally, this review highlights the opportunities to explore higher-valence metal oxides on mesoporous and microporous support material as another route toward water

sustainability in coming years by evaluating current water treatment methods and related water availability challenges.

2. Homogeneous Water Treatment

2.1 Synthesis

The synthesis of ferrate(VI), manganate(VII), chlorine (Cl), chlorine dioxide (ClO₂), ozone, and hydrogen peroxide (H₂O₂) all involve multiple, large energy consumptive steps, which are described based the many review articles in Table 1. The laboratory-scale synthesis of ferrate(VI) involves strongly basic conditions using a hypochrite anion (OCl),⁹⁰⁻⁹² an electrochemical process,⁹³⁻⁹⁹ or Cl gas (Cl₂).¹⁰⁰ Electrochemical ferrate(VI) has been inferred for large-scale water treatment. However, the purity of ferrate(VI) is greater when using a OCl or Cl₂. Potassium permanganate (KMnO₄) synthesis involves combining manganese oxide(IV) (MnO₂) with potassium hydroxide to eventually form the desired product. KMnO₄ has a wider pH range compared to ferrate(VI), but KMnO₄ has a lower redox (oxidation) potential.⁵² The lower oxidation potential is not favorable in water treatment applications. Cl is mainly produced through the alkali-Cl process. The challenge for this process is the large energy input needed to break apart sodium chloride (NaCl) into Cl₂. Cl₂ is produced by two main synthetic methods: 1) solids potassium chlorate combined with oxalic acid and 2) hydrogen chloride (HCl) combined with sodium chlorite and sodium hypochlorite.¹⁰¹ The advantage of Cl₂ over Cl gas is the ability disinfect over a wide pH range with twice the germicidal breakdown ability. This Cl agent requires many reaction steps to obtain the desired material, which is an economical challenge. Ozone is an alternative to Cl and Cl₂, but ozone must be produce onsite because of the lack of stability of this compound.¹⁰² This instable molecule is produced by cold plasma discharge of diatomic oxygen gas. The challenge for this water treatment method includes the energy, delivery, and cost.¹⁰³ Large sums of electricity are needed for producing ozone, and the amount of ozone produced is a function of the actual oxygen gas used. The air cold plasma discharge treated method liberates 50% less ozone compared to pure, dry oxygen gas.¹⁰² The economical factor is one of the major factors preventing ozone from becoming the primary mass water treatment method in North America.¹⁰²⁻¹⁰³ The final homogeneous water treatment method uses H₂O₂; nonetheless, H₂O₂ is produced by either energy intensity anthraquinone¹⁰⁴ or electrical processes.¹⁰⁵ H₂O₂ has a lower redox potential of 1.776 V compared with ozone (2.076 V), so the ability to oxidize at the sample dose with be less effective for H₂O₂, which relates to the energy and economic aspects.^{45,52} Also equally important is the stability of H₂O₂.

At concentrations greater than 30 wt% H₂O₂, the potential for safe handling becomes an issue too. Overall, these homogeneous water treatment methods do little to convert micro-pollutants to innocuous products, and these homogenous solution methods cannot be regenerated easily.

Table 1 Review publications on water remediation (homogeneous, modified, and supported)

Material(s)	Summary of the reviews	Reference
Potassium ferrate(VI) solid	Progress in synthesis and development of K ₂ FeO ₄ for water and wastewater treatment avenues has been presented. The preparation of potassium ferrate(VI) salt was described in detail. In addition, the use of K ₂ FeO ₄ in converting polluted waters is described and benefits noted for the ability to act as an oxidant and coagulant.	45
Potassium ferrate(VI) solid	K ₂ FeO ₄ has been presented as an potential avenue to remediating wastewater, and the review indicates that potassium ferrate(VI) could be used in other applications, such as super-iron (Fe) battery and radiolysis studies. The fundamental understanding properties of K ₂ FeO ₄ has been described with emphasis in water treatment application.	46
Potassium ferrate(VI) solid	Describes advantages of K ₂ FeO ₄ for environmental remediation. Wastewater treatment is the main focus with disinfection, organic contaminants, micro-pollutants, inorganic compounds, dissolved organic content, and sludge removal given significant emphasis in this review. Challenges and opportunities are indicated for future research.	47
Potassium ferrate(VI) solid	Evaluates K ₂ FeO ₄ in the treatment of wastewater and potential application in large-scale water treatment because ferrate's products acting as adsorbents. Characterization of ferrate compounds are reviewed, and ferrate compounds are suggested in the applications of bacteria, organic chemical, and heavy metal removal.	48
Potassium ferrate(VI) solid	Describes ferrate(VI) production using electrochemical method, characteristics of ferrate(VI), and wastewater treatment using ferrate(VI). Ferrate(VI) is briefly noted to be effective in converting EDCs to oxidized forms, such as with pharmaceutical compounds and other organic compounds.	49
Ferrates (VI, V, and IV)	Ferrate of variable oxidations states (VI, V, and IV) are evaluated in wastewater treatment. Ferrate is suggested for the remediation of bacteria, heavy metals, and organics. Kinetics are reviewed extensively and proposed mechanisms of ferrates contained within solution phase.	50
Ferrate(VI) and ferrate(V)	Describes the oxidation of various organics with kinetics and mechanisms using ferrate(VI) and ferrate(V).	51

Table 1 Review publications on water remediation (homogeneous, modified, and supported) (continued)

Material(s)	Summary of the reviews	Reference
Ferrate(VI)	Describes the preparation, characterization, and application of ferrate(VI) in water treatment. Difference organic compounds, such as pharmaceuticals, are evaluated against conventional treatments including H ₂ O ₂ , Fenton's reagent, and ozone. Reaction kinetics are also given within the tables.	52
Ferrate(VI)	Ferrate(VI) is presented as the green oxidant and many other potential applications including the super-Fe battery. Synthesis, characterization, and application of ferrate(VI) is discussed. Other common water treatment oxidants are also compared with ferrate(VI) including, Cl, Cl ₂ , KMnO ₄ , H ₂ O ₂ , and ozone.	5
Ferrate(VI)	Ferrate(VI) is inferred to be useful in the applications of organic transformations, breakdown of organics, and remediation of medications. Synthesis of ferrate(VI) overview is given in the review.	53
Hybrid polymer composites	Mesoporous silica and modified mesoporous silica is discussed with a focus on aqueous pollutants. The functionalized materials were described with a focus toward environmental remediation. The hybrid adsorbents were evaluated against heavy metal ions, anions, radioactive ions, and other organics for adsorption.	54
Polymer-composites	Described in detail the advantages of three polymers in adsorption: polyaniline, polypyrrole, and polythiophene. The adsorption process was compared using heavy metal ions (chromium [Cr](III/VI), and dyes (methylene blue, etc.) with another organic adsorbent (sawdust, etc.), or iron oxide (e.g., Fe ₃ O ₄). The adsorption isotherms was also presented with detailed discussion.	41
Hybrid polymer composites	Described the synthesis and water treatment application of inorganic-organic hybrid polymer matrices. Synthesis of inorganic materials, such as silica, are reviewed. Characteristics of inorganic materials and heavy metal removal are discussed.	55
Bioelectrodes	Mesoporous carbon-based materials are discussed with preparing microorganisms onto the carbon to transport electrons in redox reactions using wastewater as the media. Metal oxides are also discussed with regard to the use in redox reactions in the oxidation of organics and grown of bacteria.	57
Biopolymers	Describe use of nature biopolymers (polysaccharides) that can be converted into carbon aerogel and other highly porous materials. Adsorption of various organic chemicals briefly discussed as an application.	56

Table 1 Review publications on water remediation (homogeneous, modified, and supported) (continued)

Material(s)	Summary of the reviews	Reference
Membranes	Evaluates membranes containing polyamide for reverse-osmosis and in nano-filtration applications. The characterization techniques of these polyamide-coated membranes are extensively reviewed.	58
Membranes	Describes the differences between polymers used for developing reverse osmosis and nano-filtration materials. Different characteristics of membranes are discussed, such as spiral or hollow fiber-contained membranes. The effect of polymer sidechains are also reviewed.	59
Membranes	Describes use of nanotechnology for producing membranes made of ceramics and polymers to convert contaminated water into clean water. The major thrust of this review is employing hybrid inorganic–organic composites for obtaining the ultimate water treatment membrane.	62
Membranes	Evaluate silica membranes that are microporous in nature. Microporous silica membrane fabrication, processing, and transport mechanisms are discussed. Avenues to increase the stability of the membrane are also presented. Hybrid membranes include carbon and other metal oxide materials are evaluated.	60
Membranes	Desalination using electrical current/voltage with various carbon materials is described. The review focuses on the varied electrochemical characterization techniques in the endeavor to determine the optimal carbon material.	61
Membranes	Described nanofiber composite nanofiber membranes using electrical current/voltage. The fabrication of polymer composite membranes are evaluated in the water treatment application: organic and bacterial removal.	42
Carbon-composites	Evaluated fibrous materials as an alternative to other structures because of the high surface area and ability to fabricate relatively easily into membranes.	64
Carbon-nanomaterials	Described carbon nanomaterials, such as graphene (GE) and graphene oxide (GO), and potential materials to adsorb pollutants in wastewater. Organic chemicals, heavy metal cations, and anions (nitrate, etc.) are discussed as potential probes to remove in water treatment.	65
Carbon-modified materials	Described methods for activating activated carbon material for water treatment applications. Seven modification treatments for activated carbon are described including acidic, basic, impregnation, microwave, ozone, oxygen plasma, and biological.	66
Carbon-adsorbents	Carbon in aperiodic and periodic forms are described with emphasis given in mesoporous carbon materials. Application of carbon materials are presented for remediation of contaminated wastewater.	70

Table 1 Review publications on water remediation (homogeneous, modified, and supported) (continued)

Material(s)	Summary of the reviews	Reference
Carbon-composites	Evaluated graphene-metal oxide composites for water treatment including photocatalysis, adsorbents, and disinfectants. GE-titanium dioxide (TiO ₂), GO-TiO ₂ , and multifunctional GE-metal oxide composite are presented with degradation of various organics: dyes, and pharmaceuticals. Heavy metal ions, such as Cr(VI) with the carbon-metal oxide composite, are shown to have larger adsorption. Bacteria are broken down with the carbon-metal oxide composites because of the electron transfer.	67
Carbon-adsorbents	Described various carbon nanomaterials that can be produced in 3-D structures. Composites using Fe(III) oxide are presented, and adsorption capacity is studied for organics with recycling completed. Different synthesis methods are given, and the adsorption of dyes and heavy metal ions.	1
Carbon-composites	Evaluated activated carbon developed using sludge with pyrolysis treatment. Chemical treatment and physical activation are noted as methods for preparing activated carbon from sludge. Adsorption models, dyes, heavy metal ions, and organic chemicals are expressed through tables.	68
Carbon-adsorbents	Described development of biochar from carbon sources that are low cost. Biochar is suggested to be a material that can be used as an adsorbent beyond heavy metal collection and can adsorb organic chemicals. The author suggests converting biochar into electricity.	69
Fenton-catalysis	Described Fe ²⁺ /Fe ³⁺ couple under acidic conditions (pH = 3) using H ₂ O ₂ in the treatment of organic chemicals, such as phenol and dyes. Methods for placing Fe ³⁺ onto zeolites and mesoporous materials are described including hydrothermal and impregnation using MCM-41 or SBA-15. Fenton's reaction is described using iron oxide porous supports. Pharmaceutical wastewaters are given brief attention.	71
Fenton-reactors	Evaluates reactors in the design of Fenton reactors for large-scale water treatment. Electrochemical oxidation using Cl is also presented. Potential reactor designs and challenges are assessed for future use.	38
Iron oxides	Described the preparation, characterization, and water treatment applications, such removal of carboxylic acids, dyes, zinc (Zn), copper (Cu), Pb, As, nitrate (NO ₃ ⁻), and bromate (BrO ₃). Bacteria and viruses removal is also presented using Fe materials. Toxicity and environmental effects are evaluated.	76
Metal oxides	Described nanomaterials including metal oxides, such as FeO _x , MnO _x , alumina (Al ₂ O ₃), TiO ₂ , zinc oxide (ZnO), MgO, ceria (CeO _x), and supported metal oxides. Aqueous treatment of pollutants with these metal oxides and combinations with supports, such as silica, polymers, and hybrid organic-inorganic materials are evaluated.	77

Table 1 Review publications on water remediation (homogeneous, modified, and supported) (continued)

Material(s)	Summary of the reviews	Reference
Fenton-other metal oxides	Described potential metal oxides that could be used for replacing Fe(II/III) in the Fenton reaction with H ₂ O ₂ . Metal oxides covered included aluminum (Al), cerium (Ce), manganese (Mn), Cu, Cr, cobalt (Co), ruthenium (Ru), and polyoxometalates. Comparison of Fenton reaction with other water treatment methods are presented.	78
Metal oxides-supported materials	Evaluated various supported metal oxides on the removal of heavy metals, dyes, and organic compounds. Supports compared included clays, bio-composites, silica, Al ₂ O ₃ , and carbon. Nanoparticles presented included metal oxides with emphasis on nano-zero-valent iron (nZVI) for reducing various recalcitrant halogenated organics.	79
Clays	Described the potential advantages of clays with and without modification for water treatment applications. Organics, such as phenol and dyes, are presented as probe molecules converted using clays.	80

2.2 Characterization

The main types of characterization for homogeneous water treatment chemicals include solid and solution phases. Ferrate(VI) and manganate(VII) can be produced as metal salts. These metal salts can be characterized with typical solid techniques, which are listed in Table 2. The other four homogeneous materials are either gaseous (Cl₂, ClO₂, and ozone) or are produced as a concentrated aqueous liquid (H₂O₂). The characterization techniques applied for aqueous solutions includes UV-visible (Vis) spectroscopy from ligand-to-metal-charge transitions (LMCTs), such as with ferrate(VI) and manganate(VII) solutions.^{5,53,75} Likewise, ferrate(VI) solution is amendable to titrimetric titration with chromite, which is specific to the oxidation state of Fe.¹⁰⁶ The iodometric method is used for determining the purity or amount of Cl₂ and ClO₂ in aqueous solution, followed by using UV-Vis spectroscopy.¹⁰¹ Ozone is measured in the solution phase using the indigo method that can be measured by UV-Vis spectroscopy.¹⁰⁷ H₂O₂ aqueous solutions are evaluated with using either KMnO₄ or cerium sulfate (Ce(SO₄)₂) in volumetric analysis in conjunction with UV-Vis spectrophotometry.¹⁰⁴

Table 2 Analytical characterization employed in wastewater/water treatment

Materials evaluated	Methods	Properties determined	Method limitations	Ref
Primarily metal oxides	Powder X-ray diffraction (XRD)	Phase, phase purity, crystallinity, and material ordering	Crystallite must be 3 nm or larger for detection of typical XRD analysis.	108–111
Metal oxides, inorganic-organic hybrid structures, and porous organic structures	Nitrogen physisorption	Textural values indirectly determine the uniformity of pore arrangements from pore-size-distributions	Needs a minimum amount of catalyst for reproducible analysis of textural properties and pore size distributions.	112–115
Primarily metal oxides and hybrid inorganic-organic structures	UV-Vis-diffuse reflectance spectroscopy (DRS)	Able to differentiate between different metal oxide species	DRS has a very low detection limit depending on the metal oxide type.	115–119
Widespread use in solutions that give an absorbance from electronic transitions	UV-Vis (solution)	Able to differentiate between compounds by electronic transitions	Solutions typically need to have low ppm (mg/L) of analyte for detection	120
Primarily for metal oxides, inorganic–organic hybrid structures, and organic materials	Raman spectroscopy	Able to differentiate aggregates of metal oxides, and it is able to differentiate the purity of carbon materials	Relatively high detection limit, and the results are not qualitative in nature	121–122
Used primarily for elucidating the oxidation states encountered in supported metal oxide catalysts	X-ray photoelectron spectroscopy (XPS)	Able to differentiate the core electron structure encountered in supported metal oxides, which results in chemical shifts	Relatively large detection limit, so low metal loading is challenging to interpret qualitatively.	123–125
Primarily used on metal oxide supported materials, hybrid inorganic-organic materials, and carbon-based materials	Transmission electron microscopy (TEM)	Able to decipher pore geometries on the external particle	Challenging to create thin films for optimal viewing, and TEM requires an iterative approach to obtaining pore arrangements.	58, 109, 126
Primarily used on metal oxide supported materials, hybrid inorganic–organic materials, and carbon-based materials	Scanning electron microscopy (SEM)	Able to provide global images of external features	Challenging to obtain the actual composition in energy-dispersive X-ray spectroscopy (EDX) mapping of a given area scanned.	127
Metal oxide supported materials	Chemisorption techniques (H ₂ -TPR, CO-TPR, CO-pulse, O ₂ -pulse, TPD, and TPO)	Used for determining the reduction properties, catalytically active sites dispersion, and bonding arrangements	Relative high detection limits, so more active metal oxide is needed for accurate results	121, 128–131

Notes: TPR=temperature-programmed reduction, TPD=temperature-programmed desorption, TPO=temperature-programmed oxidation

2.3 Reactions

Homogeneous reactions can be broken down into three subsets—high-valence metal cations, disinfectants, and hydroxyl-radical-forming species. Each of these subsets comprises reactions with organics, micro-pollutants, and heavy metals. The most studied metal cations include ferrate(VI) and permanganate(VII) in conversion of organic aqueous contaminants to innocuous products. Ferrate(VI) has been studied heavily because of its large redox potential of 2.20 V compared to 1.51 V for permanganate(VII) under acidic pH conditions.^{45,52} Pharmaceutical contaminants in water have also been evaluated with ferrate(VI) and permanganate(VII), with varied results depending of the oxidation of the Fe or Mn cation. Heavy metals have also be examined with high-valence Fe and Mn, and ferrate(VI) had greater ability to oxidized followed by agglomerating as Fe_2O_3 , thereby improving the water quality. Cl and Cl_2 have been mainly evaluated for treating water-containing micro-organisms. A smaller list of studies evaluate Cl_2 and ClO_2 for reducing the activity of organics and micro-pollutants to less harmful compounds. Reactive oxygen species (ROSs) produced from ozone or H_2O_2 have been studied in organic micro-pollutants, while few to no studies evaluated either ozone or H_2O_2 in heavy metal removal.

2.3.1 Organics

Industrial organic pollutants assessed for conversion to innocuous products within aqueous media are summarized with relevant parameters in homogeneous iron, manganese, and iron oxides for organic pollutants removal, as shown in Table 3. The type of aqueous pollutant, pH, and other reaction species plays major roles in the removal efficiency, product distribution, and rate constants. Aqueous cyanide solutions removal efficiency appears to be linked to the pH and other species, such as metal cations using homogeneous K_2FeO_4 solution.¹³²⁻¹⁴¹ The pH value varies with the cyanide-containing solutions, and lower pH values lead to the potential for a lone pair of electrons on cyanide to accept a proton. In contrast, the larger pH values suggest a stabilization of cyanide that can react quickly with electron-deficient ferrate(VI) through redox chemistry from comparing the small rate constants.¹³²⁻¹³³ However, when cyanide is bound to metal complexes, the electron density is primarily occupied by the center metal cation, and this results in larger rate constants reflected in Table 3. The central metal identity also has a major influence on the ability for ferrate(VI) to attack cyanide, which implies that atomic radii and metal oxidation states are major factors in the remediation process. In addition, other nitrogen-containing chelating agents as metal complexes have been studied with ferrate(VI), such as nitrilotriacetic acid (NTA)

and iminodiacetic acid (IDA).¹⁴²⁻¹⁴⁴ The steric bulk of the ligand coupled with the electron donation to the central metal cation appear to also be major factors, as exhibited in significantly greater rate constants compared to metal cyanide compounds. The opposite of electron-rich nitrogen molecules is N-nitrosodimethylamine (NDMA).¹⁴⁵ The nitro electron-withdrawing group in NDMA causes the rate constant to increase from a few hundred to a few thousand with nitrogen-chelating ligands compared to NDMA. Therefore, the pH, atomic radii of central metal cation, central metal oxidation state, steric bulk, and electron-withdrawing substituents are leading factors affecting the reaction rate constants (Table 3). The other organic pollutants shown in Table 3 follow similar factors depending on the level of electron density present, and greater electron density provides ferrate(VI) an avenue with which to rapidly react. Finally, Mn compounds have not been evaluated greatly because of the redox potential, as reflected in Table 3; however, slightly basic conditions favor greater breakdown of aqueous pollutants, such as the flame-retardant material tetrabromobisphenol A when combined with KMnO_4 .¹⁴⁶

Table 3 Aqueous organic pollutants removal with high-valence Fe, Mn, and Fe₂O₃

Catalyst	Pollutant(s)	Reaction temperature/pH	Contact time	Removal efficiency (%)	Product(s)	Reaction rate	Reaction rate constants	Citation/reference
K ₂ FeO ₄	Cyanide	288-303 K/8.0–12	ND	ND	Cyanate Nitrite	Second order (M ⁻¹ s ⁻¹)	CN: pH 8.0, 605 ± 60	132
K ₂ FeO ₄	Cyanide	296 K/10.55–12.10	2 ms	ND	ND	Second order (M ⁻¹ s ⁻¹)	Fe(VI): pH 12, 0.76 ± 0.07 Fe(V): pH 12, 0.77 ± 0.04	133
K ₂ FeO ₄	Cu(I) cyanide	288 K/9.9	ND	ND	ND	Second order (M ⁻¹ s ⁻¹)	Fe(VI): pH = 9.9, 22.4 ± 2.0 × 10 ⁴	134
K ₂ FeO ₄	Zinc cyanide complex	298 K/9.1–10.5	20 min	100	ND	1/2 order (M ^{-0.5} s ⁻¹)	Fe(VI): pH = 9.1, 3.56 ± 0.13	135
K ₂ FeO ₄	Cd(II) cyanide Nickel(II) cyanide	298 K/9.0–10.6	ND	ND	ND	1/2 order (M ^{-0.5} s ⁻¹) Second order M ⁻¹ s ⁻¹)	Cd(CN) ₄ ²⁻ : pH 9.1, 10.6 ± 1.04 Ni(CN) ₄ ²⁻ : pH 9.0, 19.0 ± 0.95	136
K ₂ FeO ₄	Cyanide Thiocyanate Cu(I) cyanide	288 K/9.0 and 10.9	ND	ND	ND	Second order M ⁻¹ s ⁻¹)	CN: pH 10.9, Fe(VI): 7 Fe(V): 1.8 ± 0.12 × 10 ⁵ Fe(IV): 1.41 ± 0.20 × 10 ³	137
K ₂ FeO ₄	Ni(II)-cyanide Ni(II)-cyanide-EDTA	298 K/8.0–11.0	5 h	60 100	Cyanate	ND	ND	138
K ₂ FeO ₄	Cyanide Cd Cu Nickel (Ni) Pb Zn	ND/7.5–8.0	ND	99-100 95 90 70 100 100	ND	ND	ND	139
K ₂ FeO ₄	Ni(II)-cyano Co(III)-cyano	ND/9.0–11.0	300 min	95 100	NCO-	ND	ND	140
K ₂ FeO ₄	Sodium ferrocyanide Aqua petacyanoferrate(II)	298 ± 0.1 K/ND	ND	ND	ND	Second order (M ⁻¹ s ⁻¹)	5.6 ± 0.7 × 10 ⁶ 3.5 × 10 ⁸	141
K ₂ FeO ₄	Cd(II)-NTA	ND/8–12	2 h	40	ND	ND	ND	142

Table 3 Aqueous organic pollutants removal with high-valence Fe, Mn, and Fe₂O₃ (continued)

Catalyst	Pollutant(s)	Reaction temperature/pH	Contact time	Removal efficiency (%)	Product(s)	Reaction rate	Reaction rate constants	Citation/reference
K ₂ FeO ₄	Cu(II)-IDA	ND/8–12	2 h	95	ND	Second order (M ⁻¹ s ⁻¹)	Cu(II)-IDA: pH 8, 32.30	143
	Zn(II)-IDA			60			Zn(II)-IDA: pH 8, 97.42	
K ₂ FeO ₄	Cd(II)-IDA	ND/8–10	2 h	95	ND	Second order (M ⁻¹ s ⁻¹)	Cu(II)-IDA: pH 8, 126.7	144
	Ni(II)-IDA			82			Zn(II)-IDA: pH 8, 538.0	
K ₂ FeO ₄	NDMA	294 ± 0.5 K/7	30 min	ND	ND	Second order apparent (M ⁻¹ s ⁻¹)	pH 7, 2.6 × 10 ² -3.2 × 10 ⁵	145
K ₂ FeO ₄	Thiourea	283–308 K/8.80–11.70	4 s	ND	ND	Second order (M ⁻¹ s ⁻¹)	1.9 X10 ⁴	147
K ₂ FeO ₄	Thioacetamide	288–308 K/9.14–12.00	ND	Sulfate	ND	Second order (M ⁻¹ s ⁻¹)	Fe(V): pH 9.14, 1.2 × 10 ⁴	148
K ₂ FeO ₄	Phenol	298 ± 0.1 K/9.85	40 s	ND	ND	Second order (mol ⁻¹ dcm ³ s ⁻¹)	44 ± 8	149
K ₂ FeO ₄	Cysteine	295–296 K/9.0, 12.2, and 12.4	ND	ND	ND	Second order (mol ⁻¹ dcm ³ s ⁻¹)	4.00 ± 0.80 × 10 ⁹	150
	Cystine						1.95 ± 0.02 × 10 ⁴	
	Thiourea						8.10 ± 0.40 × 10 ³	
	Methionine						1.58 ± 0.09 × 10 ³	
	Glycine						8.4 ± 0.6 × 10 ⁶	
	Alanine						3.1 ± 0.2 × 10 ⁶	
	Aspartic						2.6 ± 0.1 × 10 ⁶	
	Ketomatonic						1.4 ± 0.2 × 10 ⁶	
	Tartaric						3.1 ± 0.2 × 10 ³	
	Glycolic						7.2 ± 1.0 × 10 ²	
	Malic						1.7 ± 0.2 × 10 ²	
	Lactic						1.6 ± 0.2 × 10 ²	
	Malonic						9.2 ± 1.0 × 10 ¹	
	Succinic						2.0 ± 0.2 × 10 ¹	
	Acetic						1.6 ± 0.2 × 10 ¹	
	Histidine						22.2 ± 0.1 × 10 ⁶	
	Phenylalanine						9.5 ± 0.4 × 10 ⁶	
	Tyrosine						8.1 ± 0.2 × 10 ⁶	
	Tryptophan						9.3 ± 0.4 × 10 ⁶	
	Phenol						3.8 ± 0.4 × 10 ⁶	
Proline	0.1 ± 0.01 × 10 ⁶							

Table 3 Aqueous organic pollutants removal with high-valence Fe, Mn, and Fe₂O₃ (continued)

Catalyst	Pollutant(s)	Reaction temperature/pH	Contact time	Removal efficiency (%)	Product(s)	Reaction rate	Reaction rate constants	Citation/reference
K ₂ FeO ₄	Phenol	296 ± 2 K/5.8–11	30 min	83	ND	ND	ND	151
	4-chlorophenol (4-CP)			95				
	2,4-dichlorophenol (DCP)			87				
	2,4,6-trichlorophenol (TCP)			87				
K ₂ FeO ₄	BPA	296 ± 2 K/8.2–12	20 min	100	ND	ND	ND	152
K ₂ FeO ₄	Aniline	296 ± 2 K/4.5–6.6	40 min	83	ND	ND	ND	153
	Benzene			84				
	Toluene			88				
	o-Xylene			83				
	Chlorobenzene			82				
	Nitrobenzene			47				
	2,4-dichlorophenol			57				
2,4,6-trichlorophenol	31							
K ₂ FeO ₄	Phenol	ND/9.0	1 h	60	Benzoquinone Phenoxyphenol	ND	ND	154
K ₂ FeO ₄	1H-BT	297 ± 1 K/7.0	ND	ND	ND	Second order apparent (M ⁻¹ s ⁻¹)	19.9	155
	5-methyl-1H-benzotriazole (SMBT)							
	5,6-dimethyl-1H-benzotriazole hydrate (DMBT)							
	5-chloro-1H-benzotriazole (5CBT)							
	1-hydroxybenzotriazole (HBT)							
K ₂ FeO ₄	Thiocyanate	278-318 K/7.61–10.35	ND	ND	ND	Second order (M ⁻¹ s ⁻¹)	Fe(VI): pH = 9.2, 11.0 ± 0.69	156
K ₂ FeO ₄	Thiocyanate	296 K/10.10–11.20	ND	ND	ND	Second order (M ⁻¹ s ⁻¹)	Fe(V): 3630 ± 121, pH = 10.10	157

Table 3 Aqueous organic pollutants removal with high-valence Fe, Mn, and Fe₂O₃ (continued)

Catalyst	Pollutant(s)	Reaction Temperature/pH	Contact Time	Removal Efficiency (%)	Product(s)	Reaction Rate	Reaction Rate Constants	Citation/Reference
K ₂ FeO ₄	Sulfite Thiosulfate	295 K/11.4	0.5 ms	ND	ND	Second order (M ⁻¹ s ⁻¹)	Fe(VI): 2.0 ± 0.2 × 10 ¹ (Sulfite) 2.8 ± 0.3 (Thiosulfate) Fe(V): 3.9 ± 0.3 × 10 ⁴ (Sulfite) 2.1 ± 0.1 × 10 ³ (Thiosulfate)	158
K ₂ FeO ₄	3-mercapto-propane sulfonic acid (MPS) 2-mercaptonicotinic acid (MN)	298 K/6.7–10.8	ND	ND	ND	Second order (M ⁻¹ s ⁻¹)	MPS: 3.1 × 10 ¹³ MN: 1.6 × 10 ¹³	159
K ₂ FeO ₄	Cysteine (Cys) s-Methylcysteine (Me-Cys) Cystine Methionine (Met) Selenomethionine (Se-Met) Thiourea (TU) Thioacetamide (TA) Ethionine (ET) Diethyl sulfide (DES) 2,2'-thiodiethanol (TDE) Dimethyl sulfoxide (DMSO) Mercaptoethanesulfonic acid (MES) Mercaptopropanesulfonic acid (MPS) Mercaptopropionic acid (MPA) 2-Mercaptonicotinic acid (MNA) Benzenesulfonate (BS) Thioxane (T)	298 K/7.6–11.3	ND	ND	ND	Second order apparent (M ⁻¹ s ⁻¹)	Cys: 1.8 × 10 ⁵ Me-Cys: 1.7 × 10 ² Cystine: 9.9 × 10 ² Met: 1.6 × 10 ² Se-Met: 4.9 × 10 ⁵ TU: 3.0 × 10 ⁴ TA: 1.8 × 10 ⁴ ET: 8.3 × 10 ² DES: 5.5 × 10 ² TDE: 3.1 × 10 ² DMSO: 3.1 MES: 1.5 × 10 ⁵ MPS: 2.9 × 10 ⁵ MPA: 4.0 × 10 ⁵ MNA: 6.0 × 10 ⁴ BS: 7.2 × 10 ³ T: 3.8 × 10 ²	160
K ₂ FeO ₄	Iodide	288-298 K/8.5	ND	ND	ND	Second order observed (M ⁻¹ s ⁻¹)	Fe(VI): pH = 8, 2 × 10 ⁴	161

Table 3 Aqueous organic pollutants removal with high-valence Fe, Mn, and Fe₂O₃ (continued)

Catalyst	Pollutant(s)	Reaction Temperature/pH	Contact Time	Removal Efficiency (%)	Product(s)	Reaction Rate	Reaction Rate Constants	Citation/Reference
K ₂ FeO ₄	Brilliant Red X-3B	298 K/8.5, 9, and 10	60	100	5 products	ND	ND	162
K ₂ FeO ₄	Dye effluents	ND/6.5–8.5	ND	ND	ND	ND	ND	163
KMnO ₄	Cyanide	ND/14	120 min	100	Cyanate	ND	ND	164
KMnO ₄	Trichloroethylene (TCE)	294 K/4–8	8 h	85	Formic acid Glycolic acid Glyoxylic acid Oxalic acid	First order (s ⁻¹)	TCE: pH 4, 4.30 × 10 ⁴	165
KMnO ₄ Pd/Al ₂ O ₃	Dimethylsulfide N-butyl mercaptan Sulfide Sulfite Chlorobenzene	296 ± 2 K/4–10	400 min	ND	ND	Second order (M ⁻¹ s ⁻¹)	H ₂ S: 2 × 10 ³	166
KMnO ₄	Tetrabromobisphenol A	ND/5–10	ND	0	7 products	Second order (M ⁻¹ s ⁻¹)	700, pH = 8	146
KMnO ₄	Cationic Blue	298 ± 1 K/0.5–2.0	120 min	65	ND	ND	ND	167
Fe ₂ O ₃	Ethylene glycol (EG) Phenol	ND/2–3	220 min	100 100	ND	First order (min ⁻¹)	0.371	168
Fe ₂ O ₃	Phenol	ND/6.4–8.3	30 min	100	ND	ND	ND	169

Note: ND=not determined

2.3.2 Micro-Pollutants

Among the many metal oxides employed for water treatment, the most studied metal oxides are Fe and Mn based because these metal oxides are widespread in nature and recyclable.⁷⁸ Other metal oxides used in water purification include Al, Ce, Co, Cu, Cr, and Ru. However, these metal oxides have toxicity and cost challenges compared to Fe or Mn; therefore, aluminum ($\text{Al}^0/\text{Al}^{3+}$), cerium ($\text{Ce}^{3+}/\text{Ce}^{4+}$), cobalt ($\text{Co}^{2+}/\text{Co}^{3+}$), copper ($\text{Cu}^+/\text{Cu}^{2+}$), chromium ($\text{Cr}^{3+}/\text{Cr}^{6+}$), and ruthenium ($\text{Ru}^{2+}/\text{Ru}^{3+}$) have potential applications in water treatment, assuming the environmental and economic barriers can be eliminated. Manganese oxides like KMnO_4 have lower redox potential compared to the Fe-equivalent K_2FeO_4 .⁵² Moreover, KMnO_4 (7+) and manganate (6+) are noted to be highly stable in solution, so the major factors affecting the oxidative redox potential in manganese oxides are the III and IV oxidation states: Mn_3O_4 and MnO_2 .^{24,75,78,170} Therefore, manganese and iron oxides are predominant in research studies because of environmental safety and potential for scale-up in water remediation projects from cost considerations.

The major iron oxides studied in water remediation include Fe(III) oxide and ferrate(VI).^{5,38,52,71,78,171} The iron oxide in the 2+/3+ redox system compose the needed components for the Fenton reaction in addition to a source of H_2O_2 .^{71,171} The Fenton reaction requires iron oxide, H_2O_2 , and either electrical voltage or UV light to split apart the H_2O_2 molecule into two hydroxyl radicals.³⁸ The challenge with the photo-Fenton or electrical-Fenton reaction is the tight pH that must be maintained in the acidic region using iron oxide redox couple.⁷⁸ Also, the H_2O_2 must be continually supplied for hydroxyl radicals to form and attack pollutant species in solution. Solutions to address the need for H_2O_2 formation include using a carbon membrane infiltrated with oxygen gas in iron oxide redox couple under a potential to form eventual hydroxyl radicals.¹⁷² Therefore, the challenges for the Fenton reaction using iron redox couple include the tight acidic pH range needed, rapid supply of H_2O_2 , and the catalyst, be it UV-light or electrical potential to break the H_2O_2 into two hydroxyl radicals.¹⁷³ Also, H_2O_2 is not a strong oxidant (1.776 V) compared with hydroxyl radical (2.80 V).^{5,52} The major alternative metal oxide species that has second highest redox state after hydroxyl radical is ferrate(VI) at 2.20 V. The partially empty *d*-orbital ($3d^2$) provides the opportunity for increased oxidation-reduction reactions to occur, which may be one of several reasons for ferrate(VI) use in water purification studies. The ferrate(VI) cation is not as thermodynamically stable as the Fe(III) cation because of reduced exchange energy where three of the five suborbitals having no electron density, and this is equated in the large change in Gibb's free energy.⁹⁶ The

acceptance of a hydrogen atom further stabilizes the ferrate(VI) to become ferrate(V) (HFeO_4^-), with additional electron density shared between the hydrogen atom and Fe(V) center, and this highly reactive species has been proposed as the major species that attacks the organics.¹⁷⁴ Final reduction of ferrate(V) to Fe(III) oxide involves a two-electron acceptance from the organic pollutant.

Table 4 provides an analysis of 21 Fe,^{170,175–188} Mn,^{24,189–193} and related metal oxides in aqueous pharmaceutical pollutants removal studies. Potassium ferrate(VI) in homogeneous aqueous phase directly interacts with probe molecules as an electron sink, thereby forming Fe(III) oxide in the chemical reaction. Manganese oxides initially begin as KMnO_4 in homogeneous solution before disproportion to MnO_2 and lower oxidation states. Most of the micro-pollutants listed in Table 4 have aromatic structures, which can be attacked by electron-deficient compounds, otherwise denoted as oxidants. The substituent groups attached to the aromatic ring structures determine the ability for the large π cloud to donate into ferrate(VI). The varied electron-withdrawing groups attached severely limits the breakdown with electron-deficient compounds. Comparison of a strongly withdrawing electron substituent carboxylate group in ibuprofen causes this molecule to be difficult to convert to innocuous products.¹⁷⁹ In contrast, BPA has a 100% removal efficiency with complete mineralization because this pollutant can be easily attacked by ferrate(VI).¹⁷⁶ Sulfur-containing micro-pollutants become degraded rapidly similar to other electron-rich molecules, but other functional groups will dictate the reaction rate for the degradation process. Simple placement of a nitrogen atom in a ring adjacent to an aromatic ring system favors a smaller reaction rate constant, such as with sulfamethoxazole (SMX).¹⁷⁵ However, placing an oxygen atom adjacent to the aromatic ring structure has the reverse effect, as with sulfisoxazole (SOZ). The propensity for a heteroatom to donate or remove electron density is an additional factor that influence the mineralization of micro-pollutants. Finally, the aqueous pharmaceutical pollutants all have one or more ring structures, and this provides a greater challenge in degradation because many of these compounds have stable degraded products, as reflected in Table 4.

Table 4 Aqueous pharmaceutical pollutants removal with high-valence Fe, Mn, and metal oxides

Catalyst composition	Pollutant(s)	Reaction temperature/pH	Contact time	Removal efficiency (%)	Product(s)	Reaction rate	Reaction rate constants	Reference
K ₂ FeO ₄	BPA	298 K/8.2–12	235 min	100	BPA: Complete mineralization	Second Order (M ⁻¹ s ⁻¹)	BPA: 2.80×10^2 EE2: 3.05×10^2 E1: 7.10×10^2 E2: 7.32×10^2 E3: 9.28×10^2	176
	17 α -ethynylestradiol (EE2)			90				
	Estrone (E1)			100				
	β -estradiol (E2)			100				
	Estriol (E3)			ND				
K ₂ FeO ₄ KMnO ₄	Carbamazepine (CBZ)	298 K/7.0, and 8.0	15 min	90	6 products	Second Order (M ⁻¹ s ⁻¹)	70 \pm 3	170
			30 min	100	12 products		3.0 \pm 0.3 $\times 10^2$	
K ₂ FeO ₄	Glycine (Gly) Glycylglycine (Gly-Gly)	298 K/4.0–12.4	ND	75, and 40	Acetate and ammonia	Second order (M ⁻¹ s ⁻¹)	Gly: 105 \pm 2.19, pH = 7.0; Gly-Gly: 822 \pm 60.2	177
K ₂ FeO ₄	Atenolol CBZ 17 α -ethynylestradiol (EE2) Ibuprofen SMX	297 \pm 1 K/8, and 9.2	60 min	ND	ND	Second order (M ⁻¹ s ⁻¹)	Atenolol, pH = 8, 7 CBZ, pH = 8, ND EE2, pH = 8, ND Ibuprofen, pH = 8, < 0.1 SMX, pH = 8, ND	178
K ₂ FeO ₄	Estrone	296 \pm 2 K/7	180 min	100	ND	ND	ND	179
	17- β -Estradiol			0				
	17 α -ethynylestradiol			0				
	Diethylstilbestrol			0				
	Triclosan			100				
	17 α -trenbolone			0				
	17 β -trenbolone			0				
	19-nortestosterone			0				
	4-androstene-3,17-dione (AED)			60				
	Testosterone			0				
	Methytestosterone			0				
	4-hydroxyl-anrost-2-ene-17-dione (4-OHA)			45				

Table 4 Aqueous pharmaceutical pollutants removal with high-valence Fe, Mn, and metal oxides (continued)

Catalyst composition	Pollutant(s)	Reaction temperature/pH	Contact time	Removal efficiency (%)	Product(s)	Reaction rate	Reaction rate constants	Reference
K ₂ FeO ₄	Prednisone			0				
	Cortisone			0				
	Cortisol			0				
	19-Norgestrel			0				
	Medroxyprogesterone			0				
	BPA			30				
	4-tert-octylphenol			80				
	4-nonylphenol			65				
	Triclocarban			100				
	Androsta-1,4-diene-17-dione (ADD)			100				
	17 β -Boldenone			0				
	17 α -Boldenone			50				
	Stanozolol			0				
	Epi-androsterone			0				
	Androsterone			0				
	5 α -dihydrotestosterone							
	Prednisolone			0				
	Dexamethasone			0				
	Ethynyl Testosterone			0				
	Progesterone			0				
	Diclofenac			0				
	Indometacin			100				
	Meclofenamic acid			90				
	Mefenamic acid			100				
	Tolfenamic acid			95				
	Naproxen			0				
	Bentazone			100				
	Paracetamol			0				
	CBZ			0				
	Clofibric acid			100				
	2,4-Dichlorophenoxyacetic acid (2,4-D)			40				

Table 4 Aqueous pharmaceutical pollutants removal with high-valence Fe, Mn, and metal oxides (continued)

Catalyst composition	Pollutant(s)	Reaction temperature/pH	Contact time	Removal efficiency (%)	Product(s)	Reaction rate	Reaction rate constants	Reference
K ₂ FeO ₄	2-Methyl-4-chlorophenoxyacetic acid (MCPA)			35				
	Ibuprofen			0				
	Fenoprofen			0				
	Gemfibrozil			0				
	Ketoprofen			0				
	Primidone			0				
	Cyclophosphamide			0				
	Sulfadiazine			100				
	Sulfapyridine			100				
	Trimethoprim			100				
	Ofloxacin			100				
	Norfloxacine			0				
	Ciprofloxacin			0				
	Tetracycline			75				
	Chlortetracycline			0				
	Roxithromycin			100				
	Oleandomycin			0				
	Sulfamethazine			100				
	Sulfamethoxazole			100				
	Lomefloxacin			0				
	Enrofloxacin			0				
Oxytetracycline			100					
Doxycycline			0					
Erythromycin-H ₂ O			100					
K ₂ FeO ₄	Ciprofloxacin (CIP)	ND/6.0–6.1	21 min	70	ND	ND	ND	180
K ₂ FeO ₄	Ciprofloxacin (CIP)	ND/6–8	21 min	70	ND	ND	ND	181
	Ibuprofen			25				
K ₂ FeO ₄	Amoxicillin (AMX)	298 K/6.0	ND	ND	ND	Second order (M ⁻¹ s ⁻¹)	AMX: 4.4 ± 0.9 × 10 ⁶	182
	Ampicillin (AMP)							
	6-aminopenicillanic acid							
K ₂ FeO ₄	Atenolol	293 ± 2 K/9	120 min	71.7	12 products	ND	ND	183
	Metoprolol			24.7	8 products			
	Propranolol			96.5	13 products			

Table 4 Aqueous pharmaceutical pollutants removal with high-valence Fe, Mn, and metal oxides (continued)

Catalyst Composition	Pollutant(s)	Reaction Temperature/pH	Contact Time	Removal Efficiency (%)	Product(s)	Reaction Rate	Reaction Rate Constants	Reference
K ₂ FeO ₄	Ciprofloxacin (CIP) Ibuprofen	ND/6–8	21 min	70 25	ND	ND	ND	184
K ₂ FeO ₄	Tetrabromobisphenol A (TBBPA) BPA	297 ± 1 K/7.0, and 8.0	180 min	70 75	12 products	Second order (M ⁻¹ s ⁻¹)	7.9 × 10 ³ (pH 7), and 2.6 × 10 ³ (pH 8)	185
K ₂ FeO ₄	Amoxicillin (AMX) Ampicillin (AMP) Cloxacillin (CLOX) Penicillin G (PENG) Cephalexin (CEX)	ND/6.0–9.5	180 min	ND	ND	Second order (M ⁻¹ s ⁻¹)	AMX: 771, pH 7 AMP: 418, pH 7 CLOX: 116, pH 7 PENG: 114, pH 7 CEX: 686, pH 7	186
K ₂ FeO ₄	Sulfamethoxazole (SMX) Diclofenac (DCF) CBZ Bezafibrate (BZF)	293 ± 2 K/6–8	181 min	80 82 100 20	4 products 4 products 4 products ND	Second order (M ⁻¹ s ⁻¹)	SMX: 360 ± 17, pH 8 DCF: 12.48 ± 0.98, pH 8 CBZ: 23.83 ± 0.52, pH 8 BZF: < 0.5, pH 8	187
K ₂ FeO ₄	Sulfaguanidine (SFG) Sulfisoxazole (SOZ) Sulfamethizole (SMIZ) SMX Sulfamethazine (SMAZ) Sulfadimethoxine (SDM)	298 K/4.0, 7.0, and 9.0	ND	ND	SMX: 7 products	Second order (M ⁻¹ s ⁻¹)	SFG: 0 SIX: 2.4 ± 0.1 × 10 ³ SMIZ: 2.2 ± 0.2 X10 ⁴ SMX: 3.0 ± 0.5 X10 ² SMAZ: 5.5 ± 0.5 X10 ² 5.0 ± 0.3 × 10 ² Note: pH 4	188
MnO _x : KMnO ₄ , MnO ₂	Triclosan p-nitrophenol	296 ± 2 K/5–9	50 min 160 min	100 30	CO ₂ + H ₂ O	Second order (M ⁻¹ s ⁻¹)	pH = 5, 6.5; 6, 43.3; 7, 129; 8, 349; 177, 9	24
KMnO ₄	Ciprofloxacin (CPR) Lincomycin (LCM) Trimethoprim (TMP)	298 K/5–9	80 min 18 min 35 min	75 73 75	ND	Second order (M ⁻¹ s ⁻¹)	CPR, pH = 7, 0.52 ± 0.05, 0.34 ± 0.08, 1.2 ± 0.1; LCM, pH = 7, 0.5 ± 0.1, 43 ± 6; TMP, pH = 7, 2.6 ± 0.3, 0.17 ± 0.05	189

Table 4 Aqueous pharmaceutical pollutants removal with high-valence Fe, Mn, and metal oxides (continued)

Catalyst composition	Pollutant(s)	Reaction temperature/pH	Contact time	Removal efficiency (%)	Product(s)	Reaction rate	Reaction rate constants	Reference
KMnO ₄	Ciprofloxacin (CPR)	298 K/7	80 min	75	CPR:	ND	ND	190
	Lincomycin (LCM)		18 min	73	1. C ₁₃ H ₁₁ FN ₂ O ₃			
	Trimethoprim (TMP)		35 min	75	2. C ₁₄ H ₁₁ FN ₂ O ₄ 3. C ₁₃ H ₉ FN ₂ O ₅ 4. C ₁₅ H ₁₆ FN ₃ O ₃ 5. C ₁₆ H ₁₆ FN ₃ O ₄ 6. C ₁₅ H ₁₁ FN ₂ O ₆ 7. C ₁₇ H ₁₆ FN ₃ O ₄ 8. C ₁₇ H ₁₆ FN ₃ O ₄ 9. C ₁₇ H ₁₄ FN ₃ O ₅ 10. C ₁₇ H ₁₆ FN ₃ O ₅ 11. C ₁₇ H ₁₆ FN ₃ O ₅ 12. C ₁₇ H ₁₈ FN ₃ O ₆ 13. CPR Starting C ₁₇ H ₁₈ FN ₃ O ₆ LCM: 1. C ₁₇ H ₃₂ N ₂ O ₆ S 2. C ₁₈ H ₃₃ N ₂ O ₆ S 3. C ₁₇ H ₂₉ NO ₈ S 4. C ₁₈ H ₃₂ N ₂ O ₇ S 5. C ₁₈ H ₃₄ N ₂ O ₇ S 6. C ₁₈ H ₃₄ N ₂ O ₈ S 7. C ₁₈ H ₃₂ N ₂ O ₉ S 8. LCM Starting C ₁₈ H ₃₄ N ₂ O ₆ S TMP: 1. C ₁₃ H ₁₇ N ₃ O ₄ 2. C ₁₃ H ₁₈ NO ₄ 3. C ₁₄ H ₁₆ N ₄ O ₄ 4. C ₁₄ H ₁₈ N ₄ O ₄ 5. C ₁₄ H ₁₈ N ₄ O ₅ 6. C ₁₄ H ₁₇ N ₃ O ₆ 7. C ₁₄ H ₂₀ N ₄ O ₅ 8. TMP Starting C ₁₄ H ₁₈ N ₄ O ₃			

Table 4 Aqueous pharmaceutical pollutants removal with high-valence Fe, Mn, and metal oxides (continued)

Catalyst composition	Pollutant(s)	Reaction temperature/pH	Contact time	Removal efficiency (%)	Product(s)	Reaction rate	Reaction rate constants	Reference
KMnO ₄	Estrone 17β-estradiol (E2), estriol, 17α- ethinylestradiol 4-n-nonylphenol	298 K/5–10	30 min	30	10 partially fragment organic species	Second- order (M ⁻¹ s ⁻¹) Mn(III)- NTA	E2, pH = 19735; pH = 6, 12181; pH = 7, 5288; pH = 783	191
KMnO ₄	Progestagens: Levonorgestrel (Levo) Medroxyprogesterone (Medro) Noethindrone (Nore) Progesterone (Prog)	295 ± 2 K/6, and 8	10-60 min	Levo: 89 ± 12, pH 6 Medro: 57 ± 20, pH 6 Nore: 90 ± 11, pH 6 Prog: 48 ± 11, pH 6	ND	ND	ND	192
KMnO ₄	SMX	292–294 K/8.22	60 min	100	4 partially converted organic species	ND	ND	193

A study that directly compared oxidation of a medication CBZ with KMnO_4 and K_2FeO_4 demonstrated over four times higher reaction rate of conversion of CBZ to ring-open products using K_2FeO_4 .¹⁷⁰ These results further infer that the redox potential, an empty d-orbital, and having a combination of HFeO_4^- and FeO_4^{2-} are highly favorable toward electrophilic ring attack of π -electrons. The protonated (HFeO_4^-) species has greater activity because of a lack of stability from electron sharing between the proton attached to the FeO_4^{2-} .¹⁹⁴ The reaction rate conversion of aqueous pollutants have a pH dependence for Mn, which is also seen with Fe species. Therefore, the Mn materials focused on most have lower redox potentials, such as Mn_3O_4 and MnO_2 .^{52,190} These manganese oxides are soluble in aqueous phase, and they dominate the development in wastewater treatment using alternatives to Fe.^{75,78} The Mn^{3+} forms in solution from KMnO_4 via two main routes with complexation or without ligands.¹⁹¹ Use of ligands with KMnO_4 permits the conversion of various electron-rich organic ring structures common with EDCs. In addition, KMnO_4 can directly disproportionate to Mn^{3+} although at slower rate with ligands. On the other hand, KMnO_4 without stabilizing ligands forms directly MnO_2 (Mn^{4+}) in addition to oxidizing micro-pollutants. The Mn^{3+} ion can oxidize micro-pollutants, such as EDCs, but the spontaneous disproportion reaction directly competes with the desired oxidation reaction. Therefore, ligands are needed to reduce this undesired reaction. Elevated pH values above neutral favor increased reaction conversion rates compared to K_2FeO_4 ; however, ozone treatment has been shown to have the highest product formation rates.^{191,193} These increased pH values of 9 and above provide an avenue to oxidize cyanide from gold-mine waste using KMnO_4 , as shown in Table 3.¹⁶⁴ Nonetheless, many aqueous wastewater treatment reactions will work at neutral pH values, so it is desired to operate the catalyst in this range. KMnO_4 highest oxidation potential is obtained under very acidic conditions (pH = 2).¹⁶⁷ Therefore, manganese oxides appear to work only under select conditions with optimal results. It should be noted that the compound of interest determines the pH range for manganese oxides to oxidize. Finally, the reaction rate is not always reflective of the efficiency of an oxidant because of organic matter being in real-world bodies of water.¹⁷⁸

Comparison of oxidants shows that the micro-pollutant and reaction conditions determine the kinetics, as shown in Fig. 2.¹⁷⁸ Clearly, the type of oxidant has major influence on the reaction rate. Figure 2a shows the log-normal reduction of 17 α -ethinylestradiol (EE2), which contains the electron-rich moiety phenolic group. The breakdown follows the pattern seen in Fig. 2a because selective oxidants, such as ClO_2 , HFeO_4^- , hypochlorous acid (HOCl), and ozone, selectively attack the phenolic group contained within the EE2 micro-pollutant. In contrast, hydroxyl radical ($\cdot\text{OH}$) from H_2O_2 photolysis with UV light breaks down

all organic materials nonselectively, irrespective of the type of contaminant, and this is illustrated in Fig. 2b–f. The differences among the ordering of the ClO_2 , HFeO_4^- , HOCl , and ozone can be understood to be related to type of electron donating group contained within each of these six micro-pollutants. SMX has an aniline moiety that participates with oxidants to various levels. CBZ has an olefin section that will interact with certain oxidants. ATL has a primary amine that can oxidize depending on the oxidant and dose of the oxidant. Ibuprofen has no electron-rich moieties, or there are no active aromatic rings present in this micro-pollutant, which is reflected with only hydroxyl radical and ozone reacting with ibuprofen. The final aqueous pollutant is *para*-chlorobenzonate (*p*CBA), which serves as an external scavenger of hydroxyl radicals. The ability of these micro-pollutants to donate or transfer electron density to the oxidant influences how readily an oxidation will occur. ClO_2 attacks electron-rich activated aromatic systems, such as aniline- and phenolic-containing groups. However, ClO_2 does not oxidize olefin containing micro-pollutants, such as CBZ, and ClO_2 has low oxidation ability toward primary amine containing micro-pollutants like ATL. HFeO_4^- attacks at similar doses as ozone for EE2. Nonetheless, HFeO_4^- has less attacking ability for SMX because of the aniline moiety being attached to an electron-withdrawing sulfone group contained within sulfamethoxazole. Ozone attacks all five micro-pollutants to various amounts because of forming hydroxyl radicals, but ozone can form bromates that have been suggested to be carcinogenic. Overall, ClO_2 , HFeO_4^- , HOCl , and ozone are more selective toward micro-pollutants in real-world polluted water because these oxidants do not interact with all organic matter contained within nonremediated aqueous bodies, whereas hydroxyl radical will attack any organic species in solution nonselectively, as reflected in Figs. 2–7.

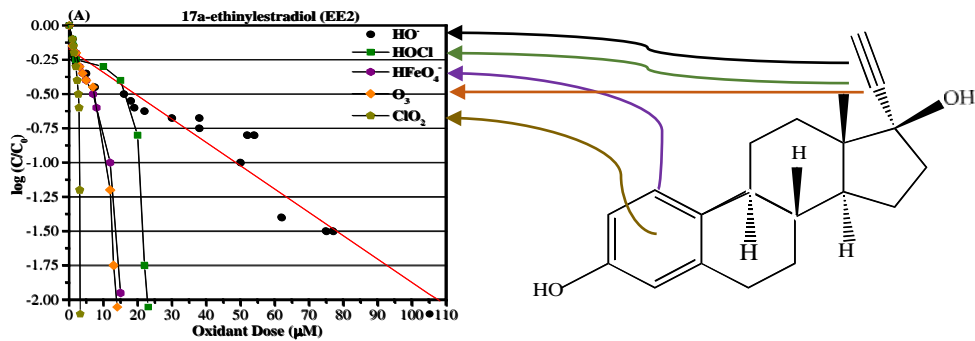


Fig. 2 Kinetics of breakdown as function of (top) micro-pollutant 17 α -ethinylestradiol (EE2) and oxidant. EE2 structure shown to the right where oxidant attack will initially take place. Data modified from Lee and von Gunten.¹⁷⁸

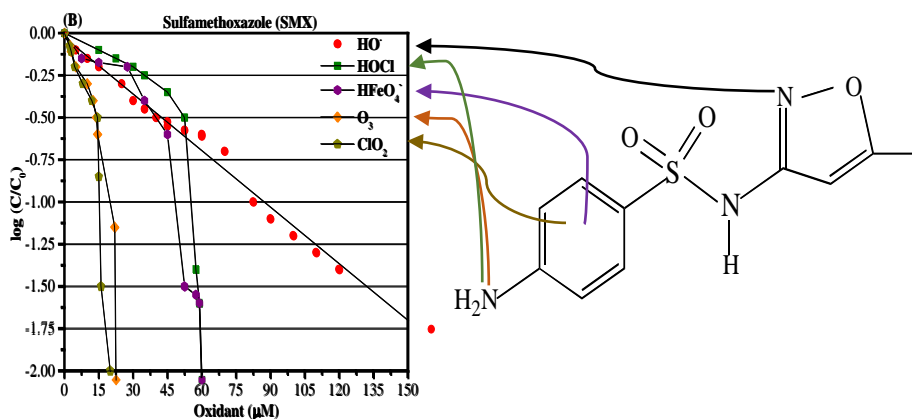


Fig. 3 Kinetics of breakdown as function of micro-pollutant sulfamethoxazole (SMX) and oxidant. SMX structure shown to the right where oxidant attack will initially take place. Data modified from Lee and von Gunten.¹⁷⁸

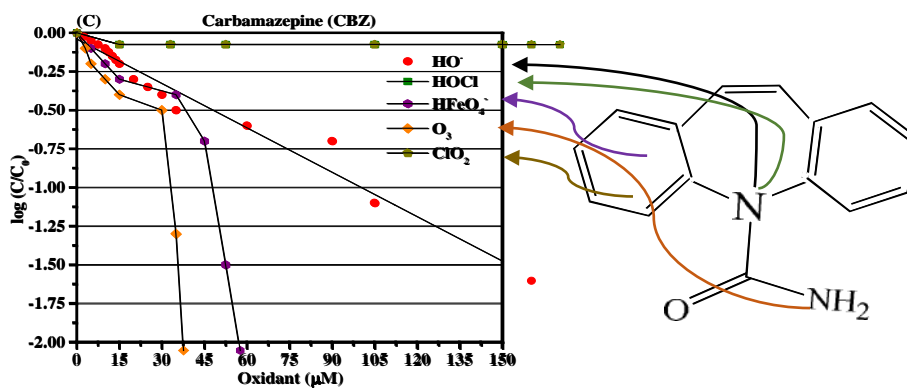


Fig. 4 Kinetics of breakdown as function of micro-pollutant carbamazepine (CBZ) and oxidant. CBZ structure shown to the right where oxidant attack will initially take place. Data modified from Lee and von Gunten.¹⁷⁸

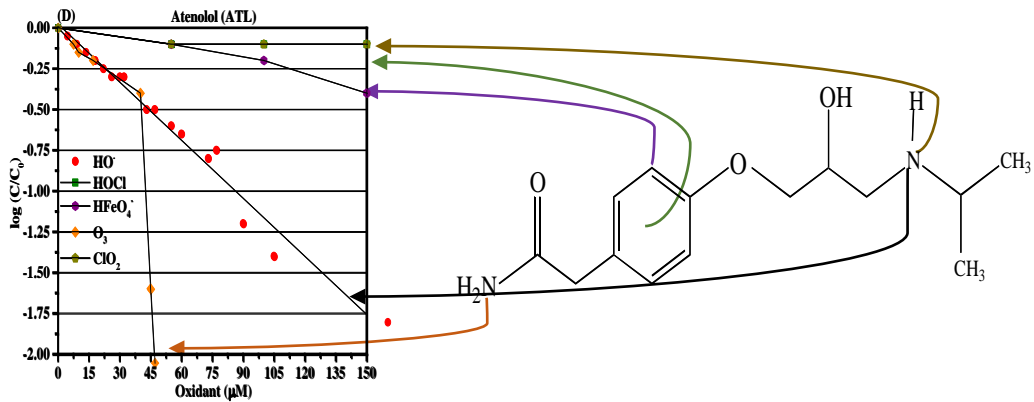


Fig. 5 Kinetics of breakdown as function of micro-pollutant atenolol (ATL) and oxidant. ATL structure shown to the right where oxidant attack will initially take place. Data modified from Lee and von Gunten.¹⁷⁸

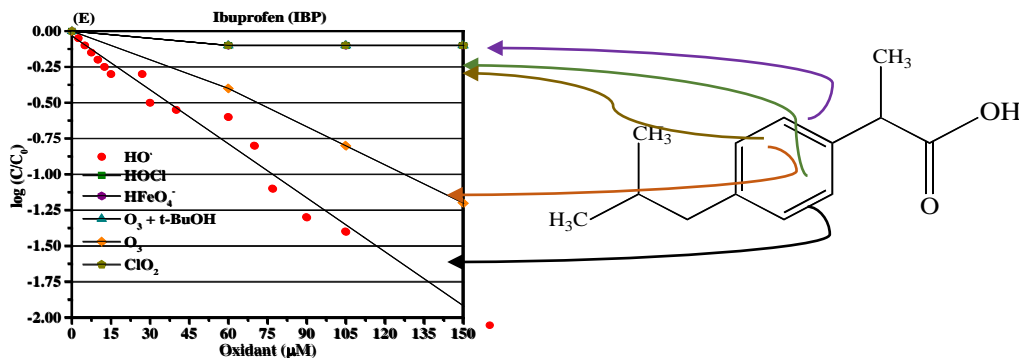


Fig. 6 Kinetics of breakdown as function of micro-pollutant ibuprofen (IBP) and oxidant. IBP structure shown to the right where oxidant attack will initially take place. Data modified from Lee and von Gunten.¹⁷⁸

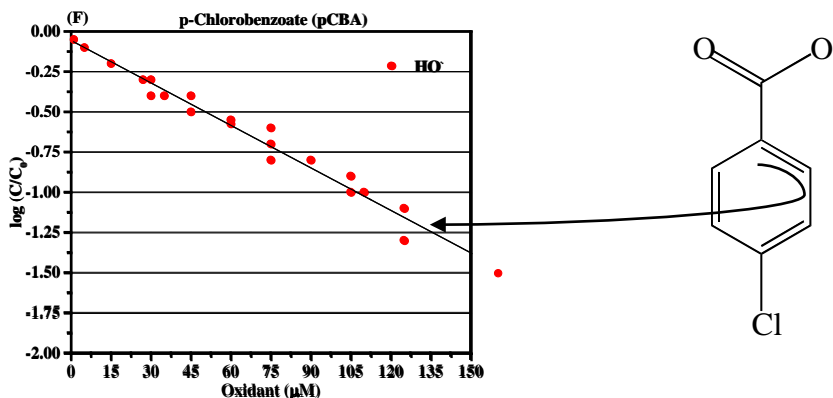


Fig. 7 Kinetics of breakdown as function of micro-pollutant *p*-chlorobenzoate (pCBA) and oxidant. pCBA structure shown to the right where oxidant attack will initially take place. Data modified from Lee and von Gunten.¹⁷⁸

Figure 8 reflects the kinetics of how quickly an oxidant is consumed in an aqueous body. Ozone is consumed within 3 min, a rapid consumption that implies mainly nonselective hydroxyl formation.¹⁷⁸ The lack of nonselectivity from ozone means that micro-pollutants will be less oxidized per a given dose. In contrast, HFeO_4^- in Fig. 8b and ClO_2 in Fig. 8d have the largest amount of residue oxidant left after 60 min of approximately 10 μM . Therefore, these two oxidants will have a greater opportunity to break down electron-rich moieties contain in certain micro-pollutants. HOCl is consumed at a slightly higher pace from interaction with organic matter, and fewer micro-pollutants will be oxidant per a dose compared with either HFeO_4^- or ClO_2 . Figures 2–8, from Lee and von Gunten,¹⁷⁸ suggest that certain oxidants are selective toward oxidants even within a real body of wastewater containing micro-pollutants, and the needed dose of selective oxidant is less than hydroxyl radicals for activated electron-rich moieties contained within micro-pollutants. Therefore, ClO_2 , HFeO_4^- , HOCl, and ozone are better per a dose basis on breaking down micro-pollutants.

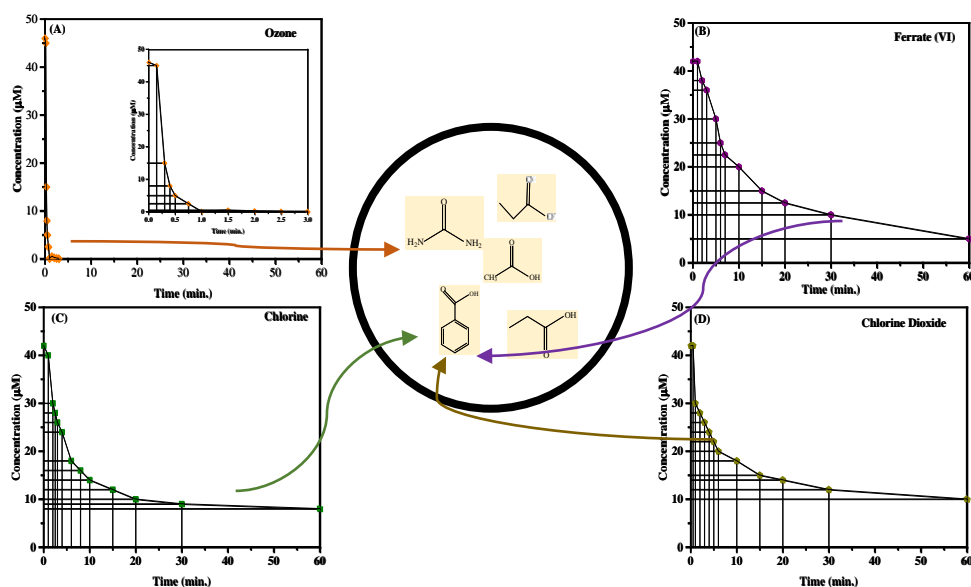


Fig. 8 Kinetics of breakdown as function of secondary wastewater pollutant and oxidant. Few secondary wastewater contaminants structures shown in center respective oxidant initial attack on organic functional group. Data modified from Lee and von Gunten.¹⁷⁸

Ferrate(VI) has been studied because of its high redox potential ability to accept electron density from donor molecules and ions common in wastewater.^{5,52} The needed component for degradation reaction to occur with ferrate(VI) requires an optimal pH value with acidic conditions favoring rapid oxidation of aqueous organics in polluted waters. In contrast, neutral and basic pH values give a less aggressive attack on electron donating organics. Nonetheless, ferrate(VI) will

function as an electron sink in pH solutions other than acidic. The major species for breaking down organics using ferrate(VI) is HFeO_4^- .¹⁹⁴ The addition of this extra electron in the partially filled 3-D orbital destabilizing ferrate(VI) into ferrate(V). The ferrate(V) accepts electron reductants in single one-electron steps until Fe(III) oxide ($3d^5$) is obtained.¹⁹⁵ Therefore, the destabilizing effect of additional electrons facilitates the high reactivity seen in ferrate materials. The major challenge for ferrate materials is regeneration after being converted to Fe(III) oxide. Avenues to explore ways to accept electrons from donor pollutant molecules and ions contained within wastewater, followed by transferring the electron density to another material, remains a major challenge for the widespread use of ferrate in water treatment. In addition, the stability of ferrate is a major struggle because it can oxidize water with moisture, causing the reduction of ferrate(VI) to Fe(III) oxide. These two challenges need to be solved before ferrate replaces current water purification technology, such as Cl, ozone, Fenton's reactant, and membranes. All of these current technologies have their own major barriers, and these conventional water treatment techniques fail to remove micro-pollutants, such as EDCs, that are encountered on a daily basis. In contrast, ferrate(VI) will convert most micro-pollutants to an oxidized form, which can be further broken down in the mineralization reaction. Finally, ferrate(VI) contained within fuel with silica gel has been shown to effectively convert organic sulfur (S) materials into their degraded products with more silica gel in solution.¹⁹⁶

The challenges for activating aliphatic organics using either Fenton's reactant or ferrate(VI) remains a major hurdle to overcome. Neither Fe(II/III) redox couple with H_2O_2 or ferrate(VI) readily activate organics comprised of only aliphatic species in aqueous phase. Also, conventional water treatment methods fail to activate saturated organics in wastewater. The major exception to slight activation of aliphatic structures is the use of a hydroxyl radical produced in photocatalysis commonly using wide-bandgap materials like TiO_2 . Combining ferrate(VI) with TiO_2 has produced less than optimal results with ferrate(VI) acting as an electron sink, and TiO_2 conduction band (LUMO) electrons being removed and holes accumulating in the valence band (HOMO).¹⁹⁷⁻¹⁹⁸ These holes form hydroxyl radicals that rapidly attack aqueous organics leading oxidized species. Lastly, the combination of ferrate(VI) with TiO_2 shows promise if the ferrate can be prevented by reducing.

2.3.3 Heavy Metals

Few studies have been directed toward homogeneous oxidants for adsorption of heavy metals. This is reflected in Table 5, with only three studies completed on Cr(III), As(III), and Ni(II) cations. Cr has been removed from radioactive waste

solid by oxidizing the Cr(III) to Cr(VI) with Fe(III) oxide forming, and this illustrates that oxidants are primarily used for removing one toxic metal cation to form an innocuous product.¹⁹⁹ Similarly, As(III) has been shown to be oxidized by ferrate(VI) to form a mixture of Fe₂O₃ bound to As(V) through coagulation process.²⁰⁰ The third study employed a reducing agent in conjunction with ferrate(VI) to bind Ni(II) cation in a similar manner as traditionally completed using alum in wastewater treatment facilities.²⁰¹ The lack of a support reduces removal efficiency in homogeneous reactions using oxidants, as shown in Table 5, and future research will need to address how to creatively remove more heavy metals using homogeneous oxidants.

Table 5 Heavy metal removal using Mn, Fe, and supported metal oxides in water treatment

Catalyst composition	Pollutant	Reaction temperature	pH	Removal efficiency (%)/mg/g	Regeneration cycles/removal efficiency (%/bed volumes)	Adsorption time	Adsorption isotherm	Citation/reference
K ₂ FeO ₄	Cr(III)	343 K	13.52	87.8 ± 2.0/NA	NA/NA/NA	24 h	NA	199
K ₂ FeO ₄	As(III)	298 ± 0.1 K	9.0	95/NA	NA/NA/NA	31 min	NA	200
Na ₄ FeO ₅	Ni(II)	ND	1.4–9.0	100/NA	NA/NA/NA	ND	NA	201
Fe ₂ O ₃ /charcoal	Cr(VI)	288 K-308 K	5.0	91/33.1	ND/ND/ND	24 h	Langmuir	202
Fe ₂ O ₃ /CMK-5	As(III) As(V)	298 K	1–11	98/81.3 65/ND	10/96-94/ND	2 min-24 h	Freundlich	203
Fe ₂ O ₃ /GE	As(V)	ND	ND	100/ND	ND/ND/80 (L)	2.1 min	ND	204
Fe ₂ O ₃ /activated carbon	As(V)	298 K	3.0–8.0	99.90/27.8	ND/ND/ND	5 min-48 h	Langmuir	205
MnO _x /activated carbon	Cu (II) Pb(II)	298 ± 1 K	4	45/2.45 45/6.24	ND/ND/ND	300 min	Langmuir	206
Fe ₂ O ₃ /polymer	Pb(II) Cd(II) Cu(II)	303 K	5.0	100/51.8 100/5.62 100/9.52	5/100/1700 5/100/450 5/100/550	48 h	Freundlich	207
Fe ⁰ /polymer	Pb(II)	298 K	3.09–7.07	97/136.11	ND/ND/ND	480 min	ND	208

Table 5 Heavy metal removal using Mn, Fe, and supported metal oxides in water treatment (continued)

Catalyst composition	Pollutant	Reaction Temperature	pH	Removal efficiency (%)	mg/g	Regeneration cycles/removal efficiency (%)	Adsorption time	Adsorption Isotherm	Citation/Reference
Fe ₂ O ₃ /sodium alginate	Cu(II)	ND	7.0	74.9/14.98		1/87-96.5/ND	ND	ND	209
	Cd(II)			94.5/18.9					
	Pb(II)			99.8/19.96					
	Co(II)			90.6/18.11					
	Ni(II)			67.4/13.48					
	Cr(III)			79.2/15.48					
Amorphous MnO ₂ /polymer	Pb(II)	298 K	4.4 ± 0.1	99/395		5/100/500	300 min	Freundlich	210
MnO ₂ /polymer	Tl(I)	298 K	5.8	90/102.2		10/78-76/1000	200 min	ND	211
Zr ₃ (PO ₄) ₄ /polymer	Pb(II)	298 K	ND	ND/115.8		ND/ND/ND	24 h	ND	212
Fe ₂ O ₃ -H ₂ O/polymer resins	As(V)	ND	7.2	ND/ND		ND/ND/8000	ND	ND	213
HZrO-H ₂ O/polymer Resins	Cu(II)					ND/ND/100			
Fe ₂ O ₃ /Fe(OH) ₃	Cr(VI)	298 K	3–8.5	100/31.5		1/95-97/ND	120 min	Langmuir	214
Fe ₂ O ₃ /Fe(OH) ₃	Se(IV)	298 K	4.0–9.5	100/95		1/95/ND	0-30 min	ND	215
	Se(VI)			13/15.1		1/98/ND			
Fe(OH) ₃ /Al ₂ O ₃	As(V)	298 ± 2 K	ND	90/61.99		ND/ND/ND	300 min-24 h	Langmuir	216
	Cr(VI)			80/24.13					
Fe ₂ O ₃ /SBA-15	Hg(II)	ND	4.5–8.2	97/310		ND/ND/ND	24 h	Langmuir	217
Fe ₂ O ₃ /MCM-41, SBA-15, and KIT-6	As(V)	298 ± 1 K	2.0–11	17.6/8.24		ND/ND/ND	5-480 min	Freundlich	218

Table 5 Heavy metal removal using Mn, Fe, and supported metal oxides in water treatment (continued)

Catalyst composition	Pollutant	Reaction temperature	pH	Removal efficiency (%) / mg/g	Regeneration cycles/removal efficiency (%/bed volumes)	Adsorption time	Adsorption Isotherm	Citation/Reference
Fe ₃ O ₄ /MCM-48	Pb(II)	298 K	4.0	97.8/127.24	ND/ND/ND	90 min	Langmuir	219
	Cu(II)			94.9/125.80				
	Cr(VI)			91.8/115.60				
	Cd(II)			88.5/114.08				
Mn-doped-Fe ₃ O ₄	Co(II)	ND	7	94/0.5	3/96-98/ND	2 h	Langmuir	220
	Ni(II)			72/0.5				
	Zn(II)			98/0.5				
	As(III)			78/0.5				
	Ag(I)			99/0.5				
	Cd(II)			100/0.5				
	Hg(II)			96/0.5				
	Tl(I)			98/0.5				
Fe ⁰ /Ni ⁰ /kaolin (clay)	Cu(II)	ND	3.0–6.0	95/80.6	ND/ND/ND	30 min	ND	221
Fe ₂ O ₃ /trioctahedral smectites (clay)	As(III)	298 K	5	ND/0.5	ND/ND/ND	2 h	ND	222
	Cd(II)			ND/1.5				
	Cr(III)			ND/1.8				
	Cu(II)			ND/1.6				
	Hg(II)			ND/0.2				
	Ni(II)			ND/1.55				
	Pb(II)			ND/1.57				
	Zn(II)			ND/1.58				

3. Classification of Materials

Nonporous materials could be classified into ceramics-sintered and carbon black, for example.^{61,223} Sintering or densification commonly using elevated heating results in relatively nonporous ceramics, which is not desired because reduced surface area leads to fewer potential opportunities for adsorption to occur.²²⁴ In a similar manner, dense carbon types, such as carbon black, have significantly reduced surface area, and adsorbents used in water purification need high surface area coupled with desired functional groups to adsorb desired aqueous pollutants. Porous materials have the benefit of large surface areas depending on given inorganic or organic solid. Mesoporous periodic silica easily can be over 1000 m²/g, with pore volumes close to 1 cc/g and pore diameters from 2 to 3 nm in size.^{108,225–226} Likewise, carbon-based materials, such as activated carbon, typically have 1000–3500 m²/g.⁶¹ In addition, the random pore network might be favorable in disordered activated carbon, and the cost of activated carbon is relatively low compared with other adsorbents. The pore size distribution (PSD) for activated carbon varies from micro-, meso-, and macroporous in nature. The other porous supports commonly encountered include Al₂O₃, MgO, and TiO₂. Al₂O₃ support surface area values vary from 300 to 500 m²/g, which suggests lower potential aqueous pollutant uptake ability.⁷⁷ Likewise, MgO generally have surface area values below 200 m²/g with basicity of this support as the major attribute in aqueous pollution remediation.^{77,227} Higher surface area values of 200 to 400 m²/g in TiO₂ have been shown to remove a larger percentage of heavy metal ions, such as Zn, Cd, Pb, Ni, and Cu.⁷⁷ Metal oxide materials are used the most in water purification currently because of their relative stability in aqueous phase.⁷⁸ Oxides have different surface potential (point-of-zero charge [PZC]) depending on the pH value, and this change in the pore wall surface can be potentially used to attract or repel various aqueous pollutants.²²⁸ Table 6 outlines the relatively large surface charges depending on the pH of the solution.

Al₂O₃,^{229–232} silica,^{232–237} CeO_x,²³⁸ zirconia,²³⁹ titania,^{240–241} carbon,^{242–245} and clay^{246–249} were the most studied to present as supports. In addition to the surface area and related textural properties, the active planes vary with smaller particle size and larger surface area, which favors greater uptake of heavy metal ions. Porous materials typically encountered in water purification as adsorbents have surface area values 200 m²/g and higher toward 3500 m²/g seen in activated carbon. Metal oxide supports generally have lower surface areas than carbon-based materials seen in water remediation from the differences in bonding arrangements. The pore volumes are also lower in metal oxides, but the pore diameters can vary from microporous (<2 nm) to macroporous (>50 nm). The

metal oxide chemistry and synthetic conditions significantly determine the resulting textural properties of the final adsorbent. The synthetic conditions in carbon-based materials are also influenced by the preparation method.

Table 6 Properties of supports employed as adsorbents

Support(s)	Density (g/cm ³)	Surface area (m ² /g)	Total pore volume (cc/g)	Pore diameter (Å)	PZC
Al ₂ O ₃ ^a	3.65–3.99	50–300	0.5	30–130	8–10
SiO ₂ ^b	0.1–2.2	600–1700	0.5–2.5	20–300	2.9
TiO ₂ ^c	3.94–4.25	50–250	0.1–0.2	7–250	5.8
Clays ^d	2.60–2.94	15–700	0.5–2.5	10–700	2.5–9.4
Carbon ^e	0.286–0.539	120–3500	0.9–2.0	10–40	2.2–11.9

^aThe phase determines the density of Al₂O₃.²⁵⁰ The Al₂O₃ textural properties vary as function of phase, preparation, and thermal treatment conditions,²⁵¹ depending on the phase of Al₂O₃ and the aqueous media.⁷²

^bThe density of silica varies depending the preparation, such as low-temperature supercritical drying (ScCO₂), templated, or precipitation.^{252–253} Nitrogen textural properties are a reflection of the synthesis conditions. The PZC value is a function of the material and pH value.¹²⁴

^c TiO₂ density a function of the phase formed.²⁵⁴ Nitrogen textural properties vary widely for synthesis of TiO₂ depending on the preparation and thermal treatment. The thermal treatment is the largest factor in the resulting textural properties obtained.²⁵⁵ The PZC value depends on the resulting titanol groups formed, which is a function of the synthesis of thermal treatment.¹²⁴

^dDehydrated clay values vary depending on the particular type of clay.²⁵⁶ The type of clay and resulting structure determines the textural properties.^{257–258} For example nanoporous clays can have an upper limit of 700 m²/g, but most clays are 15–400 m²/g in surface area. The wide range obtained for the PZC value is related to the many types of clays, which each have a different point-of-zero charge.²²⁸

^eDensity of carbon materials varies depending on the structure, such as activated carbon.²²⁴ Textural properties of carbon materials varies depending on the geometries, such as activated carbon as opposed to GE.²⁵⁹ PZC varies depending on the carbon material and the activation step.²²⁸

Figure 9 shows images four common geometric shapes commonly encountered in periodic mesoporous silica materials.

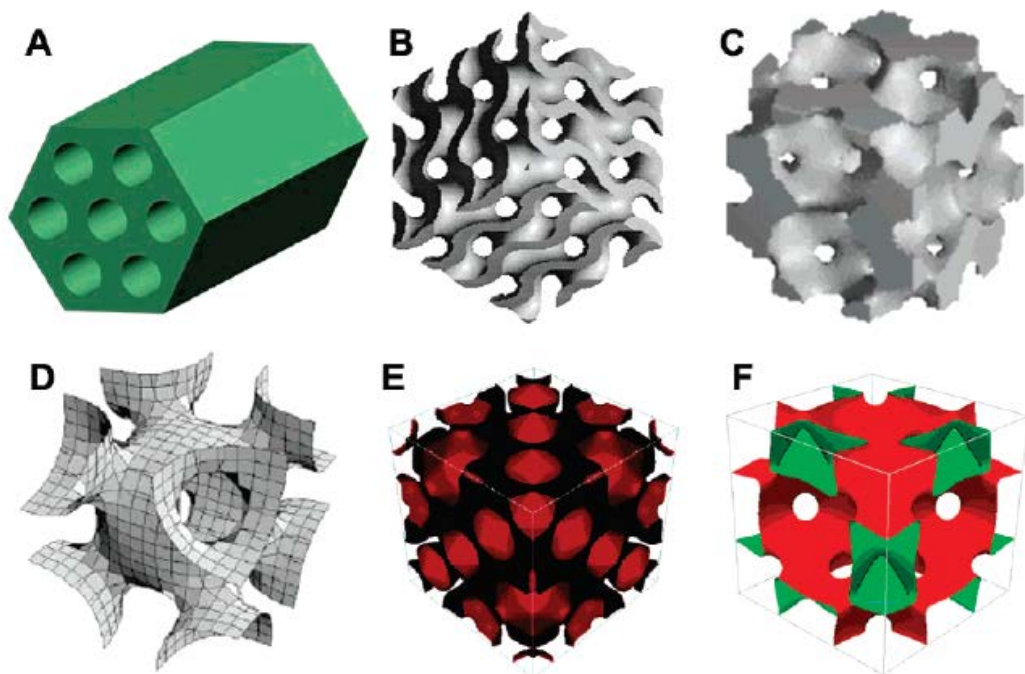


Fig. 9 Periodic mesoporous silica materials: (A) 1-D hexagonal MCM-41 pore arrangement and (B) Bi-continuous pattern in MCM-48 structure. Cubic cage pores assigned to SBA mesoporous materials: (C) SBA-6, (D) SBA-16 material, and (E) and (F) FDA-2 and FDU-1, respectively, part of class of materials from Fudan University. The symmetry of these six materials are as follows: (A) $p6mm$, (B) $Ia3d$, (C) $Pm3n$, (D) $Im3m$, (E) $Fd3m$, and (F) $Fm3m$. Other less predominant mesoporous materials can be classified into these six symmetry elements. Reprinted with permission from Wan and Zhao.²²⁶

3.1 Synthetic Methods for Support Materials

Ordered porous support synthetic strategies employ different methods depending on the type of structure needed and the composition of the support.^{1,4,55,61,65,69,77,108,223,260} The ordered porous structures can be broken into their various geometric shapes, with hexagonal pore arrangements the most studied to bi-continuous cubic as the least. In addition, laminar 2-D materials have gained research attention from the ability to carefully place desired active species for various reactions. Mesoporous periodic silica continues to be heavily studied with hexagonal pore arrays because of the relative ease compared to cubic materials, such as bi-continuous phase. Carbon supports studied thus far extensively have included carbon nanotubes (CNTs), 2-D GE materials, and hard-template carbon (CMK-3). Within periodic mesoporous silica, the sol-gel synthetic route has been applied the most from the relative ease of synthesis when using supramolecular templates. The micelles formed in aqueous acidic or basic solutions as a structure directing groups, which upon calcination lead to an ordered array of pores. Ordered carbon involves multiple methods for forming CNTs using chemical vapor deposition (CVD) onto catalyst substrate to initiate

the growth of multiwall and single-wall CNTs. Two-dimensional GE materials use exfoliation technique to split the graphite into nanosheets of GE. This technique requires strong acids and catalysts to form GE with functional groups resulting in GO.

The other periodic carbon synthetic method applied includes using a hard silica template infiltrated with carbon precursor, followed by a high heating temperature in nitrogen to form an inverse of the periodic silica template upon removal of the silica structure using either hydrogen fluoride (HF) or strong base, such as sodium hydroxide (NaOH). The hard template method can produce relatively complex carbon inverses, such as CMK-3. These synthesis strategies for periodic silica and carbon can also be applied to other metal oxide supports. TiO₂ has been hard template with Si-SBA-15 to form the inverse hexagonal structure of the silica host. Likewise, Al₂O₃ has been synthesized into porous membranes using hard template hosts, such as silica. These many synthetic methods for developing periodic materials open an avenue to increase diffusion and mass-transfer in water purification as adsorbents. Table 7 highlights synthetic methods used for producing ordered porous supports with active metal oxides in catalytic reactions. A few of the synthetic methods used for producing ordered porous supports shown in Table 7 include evaporation-induced self-assembly (EISA),²⁶¹⁻²⁶⁹ soft-template,²⁷⁰ hydrothermal (HTS),^{216,235,271-282} sol-gel,^{203,218,235,241,269,271-272,274-275,278-288} and hard-template.^{203,269,278-280,282} Synthetic methods results with EISA show macroporous periodic Al₂O₃ in the Fig. 10 TEM image. Likewise, large loading of KIT-6 periodic silica using the sol-gel synthesis method reveal excellent order from the TEM analysis in Fig. 11. Typically, periodic macroporous MgO is unheard, but, with the EISA synthetic protocol, the periodic MgO material was able to be developed as shown in Fig. 12. The final synthetic method that has become quite useful is hard templating. Infiltrating carbon precursor followed by pyrolysis a periodic carbon replicate was formed, which provided an avenue to impregnate Fe₂O₃ within the pore channels shown in Fig. 13 TEM results. Overall, EISA and hard templating have made major progress in permitting obtaining periodic metal oxides not thought possible previously.

Table 7 Synthesis of ordered porous supports containing metal oxides in catalysis

Support(s)	Metal oxide type	Synthesis type	Reaction time (h)	Reaction temperature (°C)	Reactant concentration	Reference
Al ₂ O ₃	NiO	EISA	5 rxn, 48 evaporation	60	2.0 g P123 nonionic polymer; 200 proof ethanol; aluminum isopropoxide; Ni(NO ₃) ₂ ·6H ₂ O	261
	TiO ₂	EISA	5 rxn, 48 evaporation	60	P123 nonionic copolymer; 200 proof ethanol; aluminum isopropoxide; and titanium isopropoxide: HNO ₃	262
	NiO, MgO, Fe ₂ O ₃ , Cr ₂ O ₃ , CuO, CeO ₂ , LaO ₃ , Yb ₂ O ₃ , CaO, and SnO ₂	EISA	4 rxn, 48 evaporation	60	P123 nonionic copolymer; 200 proof ethanol; aluminum isopropoxide, AlCl ₃ , or Al(NO ₃) ₃ ; dopant metal salts: Ni(NO ₃) ₃ ·6H ₂ O, NiCl ₂ ·6H ₂ O; Mg(NO ₃) ₂ ·6H ₂ O, Fe(NO ₃) ₃ ·9H ₂ O, FeCl ₃ ; CrCl ₃ ; Cu(NO ₃) ₂ ·3H ₂ O and CuCl ₂ ·2H ₂ O; CeCl ₃ ·3H ₂ O, LaCl ₃ ·6H ₂ O; YCl ₃ ·6H ₂ O; Ca(NO ₃) ₂ ·4H ₂ O; and SnCl ₄	263
	TiO ₂	EISA	4 rxn, 48 evaporation	60	P123 nonionic copolymer; 200 proof ethanol; Aluminum isopropoxide; and titanium isopropoxide: HNO ₃	264
	PdO	EISA	5 rxn and evaporation	60	P123 nonionic copolymer; 200 proof ethanol; Aluminum isopropoxide; Nitric acid; Pd(NH ₂) ₄ (NO ₃) ₂	265
	NiO V ₂ O ₅	EISA	5 rxn, 48 evaporation	60	P123 nonionic copolymer; 200 proof ethanol; Aluminum isopropoxide; Nitric acid; Ni(NO ₃) ₂ ·6H ₂ O, and V(AcAc) ₄	266
	PdO, In ₂ O ₃	EISA	2 rxn, 24 evaporation, Aging	40 evaporation, aged 65	F127 nonionic copolymer; ethanol; acetic acid; HCl; Aluminum butoxide; PdCl ₂ and In(NO ₃) ₃ ·xH ₂ O	267
	Ag, Au, Pd, and Pt	Soft-Template	NA	RT (Ambient)	F127 nonionic copolymer; poly(methyl methacrylate), (PMMA) polymer spheres; DI water; ethanol; Al(NO ₃) ₃ ·9H ₂ O and Ce(NO ₃) ₃ ·6H ₂ O; AgNO ₃ , HAuCl ₄ , PdCl ₂ , and H ₂ PtCl ₆ , and NaBH ₄	270
	Fe(OH) ₃	HTS	10	140	NaAlO ₂ , urea, polyacrylic acid sodium salt, deionized (DI water, and FeCl ₃	216

Table 7 Synthesis of ordered porous supports containing metal oxides in catalysis (continued)

Support(s)	Metal oxide type	Synthesis type	Reaction time (h)	Reaction temperature (°C)	Reactant concentration	Reference
SiO ₂	Fe ₂ O ₃	Sol-gel, HTS	2-3 days	80	TEOS, CTAB, NaOH, FeCl ₃ , and DI water	271
	Fe ₂ O ₃ , CuO, Nb ₂ O ₅ , V ₂ O ₅ , and MoO ₃	HTS and RT (Stober)	48 total, 24 h with pH adjustment, 24 h final	100, RT (ambient)	Ethanol, CTAC, DI water, TEOS, Al ₂ (SO ₄) ₃ , Cu(C ₂ H ₅ O ₂) ₂ , Fe(NO ₃) ₃ , V(SO ₄) ₂ , Nb ₂ (C ₂ O ₄) ₅ , NH ₄ MoO ₃ , H ₂ SO ₄ (dilute, pH adjustment), NaOH, NH ₄ OH.	272
	Cr ₂ O ₃ , MnO, Fe ₂ O ₃ , Co ₃ O ₄ , NiO, CuO, ZnO, CdO, SnO ₂ , and In ₂ O ₃	EISA	18 aged, 18 heating	25, 60	P123 non-ionic copolymer, HCl, TEOS, Cr(NO ₃) ₃ , Mn(NO ₃) ₂ , Fe(NO ₃) ₃ , Co(NO ₃) ₂ , Ni(NO ₃) ₂ , Cu(NO ₃) ₂ , Zn(NO ₃) ₂ , Cd(NO ₃) ₂ , SnCl ₂ , and In(NO ₃) ₃ .	268
	ZnO	Sol-gel, HTS	20 aged, 24, Total 44 h	35, 100	P123, DI water, TEOS, HCl, and [CH ₃ ZnOCH ₂ CH ₂ OCH ₃] _x	283
	MnO _x	HTS	24 h, 24h, Total 48 h	40, and 100	P123, DI water, TEOS, HCl, and Mn(C ₂ H ₅ O ₂) ₂	273
	TiO ₂ , Fe ₂ O ₃	Sol-gel, RT	2 h stir, 12 h age	25	TEOS, T(OEt) ₄ , 2-propanol, CTAB, NH ₄ OH, Fe(NO ₃) ₃ ·9H ₂ O	284
	Fe ₂ O ₃ , Clay	Sol-gel, HTS	48 h total	100	P123, HCl, DI water, Fe(NO ₃) ₃	235
	MnO _x	Sol-gel, HTS	44 h total	100	P123, HCl, DI water, Mn(NO ₃) ₂	285
	CuO	Sol-gel, HTS	24 aged, 24, Total: 48 h	35, 100	P123, DI water, TEOS, HCl, butanol, and Cu(NO ₃) ₂ ·3H ₂ O	274

Table 7 Synthesis of ordered porous supports containing metal oxides in catalysis (continued)

Support(s)	Metal oxide type	Synthesis type	Reaction time (h)	Reaction temperature (°C)	Reactant concentration	Reference
	NiO CoO _x	Sol-gel, HTS	20 aged, 24, Total: 44 h	35, 100	P123, DI water, TEOS, HCl, and Ni(NO ₃) ₂ ·6H ₂ O, Co(NO ₃) ₂ ·6H ₂ O	285
	ZrO ₂	HTS, Sol-gel	47 h total; 23 h stir period, 24 h aging period	40, and 100	P123 nonionic copolymer, HCl, ZrC ₁₀ H ₁₀ Cl ₂	275
	SnO ₂ , In ₂ O ₃ , PtO/Pt	RT/HTS	8 h RT, 15 h HTS	45, and 80	P123, HCl, DI water, TEOS, SnCl ₄ , In(NO ₃) ₃ , and H ₂ PtCl ₄ .	276
	ZnO, CuO, and Fe ₂ O ₃	HTS	24 rxn,	80	NH ₄ OH, CTAC, TMAOH, TMA Si, FeCl ₂ , FeCl ₃ , ZnCl ₂ , CuCl, CuCl ₂ , Zn(NO ₃) ₂ , Cu(NO ₃) ₂ , Fe(NO ₃) ₃ , ZnSO ₄ , CuSO ₄ , FeSO ₄ , Fe ₂ (SO ₄) ₃ , ZnCO ₃ , CuCO ₃ , Fe ₂ (CO ₃) ₃	277
	Fe ₂ O ₃	Sol-gel/ Surfactant	24 rxn	Guess, 100, Look up cited refs, on synthesis	P123, non-ionic copolymer, ethanol, HCl, CTAB, and Fe(NO ₃) ₃ ·9H ₂ O.	218
	Fe ₂ O ₃ , Al ₂ O ₃ , ZnO, CuO, NiO, ZrO ₂ , CeO ₂ , and CdO	Sol-gel/HTS	48 h total, 24 h, 24 h	35, and 60	P123, nonionic copolymer, DI water, HCl, TEOS, H ₂ SO ₄ , TMCS/toluene, Fe(NO ₃) ₃ , Al(NO ₃) ₃ , Zn(NO ₃) ₂ , Cu(NO ₃) ₂ , Ni(NO ₃) ₂ , Zr(NO ₃) ₂ , Ce(NO ₃) ₃ , and Cd(NO ₃) ₂	286
	Fe ₂ O ₃	Sol-gel, RT	1 h	60	Brij 56 nonionic copolymer, TMOS, ethanol, HCl, DI water; Check Ref.	287
	ZnO	Sol-gel, RT	16 h	RT	Zn(NO ₃) ₂ , TEOS, polyvinylpyrrolidone/styrene, HCl, methanol, ethanol.	288
TiO ₂	Fe ₂ O ₃	Sol-gel	36 h	RT	P123, ethanol, TiPP, Fe(NO ₃) ₃ , DI water, NH ₄ OH	241

Table 7 Synthesis of ordered porous supports containing metal oxides in catalysis (continued)

Support(s)	Metal oxide type	Synthesis type	Reaction time (h)	Reaction temperature (°C)	Reactant concentration	Reference
	CeO ₂	Sol-gel; Hard-template, EISA	31 h total	140 hard-SiO ₂ template; 40 evaporation; 65 aging.	Hard silica template: F127, TMB, KCl, TEOS, DI water, H ₂ O ₂ , HNO ₃ ; Ti(OBu) ₄ , and Ce(NO ₃) ₂	269
CeO ₂	CuO	Sol-gel, HTS, Hard-template	48 h	35 aging, 100 aging	P123, HCl, DI water, butanol, TEOS: (KIT-6 silica hard template); Ce(NO ₃) ₂ , and Cu(NO ₃) ₂ for impregnation of KIT-6; NaOH used to removal KIT after impregnation	278
	CuO	Sol-gel, HTS, Hard-template	48 h	35 aging, 100 aging	P123, HCl, DI water, butanol, TEOS: (KIT-6 silica hard template); Ce(NO ₃) ₃ , and Cu(NO ₃) ₂ for impregnation of KIT-6; NaOH used to removal KIT after impregnation	279
	CuO	Sol-gel, HTS, Hard-template	48 h	100	P123, HCl, DI water, TEOS, PVA (SBA-15 synthesis); Ce(NO ₃) ₃ , and Cu(NO ₃) ₂ for impregnation of KIT-6; NaOH used to removal KIT after impregnation	280
Carbon	MgO	Sol-gel, HTS,	36 h	80, 100, and 160	RHASS, P123, sucrose, sulfuric acid, HCl, DI water, Mg(NO ₃) ₂ , and NaOH; Note: RHASS: Rice husk ash silica solution.	281
	Fe ₂ O ₃	Sol-gel, EISA, hard-template; impregnation	27 h, 24 h template removal, 5 h calcination; 12 h functionalize	70, 80, 100	F127, TEOS, phenol, formalin, NaOH, HCl, ethanol, DI water, (NH ₄) ₂ S ₂ O ₈ , Fe(NO ₃) ₃ ·9H ₂ O	203
	NiO, CuO, Pt, CoO, Fe ₂ O ₃	Sol-gel, HTS, hard-template	48 h template; 18 h impregnation	100, and 160	P123, TEOS, sucrose, H ₂ PtCl ₆ , metallocene (Ni, Co, Fe, and Cu); H ₂ SO ₄ , HCl, and HF	282

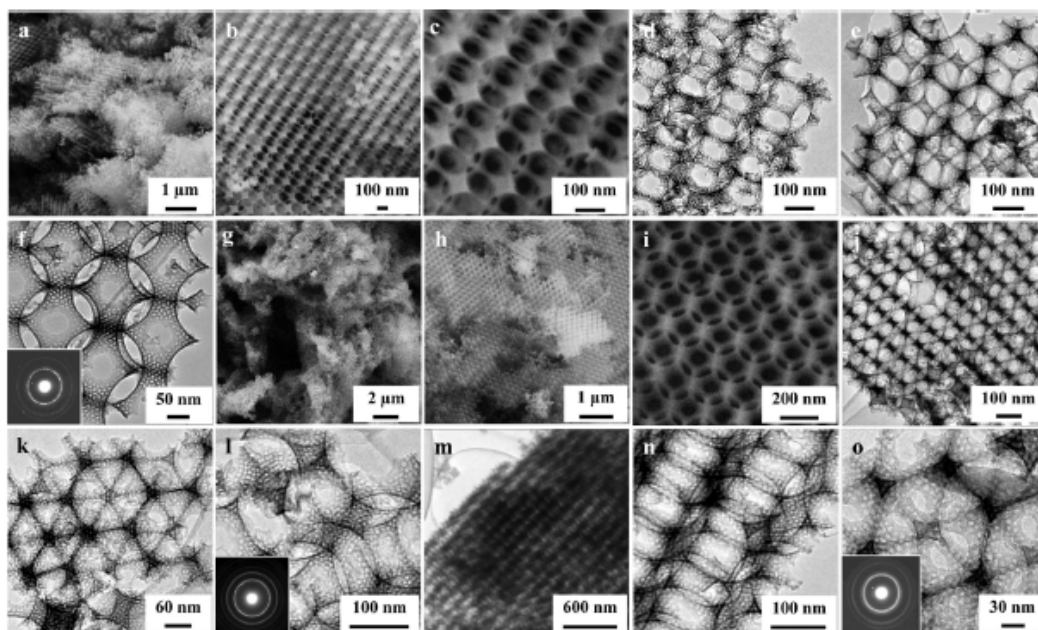


Fig. 10 Periodic Al_2O_3 using PMMA spheres in soft-template synthesis. HR-SEM and TEM with insets of selected area (electron) diffraction (SAED) patterns show the different structures depending on the Al source used holding the PMMA and nonionic F127 surfactant constant. (a–f) Using aluminum nitrate in 95% ethanol; (g–l) using aluminum isopropoxide in 95% ethanol- HNO_3 solution; and the (m–o) without Al precursor of only 95% ethanol-HCl solution. Reprinted with permission from Li et al.²⁸⁹

High resolution (HR)-SEM and TEM images suggest that the Al source has an impact on the level of periodicity resulting, but the Al structures are consistent with the structure without Al. Clearly, this suggests that the combination of PMMA spheres and use of an evaporation step similar to the EISA lead to highly ordered materials.

Overall, the results in Fig. 11 infer that high loading of 10 wt% can be placed in KIT-6 host without transformation of the bi-continuous cubic phase.

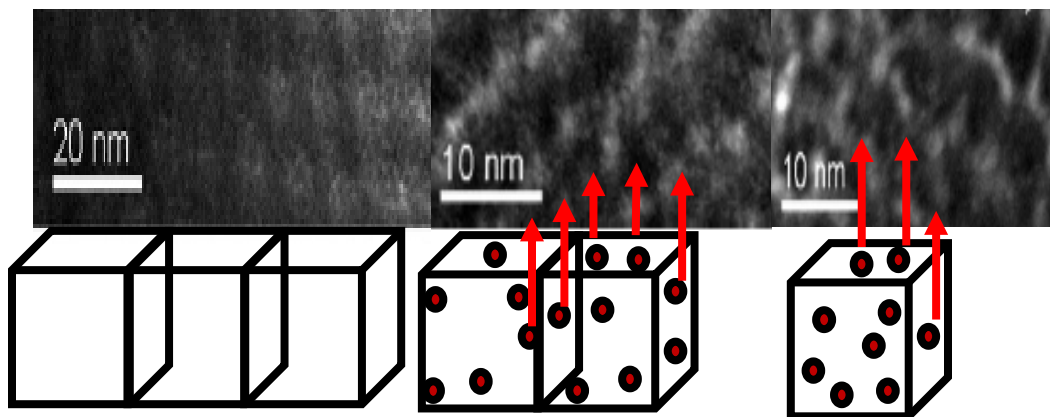


Fig. 11 TEM image of Fe-KIT-6 at 10 wt% loading with cartoon images of the cubic structure with and without iron(III) oxide nanoparticles: far left (a), center (b), and far right (c). Consistent with the bi-continuous gyroidal cubic space group Ia3d in the family of MCM-48 structures; the KIT-6 structure has larger pores than the MCM-48 structure, but it shares the same Ia3d space group. Data modified from Li.²¹⁸

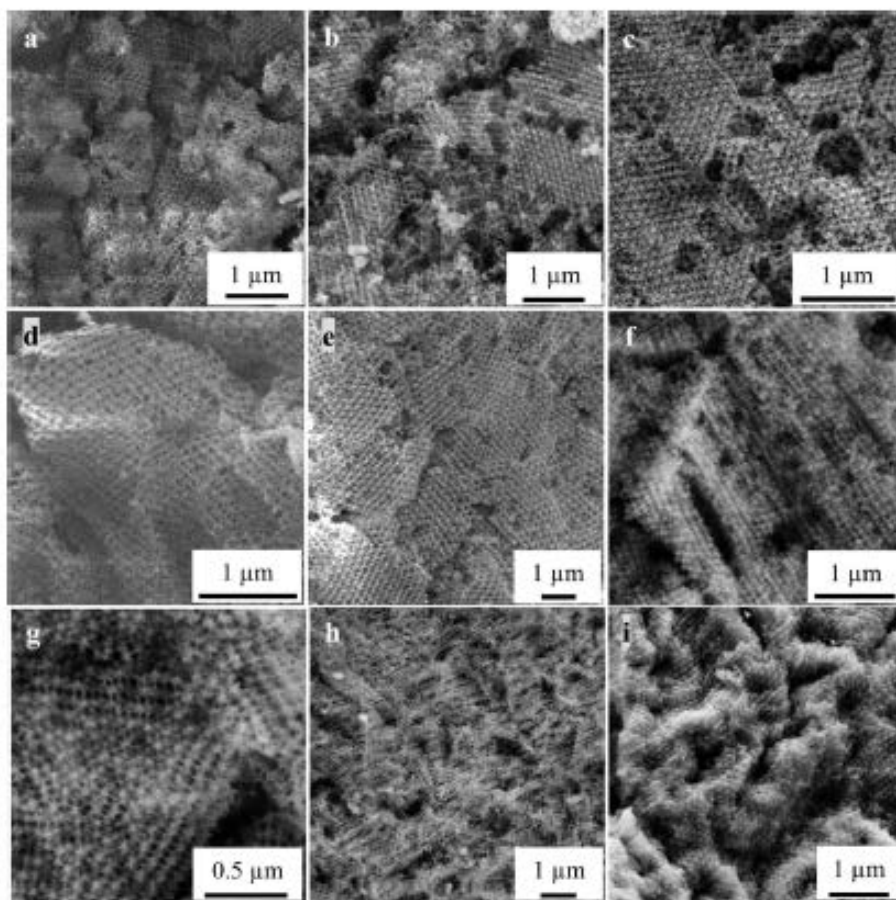


Fig. 12 HR-SEM image of periodic macroporous MgO. (a) only PMMA; (b) PMMA with 95% ethanol solution; (c) and (d) PMMA with F127 in an aqueous solution; (f) and (g) PMMA with F127 contained in 40% ethanol media; (h) PMMA with F127 in 50% ethanol; and (i) PMMA and F127 contained within a 95% ethanol solution. Reprinted with permission from Li et al.²⁸⁹

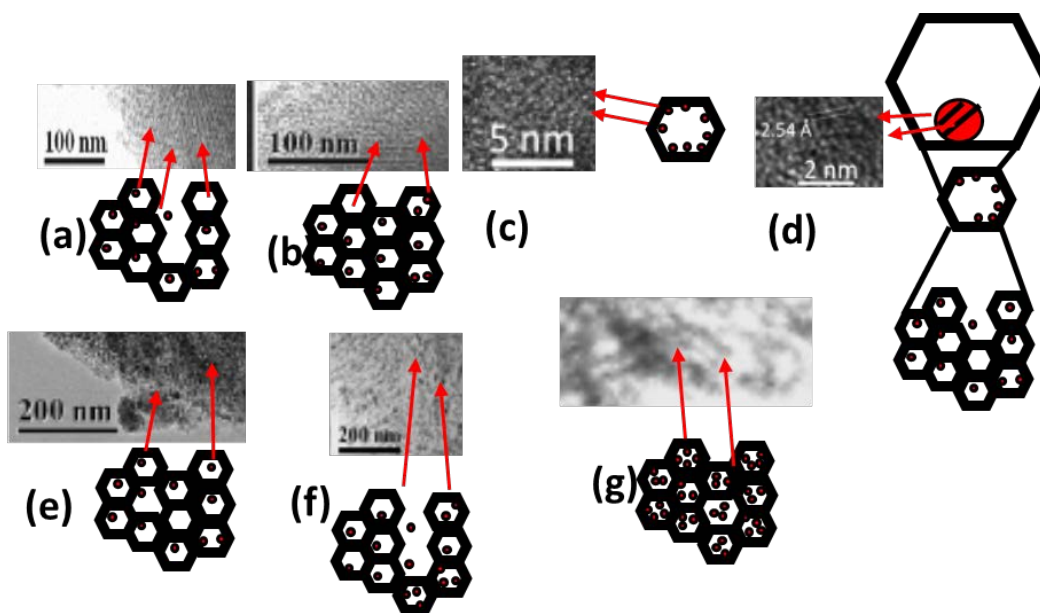


Fig. 13 TEM image of Fe_2O_3 in CMK-3 carbon pore channels. (a, b, e, f) TEM images; (c and e) SAED patterns; (c and d) HR-TEM images, and (g) DF-STEM image. (a–d) pyrolysis at 300 °C, (e) 500 °C, and (f, g) 600 °C. Data modified from Wu et al.²⁰³

3.2 Modified Water Treatment

3.2.1 Synthesis-Modification

Organic adsorbent supports are being used increasingly for filtration of water as membranes, as represented in many review articles in Table 1. Among the many advantages of organic membranes, the major highly important outcomes include low cost, ability to tune pore geometry, ability to adjust degree of hydrophobicity or hydrophilicity of the pore walls easily, and ability to tailor the polymer membranes to desired thickness depending the wastewater composition.^{37,39,41–42,55,58–59,62–64,171,290–291} Plastic scrap, including bottles and cartons, has been converted into polymer membrane materials using the electro-spun method for removal of bacteria in filtration of water.²⁹² In addition, using the electro-spun method coupled with appropriate plasma treatment forms desired distribution of surface functional groups. Therefore, plastic polymer scrap could be potentially converted into membranes in water treatment applications, depending on the treatment method. Polymer membranes can also be functionalized with different groups, such as with block copolymers or surfactants to tune the pore walls, depending on the actual water remediation task.⁶³ Likewise, the use of layer-by-layer (LBL) strategy can be incorporated into developing scrap plastic polymer films of different thicknesses and compositions, which further infer the potential of organic supports as adsorbents and filtration devices.

The standard carbon-based water treatment adsorbent has used carbon black because of its relative ease in synthesis and resulting low cost; however, recent research continues to focus on the merits of CNTs from their selective binding sites, which provides the ability to tune the adsorption process as function of binding interactions.³⁹ The CNT adsorbent has the advantage of repulsive to attractive forces of different bonding energy, such as hydrophobic with little to no hydroxyl (OH) defect groups on the pore walls, electron-donating ability from aromatic π - π , weaker hydrogen electrostatic binding, stronger covalent shared bonding, and van der Waals electrostatic forces. These five different binding interactions with different energy magnitudes provide a wealth of opportunities for using CNTs as an ideal adsorbent. In addition, the CNTs have large surface areas that have been shown to increase uptake of various pollutants, such as heavy metal cations, organic contaminants, and biological aqueous waste. Finally, the major challenge for novel carbon supports continues to be the reduction in the cost of synthesizing compared with activated carbon; nonetheless, CNTs materials have binding interactions, textural properties, and uniformity of pores as significant advantages beyond the initial cost of production.

Other carbon-based nanomaterials include GE and GO. Similar to CNTs, the binding interactions can be tuned as desired. Further, the increased surface area and ability to add hydrophilic surface functional groups (OH) provide an avenue to place metal oxides on the surface of the hybrid GO nanomaterial.⁶⁵ The result of forming a hybrid nanomaterial provides the opportunity to have mixtures of pollutants common in wastewater, such as heavy metals, organics, and biological aqueous waste. In addition, the surface functionalization with hydrophilic groups leads to higher uptake cationic and anionic species, such as heavy metal ions and anionic organic entities. The GO can be unrolled to form 2-D graphene nanosheets (GNs). The GNs have the advantage of adsorption occur in 2-D with pore arrangements as secondary issue common in 3-D materials. In summary, the major challenge for novel materials, such as GE, GO, and GNs, has been the relatively high cost of production; however, the advantages of being able to conduct adsorption in 2-D may eventually overcome the cost advantage of activated carbon.

In light of the cost challenges of carbon-based materials, other carbonaceous materials have been developed using biochar from the pyrolysis or gasification of biomaterials.⁶⁹ Biochar has the major advantage of being porous like other nanomaterials, with low-cost production similar to activated carbon. Biochar has hydrophilic character similar to GO from the incorporation of surface hydroxyl groups. In addition, the biochar has the positive attributes of carbon materials with the five binding methods present in CNTs. Even more so, biochar's low cost

provides an avenue to act as a nonregenerative adsorbent with heavy metals concentrated, followed by using the filled biochar as fuel in electricity generation. The lack of a need for regenerating the adsorbent could lead to reduced cost in water purification and added benefit of electricity. Likewise, biochar has the ability incorporate metal oxide species similar to CNTs, GE, GO, and GNs, but at a much lower cost. The many benefits of biochar, coupled with significantly lower production compared to other carbon nanomaterials, suggests that biochar may be the vehicle toward low-cost carbon material in water treatment.

The major challenge for biochar widespread use in water remediation includes developing relatively uniform arrangement of pores instead of activated carbon that has aperiodic pore arrays. In summary, carbon-based adsorbents continue to make major advances in water treatment technology, and carbon hybrid inorganics may take the advantages each nanomaterial to develop the ultimate water purification device.

3.2.2 Modified Characterization

The main techniques for characterizing modified materials like carbon include the ones listed in Table 2.

3.2.3 Modified Reactions

3.2.3.1 Organics

Many organic compounds have been evaluated with metal oxides placed onto the carbon hosts. The reactions, however, require ozone to break down the organic aqueous pollutants. The advantage of carbon supports includes the ability to tune large textural properties noted in Table 6 and related functional groups attached to the surface of the pores. Likewise, MnO₂ was attached to reduced graphene oxide (rGO) containing numerous C-OH bonds using ozone for 4-nitrophenol led to much higher breakdown rate compared to MnO₂ alone without the carbon support.²⁴⁴ Instead of confining the MnO₂ species within the pores, the firm attachment of the MnO₂ entities onto the rGO led to increase charge carrier transfer and separation, thereby providing the means to increased breakdown of the recalcitrant 4-nitrophenol. Similarly, MnO_x clusters have been placed on coconut shell activated carbon (CSAC) using a hydrothermal synthetic method, which produced highly dispersed MnO_x clusters on the carbon support.²⁴³ These highly dispersed MnO_x clusters on the carbon support provided the platform for breaking down azo dye molecules into various products. The challenge for the MnO_x-loaded carbon support materials includes preventing leaching of the active phase, and the azo dye molecules' degradation is a function of the pH value.

Lower pH values favored higher degradation rates, but the MnO_x species on the CSAC support does not have the stability present on a metal oxide support, which was apparent with the number of cycles leading to decreased catalytic activity. The lack of stability appears to be one of the most difficult challenges to overcome with metal oxide-loaded carbon support materials. Another method for placing metal oxides onto carbon-supported materials seems to be the solution, or the type of carbon geometry also might be an alternate means for developing nano-cavities much like mesopores common in periodic mesoporous silica.

Researchers have been experimenting with using carbon derivatives, such as peanut shell char,²⁹³ sewage sludge char,²⁴⁵ and multi-wall CNTs (MWCNTs).²⁴² The resulting peanut shell char impregnated with $\alpha\text{-Fe}_2\text{O}_3$ (hematite) into random porous structure was up to 12 times more effective than the active carbon prepared material, and this outcome infers that the location and dispersion of the Fe(III) oxides in fact influence positively.²⁹³ In addition, these researchers indicated that the activated carbon and wood fly ash metal oxide loaded materials had increased propanal oxidation rates when combined with water vapor, which may be from hydroxylating the surface of the other two supports. A hydrophilic support could be favorable toward propanal oxidation, depending on the level of initial hydroxylation character. Likewise, sewage sludge char has iron oxide species contained within this material.²⁴⁵ From the iron oxide species within the sewage sludge char, the ability to convert an azo dye denoted as acid orange II (AOII) was linked to the location of the iron oxide species. The stability of the iron oxide species was inferred by the repeated reactions showing similar activity; in contrast, the wood chip char loaded iron oxide material had lower degradation activity with repeated cycling of the dye degradation reactions. The use of MWCNTs for impregnating MnO_x species led to the outcome of increased degradation of antibacterial agent ciprofloxacin, with retention of the Mn species within the support.²⁴² Proof of the recyclability was done for the MnO_x -loaded MWCNTs material for five reactions, with similar degradation outcomes. Therefore, the type of pore geometry plays a major role in retaining the active metal oxide species under reaction conditions, as illustrated in this study. Moreover, the ability to have the metal oxide species with the pores of the material provide an avenue to form nano-reactors where hydroxyl radical species can form at a rapid rate, so the ideal support material has the active phase contained within the pores.

3.2.3.2 Micro-Pollutants

This area using carbon supports has not been heavily evaluated thus far. The single study evaluated MnO_x on MWCNTs in a semi-batch process, with ozone forming the reactive oxygen species hydroxyl radical.²⁴² The micro-pollutant

studied was ciprofloxacin (cip) antibacterial pollutant in wastewater. The cip solution could be broken down almost to innocuous products after 15 min of contact time with the $\text{MnO}_x/\text{MWCNTs}$, and the efficiency of ozone dose per the amount of pollutant was greater using the modified manganese oxide with carbon support. The stability of the MnO_x was also validated by reusing the catalyst five consecutive times with little to no loss in catalytic activity. This study reveals the benefits of having heterogeneous catalyst coupled in a homogeneous oxidant. Table 8 compares the other materials for other organic pollutants.

Table 8 Mn, Fe, and metal oxides in aqueous organics water treatment

Catalyst composition	Active metal oxide/support composition	Catalyst/s support surface area (m ² /g)	Water treatment evaluation	Pollutant(s) composition	Contact time	Reaction temperature/ reaction pH	Reactive oxygen species (ROS)	Reaction product(s)	Reaction rates/rate constants	Regeneration cycles/removal efficiency (%)/mg/g	Isotherm model	Ref.
MnO _x : MnO ₂	MnO _x /Al ₂ O ₃ MnO _x /SBA-15	119 650	Batch	Atrazine and Linuron	30 min	298 ± 1.5 K/6.5	·OH	ND	0.0155 ± 0.004 L kg- 1 s-1 0.123 ± 0.004 L kg- 1 s-1	ND	ND	233
MnO _x : MnO ₂	MnO ₂ /Al ₂ O ₃	ND	Batch	o-dichro- benzene (o- DCB)	7 min	773 K	ND	CO ₂ + H ₂ O	ND	1/100	ND	234
MnO _x : Mn ₂ O ₃ , Mn ₃ O ₄ , and MnO ₂	MnO _x /Al ₂ O ₃	ND	Batch	2,4-dichloro- phenoxy acetic acid (2, 4-D)	10 min	293 K/6.5	O ₂ ⁻ , HO ₂ [·]	ND	ND	1/70	ND	229
MnO _x : Mn ₃ O ₄ , Mn ₂ O ₃ , and MnO ₂	MnO _x /SBA-15	560.7	Semi-batch	Oxalic acid	60 min	298 K/3.7	·OH	ND	ND	1/84.6 2/83.5 3/83.1 4/82.6	ND	230
MnO _x : Mn ₃ O ₄ , Mn ₂ O ₃ , and MnO ₂	MnO _x /SBA-15	416.5	Batch	Butyl paraben (BPB)	175 min	298 ± 2 K/6.5 ± 2	SO ₄ ⁻ , ·OH	CO ₂ + H ₂ O	ND	1/100 2/100 3/100 4/100 5/100 6/100	ND	231
MnO _x : Mn ₃ O ₄ , and MnO ₂	MnO _x /Al ₂ O ₃ /TiO ₂	105.3	Batch	4- chlorophenol (4-CP)	10 min	293 K ± 1 K/6.57	·OH	ND	ND	1/69.4	ND	240
MnO _x : Mn ₂ O ₃ , and MnO ₂	MnO _x /ZrO ₂	232	Batch	2,4-dichloro- phenoxy- acetic acid (2,4-D)	40 min	293 K/3.7	·OH	Phenol 2-hydroxy- propanoic acid Glycolic acid Oxalic acid Glycerin	ND	1/82	ND	239

Table 8 Mn, Fe, and metal oxides in aqueous organics water treatment (continued)

Catalyst composition	Active metal oxide/support composition	Catalyst/s support surface area (m ² /g)	Water treatment evaluation	Pollutant(s) composition	Contact time	Reaction temperature/ reaction pH	Reactive oxygen species (ROS)	Reaction product(s)	Reaction rates/rate constants	Regeneration cycles/removal efficiency (%)/mg/g	Isotherm model	Ref.
MnO _x : MnO ₂	MnO _x /CeO ₂	74.9	Semi-Batch	Sulfosalicylic acid	30 min	ND/3.5, 6.5, and 9.5	·OH	Tartaric acid Oxalic acid Malic acid Acetic acid Succinic acid	ND	1/100 2/100 3/100 4/100 5/100 6/100	ND	238
MnO _x : MnO ₂	MnO ₂ /Diatomite (Clay)	17.0	Batch	Methylene blue	120 min	208 K/2, 3, 4, and 5	·OH	ND	ND	1/92.4 2/80 3/75 4/65	Langmuir	249
MnO _x	MnO _x /MWCNT	114.9	Semi-Batch	Ciprofloxacin	15 min	293 K/6.5, and 7.1	·OH	ND	ND	1/85	ND	242
MnO _x : Mn ₃ O ₄ , and MnO ₂ , Mn ₂ O ₃	MnO _x /CSAC	504.5	Batch	C.I. acid red 73	10 min	298 K/3, 4, 5, 6, and 7	·OH	Propionic acid Butyric acid Pentanoic acids Phthalic acid 4-(diphenyldiazenyl) phenol	ND	1/100 2/99.5 3/99 4/99 5/98 6/97.8 7/97.5 8/97.5 9/97.3 10/97 11/97 12/96.5 13/96 14/95.8 15/95.5 16/95 17/95 18/94 19/93 20/92	Langmuir	243

Table 8 Mn, Fe, and metal oxides in aqueous organics water treatment (continued)

Catalyst composition	Active metal oxide/support composition	Catalyst/s support surface area (m ² /g)	Water treatment evaluation	Pollutant(s) composition	Contact time	Reaction temperature/ reaction pH	Reactive oxygen species (ROS)	Reaction product(s)	Reaction rates/rate constants	Regeneration cycles/removal efficiency (%)/mg/g	Isotherm model	Ref.
MnO _x : MnO ₂	MnO _x /rGO	35.2	Semi-Batch	4-nitrophenol	30 min	298 K/ND	O ₂ ⁻ , ¹ O ₂	ND	1 order/0.123 min ⁻¹	1/80 2/80 3/80	ND	244
Fe ₃ O ₄	Fe ₃ O ₄ /Al ₂ O ₃ Fe ₃ O ₄ /SiO ₂	103.6 205.2	Batch	2,4-dichloro- phenoxy- acetic acid; p- chloro- benzoic acid	40 min	293 K/6.0	·OH	ND	ND	1/80 1/66	ND	232
Fe ₃ O ₄	Fe ₃ O ₄ /Bio-Char	19	Batch	Acid Orange II	180 min	303 K/4.0 ± 0.1	·OH	ND	Pseudo 1 order/22.45 E-3 min ⁻¹	1/90	ND	245
Fe ₂ O ₃	Fe ₂ O ₃ /SiO ₂	270	Continuous fixed bed reactor	Phenol	8 h	353 K/2.7	ND	ND	ND	1/65	ND	235
Fe ₂ O ₃	Fe ₂ O ₃ /SBA-15	294	Batch	Phenol	ND	353 K-393 K/3.0-3.3	HO ₂ [·]	Phenol Catechol Hydroquinone Maleic acid Acetic acid Oxalic acid	ND	1/25-35	ND	236
Fe ₂ O ₃	MgO@Fe ₂ O ₃ /KIT-6	327.6	Batch	Imidacloprid	2.5 h	298 K/ND	ND	ND	1 order apparent/1.4 ± 0.31 h ⁻¹	1/90 2/90 3/90	ND	237
Fe ₂ O ₃	Fe ₂ O ₃ /Al ₂ O ₃ @SBA-15	ND	Semi-batch	Ibuprofen	60 min	293 K/7	·OH, O ₂ ⁻	2-hydroxyl- propanoic acid Glycolic acid Malonic acid 3-hydroxy- hexanedioic acid p-hydroxybenzoic acid	ND	1/90 2/89 3/85 4/85 5/87 6/85	ND	317

Table 8 Mn, Fe, and metal oxides in aqueous organics water treatment (continued)

Catalyst composition	Active metal oxide/support composition	Catalyst/s support surface area (m ² /g)	Water treatment evaluation	Pollutant(s) composition	Contact time	Reaction temperature/ reaction pH	Reactive oxygen species (ROS)	Reaction product(s)	Reaction rates/rate constants	Regeneration cycles/removal efficiency (%)/mg/g	Isotherm model	Ref.
Fe ₂ O ₃	Fe ₂ O ₃ /TiO ₂	101.1	Batch	4-chlorophenol	180 min	303 K/ND	·OH	ND	ND	1/100 2/100 3/100	ND	241
Fe/Ni	Fe/Ni/clay (bentonite)	6.0	Batch	Amoxicillin	60 min	290-308 K/4-11	·OH	Amoxicillin penicilloic acid	ND	1/94	ND	246
Fe-Ni-Al	Fe-Ni-Al/clay (montmorillonite)	207.2	Batch	Orange acid II	180	333 K/3.0	ND	ND	ND	1/72.3 2/65.3 3/60.2	ND	247
AlSi ₂ Fe ₆	AlSi ₂ Fe ₆ /clay (allophane)	287	Batch	Atrazine	8 h	298 ± 1 K/3, 4, and 6	·OH	Desethyl-atrazine (DEA) desethyl-desisopropyl (DEIA)	1 order apparent 8.08 × 10 ⁻³ min ⁻¹	1/100	ND	248

Note: Not Determined, ND

3.2.3.3 Heavy Metals

Heavy metal removal has been evaluated with metal oxides placed on carbon, polymers, and biopolymers, and the results are shown in Table 5. The main two metal oxides studied are Fe_2O_3 and MnO_x on these carbon-based supports. The removal efficiency is higher for polymers compared to carbons, which may be from the type of functional groups within a given polymer. The ability to have large uptake of a given heavy metal is related to the metal oxide surface area and the support. Amorphous MnO_2 on polymer had the largest uptake of Pb(II) cations.²¹⁰ Additional studies with MnO_2 on a polymer suggest that Ti(I) , Cd(II) , and Cu(II) can be effectively removed.^{207,211} Hydrate iron oxide contained within polystyrene polymer has been studied for Cu(II) uptake, with close to 60% removal from solution at neutral pH values.²⁰⁷ However, with addition of a competing cation like calcium (Ca(II)), the Cu(II) adsorption decreases from approximately 100% removal at zero Ca to 40%–50% removal amount with a Ca cation, which can be ascribed to the charge and ionic radii. The ionic radii value is 0.87 Å for Cu(II) , and the ionic radii is 0.69 Å in Fe(III) . Moreover, the ionic radii for Ca(II) is 1.14 Å, so the dissimilar atomic radii implies that the Cu^{2+} cation can be influenced negatively by the competing Ca^{2+} ion.

This may be from the competition between the Ca^{2+} and the polymer sulfone sidechain's ability to facilitate binding the Cu^{2+} ion. In the absence of the Ca ion, the distribution coefficient (K_d) was 928 L/g. When switching from polystyrene to sodium alginate biopolymer, the result was lower Cu(II) adsorption even with Fe_3O_4 nanoparticles within the host biopolymer.²⁰⁹ Pb removal efficiency with a polystyrene backbone and hydrate iron oxide had a removal efficiency of 100% with no competing ions, such as Ca^{2+} .²⁰⁷ Upon addition of a Ca(II)/Pb(II) molar ratio of 80, the removal efficiency had decreased to approximately 80%, which was not as severe as Cd(II) or Cu(II) removal. Nonetheless, the K_d had decreased from 1063 to 6.1 L/g with the addition of a 80 molar ratio of Ca. The later the K_d value means greater adsorption and retention of the Pb(II) cation. In a follow-up work, these researchers show that the sidechains on the macroporous polystyrene zirconium phosphate nanoparticles have the largest uptake of Pb^{2+} with S-containing sidechains in the composite hybrid material.²¹² The S-containing sidechain polystyrene composite material had close to 7 meq/g at 550 mg/L concentration of Pb(II) and 1000 mg/L of competing Ca^{2+} ion. Incorporation of Fe_3O_4 onto sodium alginate biopolymer led to at 99.8% reduction in Pb^{2+} ion loading over simple use of the biopolymer of 84.5% Pb^{2+} removal efficiency.²⁰⁹ Therefore, the iron oxide assists in the binding of the Pb(II) ion from the surface defects present on the nanoparticle surface. With the use of zero-valent Fe on

commercial polystyrene resin, further research showed that depending on the pH, Fe loading, and sidechains, the removal of Pb(II) and nitrate anion could occur simultaneously.²⁰⁸ This research work shows that Pb can be converted to Pb(0) and reduction of nitrate, but how to remove the Pb is a future research work. Instead of using iron oxide, researchers have used hydrated MnO_x on polystyrene and obtained a large amount, up to 395-mg Pb/g, of sorbent.²⁰⁹ The research with MnO_x on polymers reveals the potential of using other metal oxides instead of iron oxide.

4. Inorganic Supports Water Treatment

4.1 Synthesis of Inorganic Supports

The synthesis of metal oxides can be broken down into iron and non-iron oxides. A few non-iron oxides that potentially have use in water remediation include Al₂O₃, CeO_x, magnesia, titania, copper oxide, cobalt oxide, manganese oxides, and ZnO.⁷⁷⁻⁷⁸ In addition, chromium and ruthenium oxides have been evaluated for water purification; nonetheless, these transition metal oxides are toxic, which suggests little to no actual use in water purification devices.⁷⁸ There are many avenues to developing metal oxides, but the most used method involves sol-gel synthesis, which may be from the relative ease of synthetic conditions.⁷⁷ Other synthetic methods in forming metal oxides include plasma using air or oxygen, and supercritical water similar to hydrothermal synthesis.²⁹⁴⁻²⁹⁶ In addition, there are other metal oxide synthetic preparations that are gaining attention, such as hydrothermal, microwave-hydrothermal, microwave-plasma, supercritical drying using low- and high-temperature processing, and room-temperature prepared metal oxides also called xerogels.^{295,297-305} The placement of metal oxides on supports evolves either two synthetic methods—post-impregnation or in-situ.

Post-impregnation leads to metal oxides on the support; in contrast, the in-situ synthetic can lead to the incorporation into the metal species and respective oxide known as framework or isomorphous substitution. The benefit of in-situ synthesis also provides an avenue to higher dispersion of the metal oxides on (in) the support structure. Likewise, higher dispersion of the metal oxides leads to greater catalytic activity. The synthetic methods that provide the best dispersion of metal oxides include sol-gel with xerogels having the least dispersed metal oxides within the support material. The other synthetic methods fall between sol-gel and xerogel prepared metal oxide supported materials. Synthetic methods, such as microwave, continue to gain attention from the relative ease of synthesis and rapid production. The challenge for these relatively new synthetic methods, such as microwave and others, is having similar or better catalytic characteristics, such

as textural properties, with the lowest amount of energy input. The sol-gel synthetic method requires relatively low energy input, but this synthesis method can take longer compared to the typical microwave with exception of the Stöber silica sol-gel method. Finally, the best way to determine the optimal metal oxide synthetic protocol involves determining what desired catalytic properties are needed.

Placing metal oxides in ordered host materials opens avenues for increased diffusion of reactions and products, which enhances mass-transfer of bulky aqueous pollutants common in mixed waste streams.¹⁰⁸ The increased mass-transfer occurs for inorganic supports and carbon-based nanomaterials, and the challenge for various supports is even dispersion of active sites throughout the nanomaterials because few synthetic methods have been shown to evenly disperse the active metal centers onto the porous host materials. The random dispersion of metal oxide species can be ordered to a small extent using molecular designed dispersion (MDD) with bulky ligands.^{306–310} Reaction rates typically increase with highly dispersed metal oxides to increase the number of interactions with the reactants to form products. In contrast, aperiodic supports, such as activated carbon, lead to reduced dispersion assuming comparable surface areas with periodic supports, and the results lead to fewer active site interactions. Fewer catalytic interactions or less turn-over-frequency (TOF) will directly lead to fewer products. Therefore, adsorbents or supports that have active metal oxide centers need to be highly dispersed, and periodic silica and carbon provide an avenue to high dispersion. Furthermore, the pore wall chemistry, metal precursor type, and metal loading also play major roles in forming highly dispersed metal oxides. In silica, the types of silanol groups have major effect on the distribution of metal precursor. The metal source and related ligands or counter-ions also assist in determining the minimal distance between metal oxide centers. Finally, higher metal loadings lead to lower dispersion because there is only a set surface area; above the saturation limit of the given support, the resulting metal precursor agglomerates in larger metal oxide clusters.

4.2 Inorganic Supports Characterization

The analytical techniques employed for characterizing supported metal oxides depends on the metal oxide and support used, and these primary techniques are briefly noted in Table 2. However, a few characterization techniques are employed for most supported metal oxides, such as powder XRD, nitrogen physisorption, UV-Vis DRS, Raman, XPS, TEM, SEM, and chemisorption techniques.^{5,65,108–110,225–226,260,294–296,300,311–315}

The limitation for powder XRD is the crystallite size of 3 nm or greater for detection.^{108–110} For materials comprising nanoparticles smaller than 10 nm, powder XRD may not be able to determine the given structure.³¹⁶ Nonetheless, powder XRD is a primary technique for delineated the structure and crystallinity with framework (isomorphous) substitution determined with *d*-spacing increase changes. Therefore, powder XRD analysis is one of the major analytical methods for characterization especially for metal oxide supported materials, such as silica and Al₂O₃ where isomorphous substitution can occur depending the on ionic radii of dopant ion.

Nitrogen physisorption is a complementary technique with textural properties obtained and type or porous structure elucidated.^{112–115} The importance of textural properties relates many instances to catalytic activity, so textural properties for supported materials are quite important especially in catalytic reactions. The coordination of metal clusters or a single-ion catalytic site can be determined by the peak position and broadness using UV-Vis DRS analysis.^{109–110,313} The advantage of UV-Vis DRS is its relatively simple ease of use and nondestructive nature.^{117–119} An additional advantage of UV-Vis DRS is the excellent sensitivity of this analytical technique.¹¹⁶

In contrast to UV-Vis DRS analysis, Raman is a surface sensitive technique with higher detection limits.¹²¹ For larger supported metal oxides on supports, such as silica and Al₂O₃, Raman can be helpful in determining the types of agglomerated oxides, but for single-site supported oxides Raman analysis will not provide definitive results or qualitative outcomes.¹²²

XPS provides details on the intercore electron configuration as opposed to probing the valence shell commonly with spectroscopic tools, such as UV-Vis-DRS.¹²³ The slight changes in the movement of the core electrons directly can be monitored by chemical shifts. These chemical shifts are influenced by the oxidation and geometric arrangement of atoms on a support. The chemical shifts are determined by the kinetic energy of the injected electrons from the into the XPS instrument, which are related to the binding energy of electrons in the neutral atoms and work function of the material.¹²⁴

In addition to probing the electronic properties with XPS, TEM, and SEM are complementary techniques for observing the morphology of supported metal oxides.⁵⁸ Typically, the TEM can reveal the external pore arrangement of channels, such as with hexagonal Si-MCM-41 support.^{108–109} Likewise, SEM can provide the type of particles from spherical to rod-shaped and others.¹²⁷

Chemisorption techniques, such as H₂-TPR, oxygen pulse and carbon monoxide pulse titration, H₂-TPD, and TPO, provide global understanding of the supported

metal oxide catalyst. These techniques complement the previous techniques described previously. The major challenge for chemisorption techniques has been the need for large amounts of catalyst of typically 10–200 mg and sensitive limit of 0.8 wt%.^{121,131}

These characterization methods briefly described are the major techniques for evaluating heterogeneous catalysts, and several characterization techniques are employed to gain a global understanding of a given catalyst.

4.3 Inorganic Supports Reactions

4.3.1 Organics

Organic aqueous pollutants have been evaluated using iron, manganese, and a few other metal oxides. Upon placing the Fe(III) oxide species onto a Al₂O₃-coated periodic large-pore hexagonal mesoporous silica host denoted as Al₂O₃-SBA-15, complete mineralization was obtained.³¹⁷ These researchers discovered that the reason for the increased activity was from the Lewis acidity obtained by placing Al₂O₃ onto the silica host, followed by adding Fe₂O₃. Both the Al₂O₃ and Fe(III) oxide jointly cause ozone to break apart and form highly reactive oxygen species in aqueous media. This work demonstrates the positive aspects of employing a support. Likewise, MgO-loaded Fe₂O₃-KIT-6 mesoporous cubic silica material employed in a Fenton reaction with H₂O₂ led to higher conversion values than in homogeneous phase when studying an insecticide imidacloprid degradation, which was noted from the addition of Fe(III) oxide with MgO.²³⁷ The increased reaction rate infers that Lewis acidity may be one of the reasons in addition of the dispersion of the Fe₂O₃ and MgO species onto the large-pore bi-continuous cubic mesoporous silica support (KIT-6). Phenol degradation follows a similar trend with higher conversion rates compared to homogeneous Fenton reaction when using Fe₂O₃/SBA-15 material.²³⁶ The challenge with supported metal oxides, such as Fe₂O₃ and MnO_x, is leaching of the active phase. The active species leach at an elevated rate with increased H₂O₂ concentration. However, Fe₂O₃/Al₂O₃-SBA-15 does not appear to have the leaching challenges faced with simple Fe₂O₃ on a support, which infers that Al₂O₃ binding is the key to preventing leaching from occurring.³¹⁷

Other supports, in addition to the active metal oxide species, play a major role in the ability to break down organics. Employing MnO_x onto mesoporous CeO₂ provided an avenue to attach a majority of the MnO_x species within the pores by using a capping agent when impregnating with the Mn salt solution.²³⁸ Having the active metal oxide species within the pores resulted in reduced MnO_x leaching from the CeO₂ support. Moreover, the MnO_x species within the pores provided

the means to form oxygen radical species from ozone. This ability to form oxygen radical species was realized by forming confined MnO_x species within the pores—nano-vessels or containers. An approach to using supported metal oxide species in water remediation involves using clays, porous materials that are not heavily studied. Clays use a pillar or post construction to form different pore geometries as opposed to typical zeolite construction or mesoporous materials fabrication.¹⁰⁸ Allophane clays have been evaluated in Fenton reaction under heterogeneous conditions.²⁴⁸

Employing the $\text{Fe}^{2+}/\text{Fe}^{3+}$ species on the clay led to close to complete mineralization of atrazine pesticide, with an acidic reaction pH under eight reaction periods. These researchers noted that the pH value was critical for producing the needed hydroxyl radical, which was shown with reaction completed at pH of 6. The Fe(II/III) species are, on the surface, the clay's construction, so the activity is reduced from forming ideal nano-cavities. The high reaction rate can be linked to the low Fe loading of 1 wt% or lower for this class of materials. Likewise, applying Al_2O_3 to clay material led to increased catalytic stability, which was shown by repeated reaction with orange acid II azo dye.²⁴⁷ The breakdown of the azo dye used the chemical oxygen demand (COD) parameter; this use of clay support compared to active carbon led to an approximately 72% reduction in COD, with Fe-loaded activated carbon giving 83% COD reduction. The activated carbon material had an approximate reduction of 25% of iron oxide species (5.79 ppm), starting with 2 wt% iron oxide loading initially. Employing mixed Fe-Ni nanoparticles within clay material, almost 94% of antibacterial amoxicillin was broken down occurring after 1 h. The dispersion and stability on the clay support showed to be good, which infers the need for both highly dispersed metal oxides contained within a material to slow or stop leaching from occurring. A proposed mechanism using various oxidation states of manganese oxides on periodic hexagonal silica SBA-15 with ozone for the removal of oxalic acid is shown in Fig. 14. Clearly, the three and four oxidation states are the most noted in the mechanism in Fig. 14, and further review in Table 8 shows that the active manganese oxide states are III and IV. Few research studies directly focus on the KMnO_4 compound, even though this material had d^0 orbital. The empty d orbital favors nucleophiles common in wastewater, such as aromatic ring structure compounds.

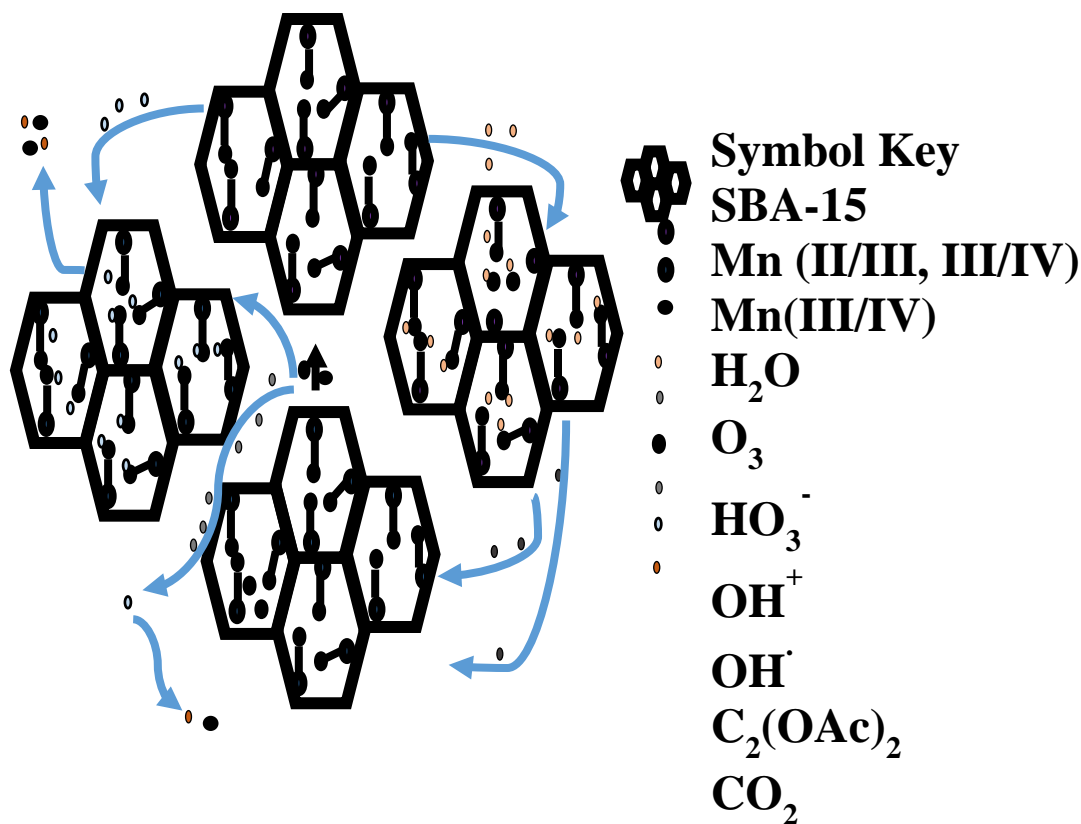


Fig. 14 Ozone mechanism of oxidation that occurs with MnO_x/SBA-15 with the probe molecule oxalic acid. Data modified from Sun et al.²³³

The initial step after forming the heterogeneous catalyst splitting water into hydroxide and proton in the upper portion of the mechanism. The ozone binds through electrostatic and hydrogen bonds to the positively charged hydroxyl group attached to the Mn cation. The third step includes the ozone lone pair of electron extracting the proton from the surface hydroxyl on the Mn cation to form HO₃⁻, which attacks the oxalic acid in solution phase resulting in CO₂ and water. Two other portions of the mechanism include the Mn(III/IV) surface hydroxyl group dissociating to form hydroxyl radical attacks on the oxalic acid, and the final portion includes oxalic acid binding through electrostatic interactions to the surface of Mn(III/IV) followed by being attacked by hydroxyl radical, thereby forming CO₂ and H₂O. The key portions of this mechanism are the Mn oxidation state and ozone binding to the MnO_x.

4.3.2 Micro-Pollutants

Two studies have been completed with heterogeneous catalysts and homogeneous oxidant, as listed in Table 8. Amoxicillin was exposed to Fe/Ni-clay (bentonite) with nZVI.²⁴⁵ The amoxicillin was broken down into secondary products after

60-min contact time from the tertiary nitrogen interacting with the small nZVI. Also, nZVI has been shown to breakdown many halogenated organics, which implies that nZVI might be an excellent reductant. Fe₂O₃/Al₂O₃ at SBA-15 heterogeneous catalyst was applied with ozone to break down ibuprofen.³¹⁷ The Al₂O₃ coating on the large-pore hexagonal SBA-15 structure was shown to be critical for converting ozone to ·OH and O₂⁻ radicals. These radicals were pivotal in the partial mineralization of ibuprofen with a 60-min contact time. These two studies show the potential of bringing a heterogeneous catalyst exposed to homogenous reductant or oxidant, as shown in Table 8. The Fe₂O₃/Al₂O₃ at SBA-15 catalyst was evaluated six times with no deactivation because of leaching, which infers excellent stability of the active metal oxide.

4.3.3 Heavy Metals

Supported iron oxide and manganese oxides have been evaluated for adsorption and removal of heavy metal ions, such as As,^{204–205,212–213,220,222} Cd,^{207,209,220,222} Cr,^{202,209,222,318} Cu,^{207,209,221–222} Zn,^{220,222} Pb,^{207–210,212,222,318} tin,^{220,222} Ni,^{209,220,222} Co,^{209,220} silver (Ag),²²⁰ and tantalum.^{211,220} Iron oxide has been placed on various supports, such as carbon, polymer, metal oxides, and clays. Figure 15 shows the typical adsorption isotherms of As on periodic mesoporous KIT-6 loaded with Fe₂O₃. Different modes of adsorption are possible depending on the homogeneity and dispersion of the Fe₂O₃ in KIT-6. Figure 16 shows the adsorption isotherms using two different adsorption models with As(V) as the model heavy metal cation.

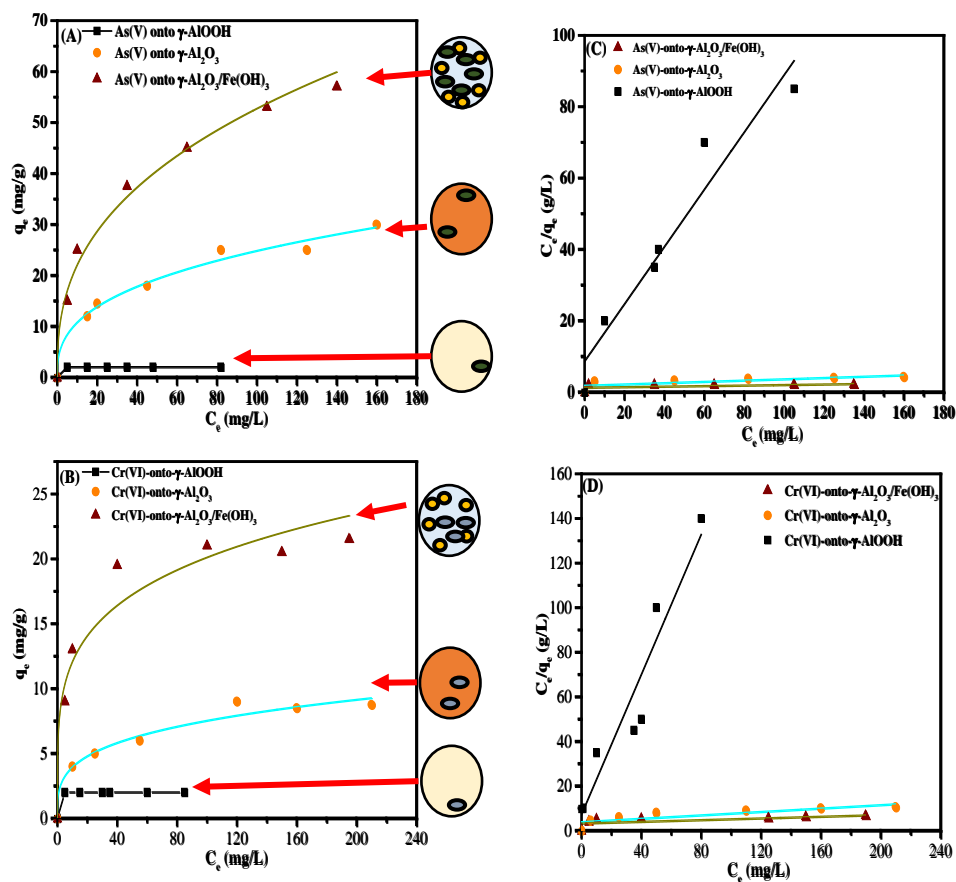


Fig. 15 Adsorption isotherms of As(V) and Cr(VI) using three materials: (a) the amount adsorbed at equilibrium (q_e) of As (V) comparing $\gamma\text{-Al}_2\text{O}_3/\text{Fe}(\text{OH})_3$ with $\gamma\text{-Al}_2\text{O}_3$ and $\gamma\text{-AlOOH}$; (b) the Cr(VI) uptake with $\gamma\text{-Al}_2\text{O}_3/\text{Fe}(\text{OH})_3$, $\gamma\text{-Al}_2\text{O}_3$, and $\gamma\text{-AlOOH}$; (c) and (d) the ratio of concentration equilibrium by adsorbed heavy metal equilibrium concentration. Data modified from Zhang et al.²¹⁶

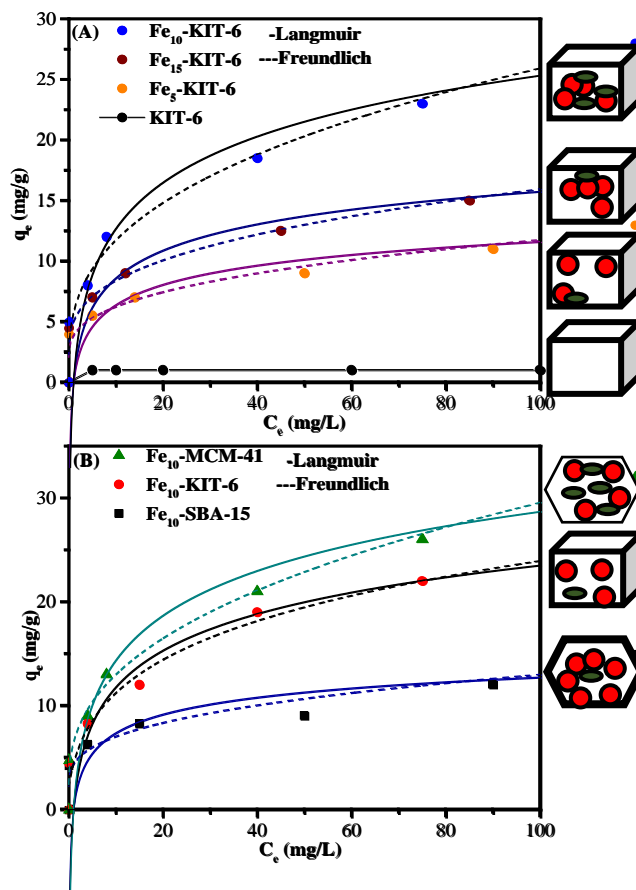


Fig. 16 Adsorption isotherms using two different adsorption models with As(V) as the model heavy metal cation. The bold lines are Langmuir monolayer adsorption model, and the dotted lines are the Freundlich model that takes into the account the heterogeneity of the active sites on a support. Data modified from Li.²¹⁸

Clearly, the Freundlich model appears to be a better fit for all three periodic mesoporous supports: small hexagonal pore MCM-41, large bi-continuous cubic pore KIT-6, and large hexagonal pore SBA-15. In Fig. 16a, the higher Fe loading starting from zero to 10 wt% show that more Fe(III) oxide favors greater uptake of As(V) cation. In addition, the different supports will have different geometries, which will also affect the adsorption modes, as seen Fig. 16b. The effects of using different supports varied depending on the heavy metal cation studied for adsorption and removal in wastewater. The two main oxidation states of As are III and V.

A study evaluated As(III) with doped coupled oxidation of Fe_3O_4 , thereby changing the surface chemistry, and the research outcomes implied As ion could be adsorbed and removed from the MnO_x -doped Fe_3O_4 nanoparticles.²²⁰ Likewise, producing aluminum oxide ($\gamma\text{-Al}_2\text{O}_3$) as a support with nanoflower

geometry embedded with iron hydroxide favored large uptake of the As(V) cation.²¹⁶ It is suggested that the coupling of γ -Al₂O₃ with Fe(OH)₃ imparts the increased adsorption of the As(V) cation because of the larger number of surface sites and greater nitrogen textural properties. Figure 15a shows the isotherms as function of type of the Al₂O₃ phase, and Fe(III) hydroxide with the As(V) cation. Figure 15b shows the Cr(VI) uptake also as function of the Al₂O₃ phase and incorporation of Fe(OH)₃. In Fig. 15a and b, the γ -Al₂O₃/Fe(OH)₃ materials has the largest uptake of heavy metal cations, which is reflected in the linearized plots in Fig. 15c and d. Overall, the adsorption isotherms support the argument that support structure, phase, support type, and loading of active phase produce the highest uptake of heavy metal cations. Similar to other adsorbents studied with relatively homogeneous adsorption sites, the γ -Al₂O₃-Fe(OH)₃ hybrid material follows Langmuir monolayer coverage, and the adsorption is 61.99 mg/g, which is attributed to the structural geometry of the support because neither Al₂O₃ or Fe(OH)₃ alone obtain such large monolayer adsorption. The clays supporting iron oxide and aluminum oxide have been evaluated for various heavy metal cations, such as As(III), and the results suggest that modifying the clay support increases the ability to uptake heavy metal cations.²²²

Plots in Fig. 15a and b suggest that As(V) uptake is greater with γ -Al₂O₃/Fe(OH)₃ compared with Cr(VI). Plots in Fig. 15c and d reflect that the phase of Al₂O₃ is critical for high adsorption of heavy metal As(V) and Cr(VI) cations. Clearly, the γ -Al₂O₃/Fe(OH)₃ has the largest uptake of over 60 mg As(V)/g support, and the γ -Al₂O₃/Fe(OH)₃ also has the highest uptake of the three compared materials with 24 mg Cr(VI)/g support. These plots infer that the monolayer Langmuir fit models best the interaction between the active adsorption sites contained on these supports.

The challenge with clay supports are the cost and very small textural properties that have been shown to be imperative for adsorption of heavy metal cations. If and when clay materials can be produced less expensively and have larger surface areas, then clay may be an idea candidate for adsorption of heavy metal cations in water treatment. Cd adsorption has been completed on polymers and clay-supported metal oxides. Natural polymer supports with iron oxide show increased binding of Cd compared with the natural polymer, which may be for the adsorption of the heavy metal cation onto the surface of the iron oxide nanoparticle.²⁰⁹

Cr has several oxidation states, with III and VI being the most common. Cr(VI) has been shown to be highly toxic, and the major hexavalent Cr species present in wastewater include CrO₄²⁻ (chromate), HCrO₄⁻ (hydrogen chromate), and Cr₂O₇²⁻ (dichromate). The other lower valence Cr species in the three oxidation state,

Cr^{3+} , is of less danger to the environment because of its solubility. Adsorption appears to be the best outcome in removing Cr^{6+} heavy metal cation, considering energy input. In addition, $\gamma\text{-Al}_2\text{O}_3\text{-FeOOH}$ has been employed with nano-flower architecture that had an adsorption of Cr^{6+} : 24.1 mg/g.²¹⁶ Therefore, the active metal oxide must also play a role in the uptake of the heavy metal Cr^{6+} ion solution. The application of a clay support showed that the charge and ionic radii could be major factors in the uptake of a heavy metal cation.²²² The iron oxide modified clay supports had the greatest uptake of Cr^{3+} ion, even with greater concentrations of Cr(III) solution (i.e., 10—70 ppb).

Co(II) bio-accumulates in the environment, so methods of adsorption are needed and used for this heavy metal ion. Incorporating MnO_x onto the surface of iron oxide led to a 94% capture of Co^{2+} and a K_d value of 160 L/g.²²⁰ Clearly, the surface effects are playing a major role in the uptake of the Co^{2+} ion. In the future, more research should focus on placing the MnO_x -coated iron oxide nanoparticles on an inert support. Similar to Co(II) bio-accumulates, Ag(I) can also accumulate; however, very few studies have attempted to study the adsorption of Ag^+ . Addleman and colleagues saw a 99% capture using the optimal 13.7% Mn loading onto the surface of the iron oxide nanoparticles, and the solid phase partition coefficient was 1300 L/g.²²⁰

MnO_x on various supports with high dispersion take advantage of the surface effects, which likely are at work in these two research endeavors.^{211,220} Table 5 summarizes use of Mn, Fe, and supported metal oxides in water treatment. MnO_x on supports showed various isotherms and removal efficiencies depending on the support.^{206,210–211} Ferrates had various removal efficiencies from approximately 88%–100%, which may be from the ability to oxidize and bind to the toxic heavy metal cation in solution.^{199–201} Among the various polymer,^{207–208,212} charcoal,²⁰² periodic silica,^{217–219} Fe(III) hydroxide,^{214–215} Mn-doped Fe_3O_4 ,²²⁰ periodic carbon,^{203–204} carbon,²⁰⁵ biopolymer,²⁰⁹ clay,^{221–222} Al_2O_3 ,²¹⁶ and hybrid metal oxide-polymer materials,²¹³ clearly the Mn-doped Fe_3O_4 had relatively larger adsorption of toxic heavy metal cations in the two oxidation state. Therefore, more emphasis needs to be placed on doping onto iron oxides, for example, to obtain the greatest removal efficiency. In summary, the adsorption of heavy metal ions needs to focus on more innovative routes toward complete removal of multiple ions using real wastewater at various pH values; otherwise, this field of study will not be able to assist the world in preventing major health and environmental disasters.

5. Conclusions

The studies completed on high-valence metal oxides are few, with exception to ferrate(VI) used as a homogenous solution. The advantages of developing advanced materials with high-valence metal oxides on supports was clear with the presentation of the aqueous organics breakdown. The analytical techniques in water purification need to be refined especially in the characterization of the support and dispersion of the metal oxide on the support. This seems to be lacking in most studies with the focus on simple modification of a known material followed by water purification study. To further the field of high-valence metal oxides on supports, the future studies need to carefully evaluate the materials according to well-known standards, such as textural properties, dispersion, and cluster versus single-site active phase.

Clearly, regeneration is not discussed or even considered in homogenous ferrate(VI) remediation. Even when using $\text{Fe}^{2+}/\text{Fe}^{3+}$ on supports, the concept of regeneration and retention of the metal oxide cluster is given little space in the study. Future studies must give thought to the regeneration of the active material or how to prevent leaching from occurring. The barriers to breakdown of aliphatic compounds seem great even with remediation of heavy metal-laden waters. The breakdown of aliphatic compounds will require developing methods for obtaining excess of hydroxyl radicals that potentially begin the attack of a saturated organic structure. Avenues to developing hydroxyl radicals in solution will need metal oxides on a support that cause rapid dissociation of either H_2O_2 to radical species or use of ozone. There has been some work in this direction with pharmaceuticals containing electron-rich aromatic structures, but more studies need to attempt to break down more difficult molecules that do not contain any electron-rich functional groups.

6. Future Outlook and Perspectives

During water remediation, all homogeneous oxidants are consumed, and the regeneration of oxidants is an energy-intensive process. The Fenton process produces hydroxyl radicals, but the needed energy to produce H_2O_2 and form the hydroxyl radical is energy intensive. The challenge for homogeneous oxidants like H_2O_2 is the nonselective nature of this oxidant, thereby requiring extremely large quantities to remove micro-pollutants. Therefore, regenerative materials are needed for widespread device application in treating wastewater. Regenerative materials that retain the textural properties even after completing thermal treatments are needed. Materials that cannot be easily regenerated with thermal

treatment are neither cost effective nor environmental friendly. In other words, the desired life-cycle assessment (LCA) should be quite long because this reduces the cost of water treatment and reduces the environmental impact of producing the oxidant. Metal oxides depending on the geometry have relatively large LCA time values, but carbon-based materials have much lower LCA outcomes, which is one of the major weaknesses that needs to be overcome with organic materials. Many studies lack the concept of how to develop a given material for large-scale water treatment. Most studies only focus on the laboratory benchtop model with little thought or discussion on how the study outcome can be translated to the pilot and industrial water treatment scale. The outlook for high-valence metal oxides suggests much more research in the design of materials is needed for placement of supports. Little to no research focuses on developing materials of high-valence metal oxides systematically using statistics for modeling purposes, which has become common in heterogeneous catalysis. Finally, the majority of studies are conducted in batch process; however, large-scale water treatment needs to evolve to the point of granule and thin films in use of columns similar to heavy metal adsorption studies currently use.

Likewise, homogeneous ferrate(VI) onto a support that could regenerate either using H_2O_2 or ozone initially has great promise in aiding in the endeavor to have potable drinking water. Methods of attaching ferrate(VI) might include changing the support surface to favor attachment of the ferrate(VI), which appears to be the most challenging aspect. If ferrate(VI) can be firmly attached to a surface modified support, it is conceivable, then, that ferrate(VI) could also be regenerated. Nonetheless, these materials challenges are large, and this suggests more research with ferrate(VI) is needed. Research toward this goal has been completed in photocatalytic water purification using Fe-doped TiO_2 , but photocatalytic water treatment suffers from the need for high-intensity UV light, so scaling Fe-doped TiO_2 in water treatment may be challenging. The water research community needs to look for ways to regenerate ferrate(VI) on a support and other higher-valence oxides in the quest to solve water-related public health issues at a reasonable cost. Using materials developed many years ago will not solve the increasing concern and related health issues of micro-pollutants that continue to evolve with time. We must use all appropriate and practical avenues related to materials design to solve the current and future water challenges.

7. References

1. Chen B, Ma Q, Tan C, Lim T-T, Huang L, Zhang H. Carbon-based sorbents with three-dimensional architectures for water remediation. *Small*. 2015;11(27):3319–3336.
2. Church J, Verbyla ME, Lee WH, Randall AA, Amundsen TJ, Zastrow DJ. Dishwashing water recycling system and related water quality standards for military use. *Science of the Total Environment*. 2015;529:275–284.
3. Schwarzenbach RP, Egli T, Hofstetter TB, Gunten Uv, Wehrli B. Global water pollution and human health. *Annual Review of Environment and Resources*. 2010;35(1):109–136.
4. Ali I. New generation adsorbents for water treatment. *Chemical Reviews*. 2012;112(10):5073–5091.
5. Sharma VK, Zboril R, Varma RS. Ferrates: greener oxidants with multimodal action in water treatment technologies. *Accounts of Chemical Research*. 2015;48(2):182–191.
6. Jasim SY, Irabelli A, Yang P, Ahmed S, Schweitzer L. Presence of pharmaceuticals and pesticides in Detroit river water and the effect of ozone on removal. *Ozone: Science & Engineering*. 2006;28(6):415–423.
7. Ikehata K, Naghashkar NJ, Gamal El-Din M. Degradation of aqueous pharmaceuticals by ozonation and advanced oxidation processes: a review. *Ozone: Science & Engineering*. 2006;28(6):353–414.
8. Cabral JPS. Water Microbiology. Bacterial pathogens and water. *International Journal of Environmental Research and Public Health*. 2010;7(10):3657–3703.
9. Azizullah A, Khattak MNK, Richter P, Häder D-P. Water pollution in Pakistan and its impact on public health — a review. *Environment International*. 2011;37(2):479–497.
10. Fawell J, Nieuwenhuijsen MJ. Contaminants in drinking water: Environmental pollution and health. *British Medical Bulletin*. 2003;68(1):199–208.
11. Cairncross S, Hunt C, Boisson S, Bostoen K, Curtis V, Fung IC, Schmidt W-P. Water, sanitation and hygiene for the prevention of diarrhoea. *International Journal of Epidemiology*. 2010;39(suppl 1):i193–i205.

12. Esrey SA, Potash JB, Roberts L, Shiff C. Effects of improved water supply and sanitation on ascariasis, diarrhoea, dracunculiasis, hookworm infection, schistosomiasis, and trachoma. *Bulletin of the World Health Organization*. 1991;69(5):609–621.
13. TB MED 577. Sanitary control and surveillance of field water supplies. Washington (DC): Army (US); 2010 May 1.
14. USAPHC, Non-potable water substitution and reuse in the field. Aberdeen Proving Ground (MD): Army Public Health Command (US); 2011. Information Paper No.: 32-002-0111.
15. Wada Y. Modeling groundwater depletion at regional and global scales: Present state and future prospects. *Surveys in Geophysics*. 2016;37(2):419–451.
16. O'Bannon C, Carr J, Seekell DA, D'Odorico P. Globalization of agricultural pollution due to international trade. *Hydrology Earth System Sciences*. 2014;18(2):503–510.
17. Törnqvist R, Jarsjö J, Karimov B. Health risks from large-scale water pollution: Trends in Central Asia. *Environment International*. 2011;37(2):435–442.
18. Kümmerer K. Significance of antibiotics in the environment. *Journal of Antimicrobial Chemotherapy*. 2003;52(1):5–7.
19. Sharma VK, Anquandah G, Kim H, Jiang J-Q, Zboril R. Ferrate(VI): A green chemistry oxidant for removal of antibiotics in water. In: *Novel solutions to water pollution*. American Chemical Society. 2013;1123:31–44.
20. Careghini A, Mastorgio AF, Saponaro S, Sezenna E. Bisphenol A, nonylphenols, benzophenones, and benzotriazoles in soils, groundwater, surface water, sediments, and food: a review. *Environ Sci Pollut Res*. 2015;22(8):5711–5741.
21. Shomar B, Dare A. Ten key research issues for integrated and sustainable wastewater reuse in the Middle East. *Environ Sci Pollut Res*. 2015;22(8):5699–5710.

22. Gaulke CA, Barton CL, Proffitt S, Tanguay RL, Sharpton TJ, Triclosan exposure is associated with rapid restructuring of the microbiome in adult zebrafish. *PLoS One*. 2016;11(5):e0154632:1–e0154632:20.
23. Tijani JO, Fatoba OO, Babajide OO, Petrik LF. Pharmaceuticals, endocrine disruptors, personal care products, nanomaterials and perfluorinated pollutants: a review. *Environmental Chemistry Letters*. 2016;14(1):27–49.
24. Jiang J, Pang S-Y, Ma J. Oxidation of triclosan by permanganate (Mn(VII)): Importance of ligands and in situ formed manganese oxides. *Environmental Science & Technology*. 2009;43(21):8326–8331.
25. Harman C, Reid M, Thomas KV. In situ calibration of a passive sampling device for selected illicit drugs and their metabolites in wastewater, and subsequent year-long assessment of community drug usage. *Environmental Science & Technology*. 2011;45(13):5676–5682.
26. Burgard DA, Banta-Green C, Field JA. Working upstream: how far can you go with sewage-based drug epidemiology? *Environmental Science & Technology*. 2014;48(3):1362–1368.
27. Rodayan A, Segura PA, Yargeau V. Ozonation of wastewater: Removal and transformation products of drugs of abuse. *Science of the Total Environment*. 2014;487:763–770.
28. Postigo C, Sirtori C, Oller I, Malato S, Maldonado MI, López de Alda M, Barceló D. Photolytic and photocatalytic transformation of methadone in aqueous solutions under solar irradiation: Kinetics, characterization of major intermediate products and toxicity evaluation. *Water Research*. 2011;45(16):4815–4826.
29. Postigo C, Sirtori C, Oller I, Malato S, Maldonado MI, López de Alda M, Barceló D. Solar transformation and photocatalytic treatment of cocaine in water: Kinetics, characterization of major intermediate products and toxicity evaluation. *Applied Catalysis B: Environmental*. 2011;104(1–2):37–48.
30. Boix C, Ibáñez M, Bijlsma L, Sancho JV, Hernández F. Investigation of cannabis biomarkers and transformation products in waters by liquid chromatography coupled to time of flight and triple quadrupole mass spectrometry. *Chemosphere*. 2014;99:64–71.

31. Bijlsma L, Boix C, Niessen WMA, Ibáñez M, Sancho JV, Hernández F. Investigation of degradation products of cocaine and benzoylecgonine in the aquatic environment. *Science of the Total Environment*. 2013;443:200–208.
32. Berg M, Tran HC, Nguyen TC, Pham HV, Schertenleib R, Giger W. Arsenic contamination of groundwater and drinking water in Vietnam: a human health threat. *Environmental Science & Technology*. 2001;35(13):2621–2626.
33. Wang X, Peng B, Tan C, Ma L, Rathinasabapathi B. Recent advances in arsenic bioavailability, transport, and speciation in rice. *Environ Sci Pollut Res*. 2015;22(8):5742–5750.
34. Navas-Acien A, Sharrett AR, Silbergeld EK, Schwartz BS, Nachman KE, Burke TA, Guallar E. Arsenic exposure and cardiovascular disease: A systematic review of the epidemiologic evidence. *American Journal of Epidemiology*. 2005;162(11):1037–1049.
35. Wang JS, Wai CM. Arsenic in drinking water—a global environmental problem. *Journal of Chemical Education*. 2004;81(2):207–212.
36. Brar SK, Verma M, Tyagi RD, Surampalli RY. Engineered nanoparticles in wastewater and wastewater sludge – evidence and impacts. *Waste Management*. 2010;30(3):504–520.
37. Shannon MA, Bohn PW, Elimelech M, Georgiadis JG, Marinas BJ, Mayes AM. Science and technology for water purification in the coming decades. *Nature*. 2008;452(7185):301–310.
38. Martínez-Huitle CA, Rodrigo MA, Sirés I, Scialdone O. Single and coupled electrochemical processes and reactors for the abatement of organic water pollutants: a critical review. *Chemical Reviews*. 2015;115(24):13362–13407.
39. Qu X, Brame J, Li Q, Alvarez PJJ. Nanotechnology for a safe and sustainable water supply: Enabling integrated water treatment and reuse. *Accounts of Chemical Research*. 2013;46(3):834–843.
40. Grafton RQ, Williams J, Jiang Q. Food and water gaps to 2050: preliminary results from the global food and water system (GFWS) platform. *Food Security*. 2015;7(2):209–220.

41. Huang Y, Li J, Chen X, Wang X. Applications of conjugated polymer based composites in wastewater purification. *RSC Advances*. 2014;4(107):62160–62178.
42. Homaeigohar S, Elbahri M. Nanocomposite electrospun nanofiber membranes for environmental remediation. *Materials*. 2014;7(2):1017–1045.
43. Mancosu N, Snyder R, Kyriakakis G, Spano D. Water scarcity and future challenges for food production. *Water*. 2015;7(3):975–992.
44. Gassert F, Luck M, Landis M. Aqueduct water stress projections: decadal projections of water supply and demand using CMIP5 GCMs. Washington (DC): Water Resources Institute; 2015 June. <https://www.wri.org/publication/aqueduct-water-stress-projections-decadal-projections-water-supply-and-demand-using>.
45. Jiang J-Q, Lloyd B. Progress in the development and use of ferrate(VI) salt as an oxidant and coagulant for water and wastewater treatment. *Water Research*. 2002;36(6):1397–1408.
46. Sharma VK. Potassium ferrate(VI): an environmentally friendly oxidant. *Advances in Environmental Research*. 2002;6(2):143–156.
47. Jiang JQ. Research progress in the use of ferrate(VI) for the environmental remediation. *Journal of Hazardous Materials*. 2007;146(3):617–623.
48. Tiwari D, Yang J-K, Lee S-M. Applications of ferrate(VI) in the treatment of wastewaters. *Environmental Engineering Research*. 2005;10(6):269–282.
49. Alsheyab M, Jiang J-Q, Stanford C. On-line production of ferrate with an electrochemical method and its potential application for wastewater treatment – a review. *Journal of Environmental Management*. 2009;90(3):1350–1356.
50. Sharma VK. Oxidation of inorganic contaminants by ferrates (VI, V, and IV)–kinetics and mechanisms: a review. *Journal of Environmental Management*. 2011;92(4):1051–1073.
51. Sharma VK. Ferrate(VI) and ferrate(V) oxidation of organic compounds: kinetics and mechanism. *Coordination Chemistry Reviews*. 2013;257(2):495–510.

52. Jiang J-Q. Advances in the development and application of ferrate(VI) for water and wastewater treatment. *Journal of Chemical Technology & Biotechnology*. 2014;89(2):165–177.
53. Sharma VK, Chen L, Zboril R. Review on high valent FeVI (Ferrate): a sustainable green oxidant in organic chemistry and transformation of pharmaceuticals. *ACS Sustainable Chemistry & Engineering*. 2016;4(1):18–34.
54. Walcarius A, Mercier L. Mesoporous organosilica adsorbents: nanoengineered materials for removal of organic and inorganic pollutants. *Journal of Materials Chemistry*. 2010;20(22):4478–4511.
55. Samiey B, Cheng C-H, Wu J. Organic-inorganic hybrid polymers as adsorbents for removal of heavy metal ions from solutions: a review. *Materials*. 2014;7(2):673–726.
56. White RJ, Brun N, Budarin VL, Clark JH, Titirici M-M. Always look on the “light” side of life: sustainable carbon aerogels. *ChemSusChem*. 2014;7(3):670–689.
57. Xie X, Criddle C, Cui Y. Design and fabrication of bioelectrodes for microbial bioelectrochemical systems. *Energy & Environmental Science*. 2015;8(12):3418–3441.
58. Cahill DG, Freger V, Kwak S-Y. Microscopy and microanalysis of reverse-osmosis and nanofiltration membranes. *MRS Bulletin*. 2008;33(01):27–32.
59. Vainrot N, Eisen MS, Semiat R. Membranes in desalination and water treatment. *MRS Bulletin*. 2008;33(01):16–20.
60. Elma M, Yacou C, Wang DK, Smart S, Diniz da Costa JC. Microporous silica based membranes for desalination. *Water*. 2012;4(3):629–649.
61. Porada S, Zhao R, van der Wal A, Presser V, Biesheuvel PM. Review on the science and technology of water desalination by capacitive deionization. *Progress in Materials Science*. 2013;58(8):1388–1442.
62. Pendergast MM, Hoek EMV. A review of water treatment membrane nanotechnologies. *Energy & Environmental Science*. 2011;4(6):1946–1971.
63. Mehwish N, Kausar A, Siddiq M. Advances in polymer-based nanostructured membranes for water treatment. *Polymer-Plastics Technology and Engineering*. 2014;53(12):1290–1316.

64. Kaur S, Gopal R, Ng WJ, Ramakrishna S, Matsuura T. Next-generation fibrous media for water treatment. *MRS Bulletin*. 2008;33(01):21–26.
65. Wang S, Sun H, Ang HM, Tadé MO. Adsorptive remediation of environmental pollutants using novel graphene-based nanomaterials. *Chemical Engineering Journal*. 2013;226:336–347.
66. Bhatnagar A, Hogland W, Marques M, Sillanpää M. An overview of the modification methods of activated carbon for its water treatment applications. *Chemical Engineering Journal*. 2013;219:499–511.
67. Upadhyay RK, Soin N, Roy SS. Role of graphene/metal oxide composites as photocatalysts, adsorbents and disinfectants in water treatment: a review. *RSC Advances*. 2014;4(8):3823–3851.
68. Hadi P, Xu M, Ning C, Sze Ki Lin C, McKay G. A critical review on preparation, characterization and utilization of sludge-derived activated carbons for wastewater treatment. *Chemical Engineering Journal*. 2015;260:895–906.
69. Shen Y. Chars as carbonaceous adsorbents/catalysts for tar elimination during biomass pyrolysis or gasification. *Renewable and Sustainable Energy Reviews*. 2015;43:281–295.
70. Tripathi PK, Gan L, Liu M, Rao NN. Mesoporous carbon nanomaterials as environmental adsorbents. *Journal of Nanoscience and Nanotechnology*. 2014;14(2):1823–1837.
71. Hartmann M, Kullmann S, Keller H. Wastewater treatment with heterogeneous Fenton-type catalysts based on porous materials. *Journal of Materials Chemistry*. 2010;20(41):9002–9017.
72. Kasprzyk-Hordern B. Chemistry of alumina, reactions in aqueous solution and its application in water treatment. *Advances in Colloid and Interface Science*. 2004;110(1–2):19–48.
73. Wang S, Peng Y. Natural zeolites as effective adsorbents in water and wastewater treatment. *Chemical Engineering Journal*. 2010;156(1):11–24.
74. Chaplin BP, Reinhard M, Schneider WF, Schüth C, Shapley JR, Strathmann TJ, Werth CJ. Critical review of Pd-based catalytic treatment of priority contaminants in water. *Environmental Science & Technology*. 2012;46(7):3655–3670.

75. Najafpour MM, Hołyńska M, Salimi S. Applications of the “nano to bulk” Mn oxides: Mn oxide as a Swiss army knife. *Coordination Chemistry Reviews*. 2015;285:65–75.
76. Kharisov BI, Rasika Dias HV, Kharissova OV, Jimenez-Perez VM, Perez BO, Flores BM. Iron-containing nanomaterials: synthesis, properties, and environmental applications. *RSC Advances*. 2012;2(25):9325–9358.
77. Hua M, Zhang S, Pan B, Zhang W, Lv L, Zhang Q. Heavy metal removal from water/wastewater by nanosized metal oxides: a review. *Journal of Hazardous Materials*. 2012;211–212:317–331.
78. Bokare AD, Choi W. Review of iron-free Fenton-like systems for activating H₂O₂ in advanced oxidation processes. *Journal of Hazardous Materials*. 2014;275:121–135.
79. Trujillo-Reyes J, Peralta-Videa JR, Gardea-Torresdey JL. Supported and unsupported nanomaterials for water and soil remediation: are they a useful solution for worldwide pollution? *Journal of Hazardous Materials*. 2014;280:487–503.
80. Lee SM, Tiwari D. Organo and inorgano-organo-modified clays in the remediation of aqueous solutions: an overview. *Applied Clay Science*. 2012;59–60:84–102.
81. Ribeiro AR, Nunes OC, Pereira MFR, Silva AMT. An overview on the advanced oxidation processes applied for the treatment of water pollutants defined in the recently launched Directive 2013/39/EU. *Environment International*. 2015;75:33–51.
82. Miller EL, Nason SL, Karthikeyan KG, Pedersen JA. Root uptake of pharmaceuticals and personal care product ingredients. *Environmental Science & Technology*. 2016;50(2):525–541.
83. Verlicchi P, Zambello E. Pharmaceuticals and personal care products in untreated and treated sewage sludge: occurrence and environmental risk in the case of application on soil — a critical review. *Science of the Total Environment*. 2015;538:750–767.
84. Wu X, Dodgen LK, Conkle JL, Gan J. Plant uptake of pharmaceutical and personal care products from recycled water and biosolids: a review. *Science of the Total Environment*. 2015;536:655–666.
85. Tang LL, DeNardo MA, Gayathri C, Gil RR, Kanda R, Collins TJ. TAML/H₂O₂ oxidative degradation of metaldehyde: pursuing better water

- treatment for the most persistent pollutants. *Environmental Science & Technology*. 2016;50(10):5261–5268.
86. Choina J, Kosslick H, Fischer C, Flechsig GU, Frunza L, Schulz A. Photocatalytic decomposition of pharmaceutical ibuprofen pollutions in water over titania catalyst. *Applied Catalysis B: Environmental*. 2013;129:589–598.
 87. Tixier C, Singer HP, Oellers S, Müller SR. Occurrence and fate of carbamazepine, clofibrac acid, diclofenac, ibuprofen, ketoprofen, and naproxen in surface waters. *Environmental Science & Technology*. 2003;37(6):1061–1068.
 88. Kümmerer K. Pharmaceuticals in the environment. *Annual Review of Environment and Resources*. 2010;35(1):57–75.
 89. Chakma S, Moholkar VS. Investigations in sono-enzymatic degradation of ibuprofen. *Ultrasonics Sonochemistry*. 2016;29:485–494.
 90. Thompson GW, Ockerman LT, Schreyer JM. Preparation and purification of potassium ferrate VI. *Journal of the American Chemical Society*. 1951;73(3):1379–1381.
 91. Audette RJ, Quail JW. Potassium, rubidium, cesium, and barium ferrates(VI): preparations, infrared spectra, and magnetic susceptibilities. *Inorganic Chemistry*. 1972;11(8):1904–1908.
 92. Wei Y-L, Wang Y-S, Liu C-H. Preparation of potassium ferrate from spent steel pickling liquid. *Metals*. 2015;5(4):1770–1787.
 93. Bouzek K, Lipovská M, Schmidt M, Roušar I, Wragg AA. Electrochemical production of ferrate(VI) using sinusoidal alternating current superimposed on direct current: grey and white cast iron electrodes. *Electrochimica Acta*. 1998;44(4):547–557.
 94. Bouzek K, Schmidt MJ, Wragg AA. Influence of electrolyte composition on current yield during ferrate(VI) production by anodic iron dissolution. *Electrochemistry Communications*. 1999;1(9):370–374.
 95. Lapique F, Valentin G. Direct electrochemical preparation of solid potassium ferrate. *Electrochemistry Communications*. 2002;4(10):764–766.
 96. Ibanez JG, Tellez-Giron M, Alvarez D, Garcia-Pintor E. Laboratory experiments on the electrochemical remediation of the environment. Part 6: Microscale production of ferrate. *Journal of Chemical Education*. 2004;81(2):251–254.

97. Licht S, Yu X. Electrochemical alkaline Fe(VI) water purification and remediation. *Environmental Science & Technology*. 2005;39(20):8071–8076.
98. Yang W, Zhou Y, Wang H, Bi D. Studies on the influence of various experimental conditions on electrochemical generation of ferrate(VI) in NaOH-KOH mixed electrolyte. *Russian Journal of Electrochemistry*. 2009;45(7):795–799.
99. Perez-Sicairos S, Carrillo-Mandujano AJ, Lopez-Lopez JR, Lin-Ho SW. Wastewater treatment via electrochemically generated ferrate and commercial ferrate. *Desalination and Water Treatment*. 2014;52(37-39):6904–6913.
100. Licht S, Naschitz V, Liu B, Ghosh S, Halperin N, Halperin L, Rozen D. Chemical synthesis of battery grade super-iron barium and potassium Fe(VI) ferrate compounds. *Journal of Power Sources*. 2001;99(1–2):7–14.
101. Chris D, Bogatu C, Vlaicu I, Iovi A, Botau D, Ursoiu I. Chlorine dioxide synthesis and its analysis by chemical methods. *Journal of Environmental Protection and Ecology*. 2006;7(1):36–42.
102. Glaze WH. Drinking-water treatment with ozone. *Environmental Science & Technology*. 1987;21(3):224–230.
103. Martínez SB, Pérez-Parra J, Suay R. Use of ozone in wastewater treatment to produce water suitable for irrigation. *Water Resources Management*. 2011;25(9):2109–2124.
104. Campos-Martin JM, Blanco-Brieva G, Fierro JLG. Hydrogen peroxide synthesis: An outlook beyond the anthraquinone process. *Angewandte Chemie International Edition*. 2006;45(42):6962–6984.
105. Martínez-Huitle CA, Brillas E. Electrochemical alternatives for drinking water disinfection. *Angewandte Chemie International Edition*. 2008;47(11):1998–2005.
106. Licht S, Naschitz V, Halperin L, Halperin N, Lin L, Chen J, Ghosh S, Liu, B. Analysis of ferrate(VI) compounds and super-iron Fe(VI) battery cathodes: FTIR, ICP, titrimetric, XRD, UV/VIS, and electrochemical characterization. *Journal of Power Sources*. 2001;101(2):167–176.
107. Westerhoff P, Yoon Y, Snyder S, Wert E. Fate of endocrine-disruptor, pharmaceutical, and personal care product chemicals during simulated

- drinking water treatment processes. *Environmental Science & Technology*. 2005;39(17):6649–6663.
108. Corma A. From microporous to mesoporous molecular sieve materials and their use in catalysis. *Chemical Reviews*. 1997;97(6):2373–2420.
 109. Copéret C, Comas-Vives A, Conley MP, Estes DP, Fedorov A, Mougél V, Nagae H, Núñez-Zarur F, Zhizhko PA. Surface organometallic and coordination chemistry toward single-site heterogeneous catalysts: Strategies, methods, structures, and activities. *Chemical Reviews*. 2016;116(2):323–421.
 110. Weckhuysen BM, Rao RR, Martens J, Schoonheydt RA. Transition metal ions in microporous crystalline aluminophosphates: Isomorphous substitution. *European Journal of Inorganic Chemistry*. 1999;1999(4):565–577.
 111. Langford JI, Daniel L. Powder diffraction. *Reports on Progress in Physics*. 1996;59(2):131–234.
 112. Ng E-P, Mintova S. Nanoporous materials with enhanced hydrophilicity and high water sorption capacity. *Microporous and Mesoporous Materials*. 2008;114(1–3):1–26.
 113. Zhao XS, Lu GQ, Millar GJ. Advances in mesoporous molecular sieve MCM-41. *Industrial & Engineering Chemistry Research*. 1996;35(7):2075–2090.
 114. Kruk M, Jaroniec M. Gas adsorption characterization of ordered organic–inorganic nanocomposite materials. *Chemistry of Materials*. 2001;13(10):3169–3183.
 115. Sing KSW, Everett DH, Haul RAW, Moscou L, Pierotti RA, Rouquerol J, Siemieniowska T. Reporting physisorption data for gas/solid systems with special reference to the determination of surface area and porosity. *Pure and Applied Chemistry*. 1985;57(4):603–619.
 116. Wachs IE. Recent conceptual advances in the catalysis science of mixed metal oxide catalytic materials. *Catalysis Today*. 2005;100(1–2):79–94.
 117. Weckhuysen BM, Schoonheydt RA. Recent progress in diffuse reflectance spectroscopy of supported metal oxide catalysts. *Catalysis Today*. 1999;49(4):441–451.

118. Schoonheydt RA. UV-VIS-NIR spectroscopy and microscopy of heterogeneous catalysts. *Chemical Society Reviews*. 2010;39(12):5051–5066.
119. Jentoft FC. Chapter 3 ultraviolet–visible–near infrared spectroscopy in catalysis: theory, experiment, analysis, and application under reaction conditions. In: *Advances in catalysis*. Cambridge (MA): Academic Press; 2009;52:129–211.
120. Ojeda CB, Rojas FS. Process analytical chemistry: Applications of ultraviolet/visible spectrometry in environmental analysis: an overview. *Applied Spectroscopy Reviews*. 2009;44(3):245–265.
121. Weckhuysen BM, Wachs IE, Schoonheydt RA. Surface chemistry and spectroscopy of chromium in inorganic oxides. *Chemical Reviews*. 1996;96(8):3327–3350.
122. Bentrup U. Combining in situ characterization methods in one set-up: looking with more eyes into the intricate chemistry of the synthesis and working of heterogeneous catalysts. *Chemical Society Reviews*. 2010;39(12):4718–4730.
123. Guo T. More power to X-rays: new developments in X-ray spectroscopy. *Laser & Photonics Reviews*. 2009;3(6):591–622.
124. Al-Abadleh HA, Grassian VH. Oxide surfaces as environmental interfaces. *Surface Science Reports*. 2003;52(3–4):63–161.
125. Stickle WF, Bomben KD. X-ray photoelectron spectroscopy applied to microelectronic materials. In: *Microelectronics Processing: Inorganic Materials Characterization*. 1986;295:144–162. American Chemical Society.
126. Grunwaldt J-D, Wagner JB, Dunin-Borkowski RE. Imaging catalysts at work: A hierarchical approach from the macro- to the meso- and nano-scale. *ChemCatChem*. 2013;5(1):62–80.
127. Newbury DE, Williams DB. The electron microscope: the materials characterization tool of the millennium. *Acta Materialia*. 2000;48(1):323–346.
128. Hurst NW, Gentry SJ, Jones A, McNicol BD. Temperature programmed reduction. *Catalysis Reviews*. 1982;24(2):233–309.

129. Falconer JL, Schwarz JA. Temperature-programmed desorption and reaction: applications to supported catalysts. *Catalysis Reviews*. 1983;25(2):141–227.
130. Kock AJHM, Geus JW. The characterization of iron surfaces. *Progress in Surface Science*. 1985;20(3):165–272.
131. Dixit L, Rao TSRP. Spectroscopy in the measurements of acido-basic properties of solids. *Applied Spectroscopy Reviews*. 1996;31(4):369–472.
132. Sharma VK, Rivera W, Smith JO, O'Brien B. Ferrate(VI) oxidation of aqueous cyanide. *Environmental Science & Technology*. 1998;32(17):2608–2613.
133. Sharma V.K, O'Connor DB, Cabelli DE. Sequential one-electron reduction of Fe(V) to Fe(III) by cyanide in alkaline medium. *Journal of Physical Chemistry B*. 2001;105(46):11529–11532.
134. Sharma VK, Burnett CR, Yngard RA, Cabelli DE. Iron(VI) and iron(V) oxidation of copper(I) cyanide. *Environmental Science & Technology*. 2005;39(10):3849–3854.
135. Yngard R, Damrongsiri S, Osathaphan K, Sharma VK. Ferrate(VI) oxidation of zinc–cyanide complex. *Chemosphere*. 2007;69(5):729–735.
136. Yngard RA, Sharma VK, Filip J, Zboril R. Ferrate(VI) oxidation of weak-acid dissociable cyanides. *Environmental Science & Technology*. 2008;42(8):3005–3010.
137. Sharma VK, Yngard RA, Cabelli DE, Clayton Baum J. Ferrate(VI) and ferrate(V) oxidation of cyanide, thiocyanate, and copper(I) cyanide. *Radiation Physics and Chemistry*. 2008;77(6):761–767.
138. Osathaphan K, Tiyanont P, Yngard RA, Sharma VK. Removal of cyanide in Ni(II)–cyanide, Ni(II)–cyanide–EDTA, and electroplating rinse wastewater by ferrate(VI). *Water Air Soil Pollut*. 2011;219(1):527–534.
139. Reed B, Islam A, Bendick J. Ferrate and alkaline chlorination treatment of cyanide-heavy metal maritime wastewater. *Journal of Environmental Engineering*. 2013;139(5):661–666.
140. Osathaphan K, Kittisarn W, Chatchaitanawat P, Yngard RA, Kim H, Sharma VK. Oxidation of Ni(II)-cyano and Co(III)-cyano complexes by ferrate(VI): effect of pH. *Journal of Environmental Science and Health, Part A*. 2014;49(12):1380–1384.

141. Johnson MD, Sharma KD. Kinetics and mechanism of the reduction of ferrate by one-electron reductants. *Inorganica Chimica Acta*. 1999;293(2):229–233.
142. Yu MR, Chang YY, Tiwari D, Pachuau L, Lee SM, Yang JK. Treatment of wastewater contaminated with Cd(II)–NTA using Fe(VI). *Desalination and Water Treatment*. 2012;50(1-3):43–50.
143. Pachuau L, Lee SM, Tiwari D. Ferrate(VI) in wastewater treatment contaminated with metal(II)-iminodiacetic acid complexed species. *Chemical Engineering Journal*. 2013;230:141–148.
144. Tiwari D, Sailo L, Pachuau L. Remediation of aquatic environment contaminated with the iminodiacetic acid metal complexes using ferrate(VI). *Separation and Purification Technology*. 2014;132:77–83.
145. Lee C, Lee Y, Schmidt C, Yoon J, Von Gunten U. Oxidation of suspected N-nitrosodimethylamine (NDMA) precursors by ferrate(VI): kinetics and effect on the NDMA formation potential of natural waters. *Water Research*. 2008;42(1–2):433–441.
146. Pang S-Y, Jiang J, Gao Y, Zhou Y, Huangfu X, Liu Y, Ma J. Oxidation of flame retardant tetrabromobisphenol A by aqueous permanganate: reaction kinetics, brominated products, and pathways. *Environmental Science & Technology*. 2014;48(1):615–623.
147. Sharma VK, Rivera W, Joshi VN, Millero FJ, O'Connor D. Ferrate(VI) oxidation of thiourea. *Environmental Science & Technology*. 1999;33(15):2645–2650.
148. Sharma VK, Rendon RA, Millero FJ, Vazquez FG. Oxidation of thioacetamide by ferrate(VI). *Marine Chemistry*. 2000;70(1–3):235–242.
149. Huang H, Sommerfeld D, Dunn BC, Eyring EM, Lloyd CR. Ferrate(VI) oxidation of aqueous phenol: Kinetics and mechanism. *Journal of Physical Chemistry A*. 2001;105(14):3536–3541.
150. Sharma VK. Ferrate(V) oxidation of pollutants: a premix pulse radiolysis study. *Radiation Physics and Chemistry*. 2002;65(4–5):349–355.
151. Graham N, Jiang C-c, Li X-Z, Jiang J-Q, Ma J. The influence of pH on the degradation of phenol and chlorophenols by potassium ferrate. *Chemosphere*. 2004;56(10):949–956.
152. Li C, Li XZ, Graham N. A study of the preparation and reactivity of potassium ferrate. *Chemosphere*. 2005;61(4):537–543.

153. Liu X, Li Y, Zhang X, Lei L. Retention–oxidation–adsorption process for emergent treatment of organic liquid spills. *Journal of Hazardous Materials*. 2011;195:162–169.
154. Peings V, Frayret J, Pigot T. Mechanism for the oxidation of phenol by sulfatoferrate(VI): comparison with various oxidants. *Journal of Environmental Management*. 2015;157:287–296.
155. Yang B, Ying G-G, Zhang L-J, Zhou L-J, Liu S, Fang Y-X. Kinetics modeling and reaction mechanism of ferrate(VI) oxidation of benzotriazoles. *Water Research*. 2011;45(6):2261–2269.
156. Sharma VK, Burnett CR, O'Connor DB, Cabelli D. Iron(VI) and iron(V) oxidation of thiocyanate. *Environmental Science & Technology*. 2002;36(19):4182–4186.
157. Sharma VK, O'Connor DB, Cabelli D. Oxidation of thiocyanate by iron(V) in alkaline medium. *Inorganica Chimica Acta*. 2004;357(15):4587–4591.
158. Sharma VK, Cabelli D. Reduction of oxyiron(V) by sulfite and thiosulfate in aqueous solution. *Journal of Physical Chemistry A*. 2009;113(31):8901–8906.
159. Read JF, Graves CR, Jackson E. The kinetics and mechanism of the oxidation of the thiols 3-mercapto-1-propane sulfonic acid and 2-mercaptonicotinic acid by potassium ferrate. *Inorganica Chimica Acta*. 2003;348:41–49.
160. Sharma VK, Luther III GW, Millero FJ. Mechanisms of oxidation of organosulfur compounds by ferrate(VI). *Chemosphere*. 2011;82(8):1083–1089.
161. Sharma VK. Oxidation of inorganic compounds by ferrate(VI) and ferrate(V): one-electron and two-electron transfer steps. *Environmental Science & Technology*. 2010;44(13):5148–5152.
162. Xu GR, Zhang YP, Li GB. Degradation of azo dye active brilliant red X-3B by composite ferrate solution. *Journal of Hazardous Materials*. 2009;161(2–3):1299–1305.
163. Ciabatti I, Tognotti F, Lombardi L. Treatment and reuse of dyeing effluents by potassium ferrate. *Desalination*. 2010;250(1):222–228.
164. Ordiales M, Fernández D, Verdeja LF, Sancho J. Potassium permanganate as an alternative for gold mining wastewater treatment. *JOM*. 2015;67(9):1975–1985.

165. Yan YE, Schwartz FW. Kinetics and mechanisms for TCE oxidation by permanganate. *Environmental Science & Technology*. 2000;34(12):2535–2541.
166. Angeles-Wedler D, Mackenzie K, Kopinke F-D. Permanganate oxidation of sulfur compounds to prevent poisoning of Pd catalysts in water treatment processes. *Environmental Science & Technology*. 2008;42(15):5734–5739.
167. Liu R, Liu H, Zhao X, Qu J, Zhang R. Treatment of dye wastewater with permanganate oxidation and in situ formed manganese dioxides adsorption: cation blue as model pollutant. *Journal of Hazardous Materials*. 2010;176(1–3):926–931.
168. Zelmanov G, Semiat R. Iron(3) oxide-based nanoparticles as catalysts in advanced organic aqueous oxidation. *Water Research*. 2008;42(1–2):492–498.
169. Zelmanov G, Semiat R. Phenol oxidation kinetics in water solution using iron(3)-oxide-based nano-catalysts. *Water Research*. 2008;42(14):3848–3856.
170. Hu L, Martin HM, Arce-Bulted O, Sugihara MN, Keating KA, Strathmann TJ. Oxidation of carbamazepine by Mn(VII) and Fe(VI): reaction kinetics and mechanism. *Environmental Science & Technology*. 2009;43(2):509–515.
171. Uribe IO, Mosquera-Corral A, Rodicio JL, Esplugas S. Advanced technologies for water treatment and reuse. *AIChE Journal*. 2015;61(10):3146–3158.
172. Roth H, Gendel Y, Buzatu P, David O, Wessling M. Tubular carbon nanotube-based gas diffusion electrode removes persistent organic pollutants by a cyclic adsorption – electro-Fenton process. *Journal of Hazardous Materials*. 2016;307:1–6.
173. Jack RS, Ayoko GA, Adebajo MO, Frost RL. A review of iron species for visible-light photocatalytic water purification. *Environ Sci Pollut Res*. 2015;22(10):7439–7449.
174. Sharma VK, Burnett CR, Millero FJ. Dissociation constants of the monoprotic ferrate(VI) ion in NaCl media. *Physical Chemistry Chemical Physics*. 2001;3(11):2059–2062.

175. Sharma VK, Mishra SK, Nesnas N. Oxidation of sulfonamide antimicrobials by ferrate(VI) $[\text{FeVIO}_4^{2-}]^\dagger$. *Environmental Science & Technology*. 2006;40(23):7222–7227.
176. Li C, Li XZ, Graham N, Gao NY. The aqueous degradation of bisphenol A and steroid estrogens by ferrate. *Water Research*. 2008;42(1–2):109–120.
177. Noorhasan N, Patel B, Sharma VK. Ferrate(VI) oxidation of glycine and glycyglycine: kinetics and products. *Water Research*. 2010;44(3):927–935.
178. Lee Y, von Gunten U. Oxidative transformation of micropollutants during municipal wastewater treatment: comparison of kinetic aspects of selective (chlorine, chlorine dioxide, ferrateVI, and ozone) and non-selective oxidants (hydroxyl radical). *Water Research*. 2010;44(2):555–566.
179. Yang B, Ying G-G, Zhao J-L, Liu S, Zhou L-J, Chen F. Removal of selected endocrine disrupting chemicals (EDCs) and pharmaceuticals and personal care products (PPCPs) during ferrate(VI) treatment of secondary wastewater effluents. *Water Research*. 2012;46(7):2194–2204.
180. Jiang J-Q, Zhou Z, Pahl O. Preliminary study of ciprofloxacin (cip) removal by potassium ferrate(VI). *Separation and Purification Technology*. 2012;88:95–98.
181. Jiang J-Q, Zhou Z, Patibandla S, Shu X. Pharmaceutical removal from wastewater by ferrate(VI) and preliminary effluent toxicity assessments by the zebrafish embryo model. *Microchemical Journal*. 2013;110:239–245.
182. Sharma VK, Liu F, Tolan S, Sohn M, Kim H, Oturan MA. Oxidation of β -lactam antibiotics by ferrate(VI). *Chemical Engineering Journal*. 2013;221:446–451.
183. Wilde ML, Mahmoud WMM, Kümmerer K, Martins AF. Oxidation–coagulation of β -blockers by K_2FeVIO_4 in hospital wastewater: assessment of degradation products and biodegradability. *Science of the Total Environment*. 2013;452–453:137–147.
184. Jiang J, Zhou Z. Removal of pharmaceutical residues by ferrate(VI). *PLoS One*. 2013;8(2):e55729.
185. Yang B, Ying G-G, Chen Z-F, Zhao J-L, Peng F-Q, Chen X-W. Ferrate(VI) oxidation of tetrabromobisphenol A in comparison with bisphenol A. *Water Research*. 2014;62:211–219.
186. Karlesa A, De Vera GAD, Dodd MC, Park J, Espino MPB, Lee Y. Ferrate(VI) oxidation of β -Lactam antibiotics: reaction kinetics,

- antibacterial activity changes, and transformation products. *Environmental Science & Technology*. 2014;48(17):10380–10389.
187. Zhou Z, Jiang J-Q. Treatment of selected pharmaceuticals by ferrate(VI): Performance, kinetic studies and identification of oxidation products. *Journal of Pharmaceutical and Biomedical Analysis*. 2015;106:37–45.
 188. Kim C, Panditi VR, Gardinali PR, Varma RS, Kim H, Sharma VK. Ferrate promoted oxidative cleavage of sulfonamides: kinetics and product formation under acidic conditions. *Chemical Engineering Journal*. 2015;279:307–316.
 189. Hu L, Martin HM, Strathmann TJ. Oxidation kinetics of antibiotics during water treatment with potassium permanganate. *Environmental Science & Technology*. 2010;44(16):6416–6422.
 190. Hu L, Stemig AM, Wammer KH, Strathmann TJ. Oxidation of antibiotics during water treatment with potassium permanganate: reaction pathways and deactivation. *Environmental Science & Technology*. 2011;45(8):3635–3642.
 191. Jiang J, Pang S-Y, Ma J, Liu H. Oxidation of phenolic endocrine disrupting chemicals by potassium permanganate in synthetic and real waters. *Environmental Science & Technology*. 2012;46(3):1774–1781.
 192. Fayad PB, Zamyadi A, Broseus R, Prévost M, Sauvé S. Degradation of progestagens by oxidation with potassium permanganate in wastewater effluents. *Chemistry Central Journal*. 2013;7(1):1–11.
 193. Gao S, Zhao Z, Xu Y, Tian J, Qi H, Lin W, Cui F. Oxidation of sulfamethoxazole (SMX) by chlorine, ozone and permanganate—A comparative study. *Journal of Hazardous Materials*. 2014;274:258–269.
 194. Sharma VK. Disinfection performance of Fe(VI) in water and wastewater: a review. *Water Science and Technology*. 2007;55(1-2):225–232.
 195. Sharma VK. Use of iron(VI) and iron(V) in water and wastewater treatment. *Water Science and Technology*. 2004;49(4):69–74.
 196. Al-Abdul A, Sharma VK. Oxidation of benzothiophene, dibenzothiophene, and methyl-dibenzothiophene by ferrate(VI). *Journal of Hazardous Materials*. 2014;279:296–301.
 197. Winkelmann K, Sharma VK, Lin Y, Shreve KA, Winkelmann C, Hoisington LJ, Yngard RA. Reduction of ferrate(VI) and oxidation of

- cyanate in a Fe(VI)-TiO₂-UV-NCO- system. *Chemosphere*. 2008;72(11):1694-1699.
198. Sharma V, Graham ND, Li X-Z, Yuan B-L. Ferrate(VI) enhanced photocatalytic oxidation of pollutants in aqueous TiO₂ suspensions. *Environ Sci Pollut Res*. 2010;17(2):453-461.
 199. Sylvester P, Rutherford LA, Gonzalez-Martin A, Kim J, Rapko BM, Lumetta GJ. Ferrate treatment for removing chromium from high-level radioactive tank waste. *Environmental Science & Technology*. 2001;35(1):216-221.
 200. Lee Y, Um I-h, Yoon J. Arsenic(III) oxidation by iron(VI) (ferrate) and Subsequent removal of arsenic(V) by iron(III) coagulation. *Environmental Science & Technology*. 2003;37(24):5750-5756.
 201. Stupin DY, Ozernoi MI. Removal of Ni(II) with sodium ferrate(VI) from EDTA-containing aqueous solutions. *Russian Journal of Applied Chemistry*. 2004;77(8):1312-1315.
 202. Wang XJ, Wang Y, Wang X, Liu M, Xia SQ, Yin DQ, Zhang YL, Zhao JF. Microwave-assisted preparation of bamboo charcoal-based iron-containing adsorbents for Cr(VI) removal. *Chemical Engineering Journal*. 2011;174(1):326-332.
 203. Wu Z, Li W, Webley PA, Zhao D. General and controllable synthesis of novel mesoporous magnetic iron Oxide@Carbon encapsulates for efficient arsenic removal. *Advanced Materials*. 2012;24(4):485-491.
 204. Li L, Zhou G, Weng Z, Shan X-Y, Li F, Cheng H-M. Monolithic Fe₂O₃/graphene hybrid for highly efficient lithium storage and arsenic removal. *Carbon*. 2014;67:500-507.
 205. Yürüm A, Kocabaş-Ataklı ZÖ, Sezen M, Semiat R, Yürüm Y. Fast deposition of porous iron oxide on activated carbon by microwave heating and arsenic (V) removal from water. *Chemical Engineering Journal*. 2014;242:321-332.
 206. Lalhmunsiam L, Lee SM, Tiwari D. Manganese oxide immobilized activated carbons in the remediation of aqueous wastes contaminated with copper(II) and lead(II). *Chemical Engineering Journal*. 2013;225:128-137.
 207. Pan B, Qiu H, Pan B, Nie G, Xiao L, Lv L, Zhang W, Zhang Q, Zheng S. Highly efficient removal of heavy metals by polymer-supported nanosized

- hydrated Fe(III) oxides: behavior and XPS study. *Water Research*. 2010;44(3):815–824.
208. Shi J, Yi S, He H, Long C, Li A. Preparation of nanoscale zero-valent iron supported on chelating resin with nitrogen donor atoms for simultaneous reduction of Pb^{2+} . *Chemical Engineering Journal*. 2013;230:166–171.
209. Lakouraj MM, Mojerlou F, Zare EN. Nanogel and superparamagnetic nanocomposite based on sodium alginate for sorption of heavy metal ions. *Carbohydrate Polymers*. 2014;106:34–41.
210. Su Q, Pan B, Pan B, Zhang Q, Zhang W, Lv L, Wang X, Wu J, Zhang Q. Fabrication of polymer-supported nanosized hydrous manganese dioxide (HMO) for enhanced lead removal from waters. *Science of the Total Environment*. 2009;407(21):5471–5477.
211. Pan B, Wan S, Zhang S, Guo Q, Xu Z, Lv L, Zhang W. Recyclable polymer-based nano-hydrous manganese dioxide for highly efficient Tl(I) removal from water. *Science China Chemistry*. 2013;57(5):763–771.
212. Zhang Q, Pan B, Zhang S, Wang J, Zhang W, Lv L. New insights into nanocomposite adsorbents for water treatment: a case study of polystyrene-supported zirconium phosphate nanoparticles for lead removal. *J Nanopart Res*. 2011;13(10):5355–5364.
213. Smith RC, Li J, Padungthon S, Sengupta AK. Nexus between polymer support and metal oxide nanoparticles in hybrid nanosorbent materials (HNMs) for sorption/desorption of target ligands. *Frontiers of Environmental Science & Engineering*. 2015;9(5):929–938.
214. Zelmanov G, Semiat R. Iron (Fe^{+3}) oxide/hydroxide nanoparticles-based agglomerates suspension as adsorbent for chromium (Cr^{+6}) removal from water and recovery. *Separation and Purification Technology*. 2011;80(2):330–337.
215. Zelmanov G, Semiat R. Selenium removal from water and its recovery using iron (Fe^{3+}) oxide/hydroxide-based nanoparticles sol (NanoFe) as an adsorbent. *Separation and Purification Technology*. 2013;103:167–172.
216. Zhang Y, Ye Y, Liu Z, Li B, Liu Q, Liu Q, Li X. Monodispersed hierarchical aluminum/iron oxides composites micro/nanoflowers for efficient removal of As(V) and Cr(VI) ions from water. *Journal of Alloys and Compounds*. 2016;662:421–430.

217. Kim BC, Lee J, Um W, Kim J, Joo J, Lee JH, Kwak JH, Kim JH, Lee C, Lee H, Addleman RS, Hyeon T, Gu MB, Kim J. Magnetic mesoporous materials for removal of environmental wastes. *Journal of Hazardous Materials*. 2011;192(3):1140–1147.
218. Li F. Layer-by-layer loading iron onto mesoporous silica surfaces: Synthesis, characterization and application for As(V) removal. *Microporous and Mesoporous Materials*. 2013;171:139–146.
219. Anbia M, Kargosha K, Khoshbooei S. Heavy metal ions removal from aqueous media by modified magnetic mesoporous silica MCM-48. *Chemical Engineering Research and Design*. 2015;93:779–788.
220. Warner CL, Chouyyok W, Mackie KE, Neiner D, Saraf LV, Droubay TC, Warner MG, Addleman RS. Manganese doping of magnetic iron oxide nanoparticles: tailoring surface reactivity for a regenerable heavy metal sorbent. *Langmuir*. 2012;28(8):3931–3937.
221. Cai X, Gao Y, Sun Q, Chen Z, Megharaj M, Naidu R. Removal of co-contaminants Cu (II) and nitrate from aqueous solution using kaolin-Fe/Ni nanoparticles. *Chemical Engineering Journal*. 2014;244:19–26.
222. Franco F, Benítez-Guerrero M, Gonzalez-Triviño I, Pérez-Recuerda R, Assiego C, Cifuentes-Melchor J, Pascual-Cosp J. Low-cost aluminum and iron oxides supported on dioctahedral and trioctahedral smectites: a comparative study of the effectiveness on the heavy metal adsorption from water. *Applied Clay Science*. 2016;119(Part 2):321–332.
223. Ohji T, Fukushima M. Macro-porous ceramics: processing and properties. *International Materials Reviews*. 2012;57(2):115–131.
224. San Miguel G, Lambert SD, Graham NJD. A practical review of the performance of organic and inorganic adsorbents for the treatment of contaminated waters. *Journal of Chemical Technology & Biotechnology*. 2006;81(10):1685–1696.
225. Soler-Illia GJdAA, Sanchez C, Lebeau B, Patarin J. Chemical strategies to design textured materials: from microporous and mesoporous oxides to nanonetworks and hierarchical structures. *Chemical Reviews*. 2002;102(11):4093–4138.
226. Wan Y, Zhao D. On the controllable soft-templating approach to mesoporous silicates. *Chemical Reviews*. 2007;107(7):2821–2860.

227. Purwajanti S, Zhou L, Ahmad Nor Y, Zhang J, Zhang H, Huang X, Yu C. Synthesis of magnesium oxide hierarchical microspheres: A dual-functional material for water remediation. *ACS Applied Materials & Interfaces*. 2015;7(38):21278–21286.
228. Kosmulski M. pH-dependent surface charging and points of zero charge. IV. Update and new approach. *Journal of Colloid and Interface Science*. 2009;337(2):439–448.
229. Rosal R, Gonzalo MS, Rodríguez A, Perdigón-Melón JA, García-Calvo E. Catalytic ozonation of atrazine and linuron on $\text{MnO}_x/\text{Al}_2\text{O}_3$ and $\text{MnO}_x/\text{SBA-15}$ in a fixed bed reactor. *Chemical Engineering Journal*. 2010;165(3):806–812.
230. Saleh FS, Rahman MM. Oxidative destruction of o-DCB on supported manganese oxide catalyst. *Journal of Hazardous Materials*. 2009;162(2–3):1574–1577.
231. Nie Y, Hu C, Yang L, Hu J. Inhibition mechanism of formation over $\text{MnO}_x/\text{Al}_2\text{O}_3$ during the catalytic ozonation of 2,4-dichlorophenoxyacetic acid in water. *Separation and Purification Technology*. 2013;117:41–45.
232. Yang Z, Lv A, Nie Y, Hu C. Catalytic ozonation performance and surface property of supported Fe_3O_4 catalysts dispersions. *Frontiers of Environmental Science & Engineering*. 2013;7(3):451–456.
233. Sun Q, Li L, Yan H, Hong X, Hui KS, Pan Z. Influence of the surface hydroxyl groups of $\text{MnO}_x/\text{SBA-15}$ on heterogeneous catalytic ozonation of oxalic acid. *Chemical Engineering Journal*. 2014;242:348–356.
234. Yang J-CE, Lan H, Lin X-Q, Yuan B, Fu M-L. Synthetic conditions-regulated catalytic Oxone efficacy of $\text{MnO}_x/\text{SBA-15}$ towards butyl paraben (BPB) removal under heterogeneous conditions. *Chemical Engineering Journal*. 2016;289:296–305.
235. Botas JA, Melero JA, Martínez F, Pariente MI. Assessment of $\text{Fe}_2\text{O}_3/\text{SiO}_2$ catalysts for the continuous treatment of phenol aqueous solutions in a fixed bed reactor. *Catalysis Today*. 2010;149(3–4):334–340.
236. Pariente MI, Molina R, Melero JA, Botas JÁ, Martínez F. Intensified-Fenton process for the treatment of phenol aqueous solutions. *Water Science and Technology*. 2015;71(3):359–365.
237. Zheng C, Cheng X, Chen P, Yang C, Bao S, Xia J, Guo M, Sun X. Highly porous $\text{Fe}_2\text{O}_3/\text{KIT-6}$ with Mg substitution for heterogeneous Fenton

- oxidation of imidacloprid with enhanced catalytic activity. *Chemistry Letters*. 2015;44(5):601–603.
238. Xing S, Lu X, Liu J, Zhu L, Ma Z, Wu Y. Catalytic ozonation of sulfosalicylic acid over manganese oxide supported on mesoporous ceria. *Chemosphere*. 2016;144:7–12.
239. Xing S, Hu C, Qu J, He H, Yang M. Characterization and reactivity of MnO_x supported on mesoporous zirconia for herbicide 2,4-D mineralization with ozone. *Environmental Science & Technology*. 2008;42(9):3363–3368.
240. Qi L, You H, Zhang Z, Feng C, Agtmaal Sv. Degradation of 4-chlorophenol by catalytic ozonation using $\gamma-Al_2O_3/TiO_2$ supported manganese oxides in aqueous solution. *International Journal of Electrochemical Science*. 2013;8(4):5457–5468.
241. Palanisamy B, Babu CM, Sundaravel B, Anandan S, Murugesan V. Sol–gel synthesis of mesoporous mixed Fe_2O_3/TiO_2 photocatalyst: Application for degradation of 4-chlorophenol. *Journal of Hazardous Materials*. 2013;252–253:233–242.
242. Sui M, Xing S, Sheng L, Huang S, Guo H. Heterogeneous catalytic ozonation of ciprofloxacin in water with carbon nanotube supported manganese oxides as catalyst. *Journal of Hazardous Materials*. 2012;227–228:227–236.
243. Xu L, Li X, Ma J, Wen Y, Liu W. Nano- MnO_x on activated carbon prepared by hydrothermal process for fast and highly efficient degradation of azo dyes. *Applied Catalysis A: General*. 2014;485:91–98.
244. Wang Y, Xie Y, Sun H, Xiao J, Cao H, Wang S. 2D/2D nano-hybrids of $\gamma-MnO_2$ on reduced graphene oxide for catalytic ozonation and coupling peroxydisulfate activation. *Journal of Hazardous Materials*. 2016;301:56–64.
245. Tu Y, Tian S, Kong L, Xiong Y. Co-catalytic effect of sewage sludge-derived char as the support of Fenton-like catalyst. *Chemical Engineering Journal*. 2012;185–186:44–51.
246. Weng X, Sun Q, Lin S, Chen Z, Megharaj M, Naidu R. Enhancement of catalytic degradation of amoxicillin in aqueous solution using clay supported bimetallic Fe/Ni nanoparticles. *Chemosphere*. 2014;103:80–85.

247. Gao H, Zhao B-X, Luo J-C, Wu D, Ye W, Wang Q, Zhang X-L. Fe–Ni–Al pillared montmorillonite as a heterogeneous catalyst for the catalytic wet peroxide oxidation degradation of orange acid II: preparation condition and properties study. *Microporous and Mesoporous Materials*. 2014;196:208–215.
248. Garrido-Ramírez EG, Mora ML, Marco JF, Ureta-Zañartu MS. Characterization of nanostructured allophane clays and their use as support of iron species in a heterogeneous electro-Fenton system. *Applied Clay Science*. 2013;86:153–161.
249. Zhang YX, Hao XD, Li F, Diao ZP, Guo ZY, Li J. pH-dependent degradation of methylene blue via rational-designed MnO₂ Nanosheet-decorated diatomites. *Industrial & Engineering Chemistry Research*. 2014;53(17):6966–6977.
250. Busca G. Chapter three – structural, surface, and catalytic properties of aluminas. In: *Advances in catalysis*, Friederike CJ, ed. Cambridge (MA): Academic Press. 2014;57:319–404.
251. Čejka J. Organized mesoporous alumina: synthesis, structure and potential in catalysis. *Applied Catalysis A: General*. 2003;254(2):327–338.
252. Sinkó K. Influence of chemical conditions on the nanoporous structure of silicate aerogels. *Materials*. 2010;3(1):704–740.
253. Soleimani Dorcheh A, Abbasi MH. Silica aerogel; synthesis, properties and characterization. *Journal of Materials Processing Technology*. 2008;199(1–3):10–26.
254. Linsebigler AL, Lu G, Yates JT. Photocatalysis on TiO₂ surfaces: principles, mechanisms, and selected results. *Chemical Reviews*. 1995;95(3):735–758.
255. Bagheri S, Mohd Hir ZA, Yousefi AT, Abdul Hamid SB. Progress on mesoporous titanium dioxide: synthesis, modification and applications. *Microporous and Mesoporous Materials*. 2015;218:206–222.
256. Osipov VI. Density of clay minerals. *Soil Mechanics and Foundation Engineering* 2012;48(6):231–240.
257. Hussin F, Aroua MK, Daud WMAW. Textural characteristics, surface chemistry and activation of bleaching earth: a review. *Chemical Engineering Journal*. 2011;170(1):90–106.

258. Woignier T, Duffours L, Colombel P, Dieudonné P. Nanoporous clay with carbon sink and pesticide trapping properties. *The European Physical Journal Special Topics*. 2015;224(9):1945–1962.
259. Gu W, Yushin G. Review of nanostructured carbon materials for electrochemical capacitor applications: advantages and limitations of activated carbon, carbide-derived carbon, zeolite-templated carbon, carbon aerogels, carbon nanotubes, onion-like carbon, and graphene. *Wiley Interdisciplinary Reviews: Energy and Environment*. 2014;3(5):424–473.
260. AlOthman Z. A review: Fundamental aspects of silicate mesoporous materials. *Materials*. 2012;5(12):2874–2902.
261. Morris SM, Fulvio PF, Jaroniec M. Ordered mesoporous alumina-supported metal oxides. *Journal of the American Chemical Society*. 2008;130(45):15210–15216.
262. Morris SM, Horton JA, Jaroniec M. Soft-templating synthesis and properties of mesoporous alumina–titania. *Microporous and Mesoporous Materials*. 2010;128(1–3):180–186.
263. Cai W, Yu J, Anand C, Vinu A, Jaroniec M. Facile synthesis of ordered mesoporous alumina and alumina-supported metal oxides with tailored adsorption and framework properties. *Chemistry of Materials*. 2011;23(5):1147–1157.
264. Grant SM, Jaroniec M. Effect of acid concentration on pore size in polymer-templated mesoporous alumina. *Journal of Materials Chemistry*. 2012;22(1):86–92.
265. Parlett CMA, Durndell LJ, Wilson K, Bruce DW, Hondow NS, Lee AF. Selective oxidation of allylic alcohols over highly ordered Pd/meso- Al_2O_3 catalysts. *Catalysis Communications*. 2014;44:40–45.
266. Liu Q, Gao J, Gu F, Lu X, Liu Y, Li H, Zhong Z, Liu B, Xu G, Su F. One-pot synthesis of ordered mesoporous Ni–V–Al catalysts for CO methanation. *Journal of Catalysis*. 2015;326:127–138.
267. Gao Z, Zhang Y, Li D, Werth CJ, Zhang Y, Zhou X. Highly active Pd–In/mesoporous alumina catalyst for nitrate reduction. *Journal of Hazardous Materials*. 2015;286:425–431.

268. Yang H, Lu Q, Gao F, Shi Q, Yan Y, Zhang F, Xie S, Tu B, Zhao D. One-step synthesis of highly ordered mesoporous silica monoliths with metal oxide nanocrystals in their channels. *Advanced Functional Materials*. 2005;15(8):1377–1384.
269. Xu S, Hong Y, Chen C, Li S, Xiao L, Fan J. A general synthetic strategy for ordered, extra-large mesoporous metal oxides via uniform sol-gel coating. *Journal of Materials Chemistry A*. 2013;1(20):6191–6198.
270. Yang H, Deng J, Liu Y, Xie S, Wu Z, Dai H. Preparation and catalytic performance of Ag, Au, Pd or Pt nanoparticles supported on 3DOM CeO₂–Al₂O₃ for toluene oxidation. *Journal of Molecular Catalysis A: Chemical*. 2016;414:9–18.
271. Samanta S, Giri S, Sastry PU, Mal NK, Manna A, Bhaumik A. Synthesis and characterization of iron-rich highly ordered mesoporous Fe-MCM-41. *Industrial & Engineering Chemistry Research*. 2003;42(13):3012–3018.
272. Ziolk M, Nowak I, Kilos B, Sobczak I, Decyk P, Trejda M, Volta JC. Template synthesis and characterisation of MCM-41 mesoporous molecular sieves containing various transition metal elements—TME (Cu, Fe, Nb, V, Mo). *Journal of Physics and Chemistry of Solids*. 2004;65(2–3):571–581.
273. Kumar GS, Palanichamy M, Hartmann M, Murugesan V. A new route for the synthesis of manganese incorporated SBA-15. *Microporous and Mesoporous Materials*. 2008;112(1–3):53–60.
274. Tsoncheva T, Dal Santo V, Gallo A, Scotti N, Dimitrov M, Kovacheva D. Structure and catalytic activity of hosted in mesoporous silicas copper species: effect of preparation procedure and support pore topology. *Applied Catalysis A: General*. 2011;406(1–2):13–21.
275. Iglesias J, Melero JA, Bautista LF, Morales G, Sánchez-Vázquez R, Andreola MT, Lizarraga-Fernández A. Zr-SBA-15 as an efficient acid catalyst for FAME production from crude palm oil. *Catalysis Today*. 2011;167(1):46–55.
276. Seftel EM, Cool P, Lloyd-Spetz A, Latic D. Synthesis and characterization of catalytic metal semiconductor-doped siliceous materials with ordered structure for chemical sensing. *Journal of Porous Materials*. 2013;20(5):1119–1128.

277. Furtado AMB, Wang Y, Glover TG, LeVan MD. MCM-41 impregnated with active metal sites: synthesis, characterization, and ammonia adsorption. *Microporous and Mesoporous Materials*. 2011;142(2–3):730–739.
278. Djinović P, Kocjan U, Batista J, Pintar A. Synthesis and characterization of ordered CuO–CeO₂ mixed oxides using KIT-6 silica as a hard template. *Acta Chimica Slovenica*. 2009;56(4):868–877.
279. Wan L, Cui X, Chen H, Shi J. Synthesis of ordered mesoporous CuO/CeO₂ composite via co-nanocasting replication method and its improved reactivity towards hydrogen. *Materials Letters*. 2010;64(12):1379–1382.
280. Markoulaki VI, Papadas IT, Kornarakis I, Armatas GS. Synthesis of ordered mesoporous CuO/CeO₂ composite frameworks as anode catalysts for water oxidation. *Nanomaterials*. 2015;5(4):1971–1984.
281. Bhagiyalakshmi M, Hemalatha P, Ganesh M, Mei PM, Jang HT. A direct synthesis of mesoporous carbon supported MgO sorbent for CO₂ capture. *Fuel*. 2011;90(4):1662–1667.
282. Samiee L, Shoghi F, Vinu A. Fabrication and electrocatalytic application of functionalized nanoporous carbon material with different transition metal oxides. *Applied Surface Science*. 2013;265:214–221.
283. Polarz S, Neues F, van den Berg MWE, Grünert W, Khodeir L. Mesosynthesis of ZnO–silica composites for methanol nanocatalysis. *Journal of the American Chemical Society*. 2005;127(34):12028–12034.
284. Popova M, Szegedi Á, Cherkezova-Zheleva Z, Mitov I, Kostova N, Tsoncheva T. Toluene oxidation on titanium- and iron-modified MCM-41 materials. *Journal of Hazardous Materials*. 2009;168(1):226–232.
285. Wolters M, van Grotel LJW, Eggenhuisen TM, Sietsma JRA, de Jong KP, de Jongh PE. Combining confinement and NO calcination to arrive at highly dispersed supported nickel and cobalt oxide catalysts with a tunable particle size. *Catalysis Today*. 2011;163(1):27–32.
286. Liu C-H, Lai N-C, Liou S-C, Chu M-W, Chen C-H, Yang C-M. Deposition and thermal transformation of metal oxides in mesoporous SBA-15 silica with hydrophobic mesopores. *Microporous and Mesoporous Materials*. 2013;179:40–47.

287. Van Quy N, Hung TM, Thong TQ, Tuan LA, Huy TQ, Hoa ND. Novel synthesis of highly ordered mesoporous Fe₂O₃/SiO₂ nanocomposites for a room temperature VOC sensor. *Current Applied Physics*. 2013;13(8):1581–1588.
288. Wang L-J, Fan H-L, Shangguan J, Croiset E, Chen Z, Wang H, Mi J. Design of a sorbent to enhance reactive adsorption of hydrogen sulfide. *ACS Applied Materials & Interfaces*. 2014;6(23):21167–21177.
289. Li H, Zhang L, Dai H, He H. Facile synthesis and unique physicochemical properties of three-dimensionally ordered macroporous magnesium oxide, gamma-alumina, and ceria–zirconia solid solutions with crystalline mesoporous walls. *Inorganic Chemistry*. 2009;48(10):4421–4434.
290. Pierre AC, Pajonk GM. Chemistry of aerogels and their applications. *Chemical Reviews*. 2002;102(11):4243–4266.
291. Shannon MA, Semiat R. Advancing materials and technologies for water purification. *MRS Bulletin*. 2008;33(01):9–15.
292. Zander N, Gillan M, Sweetser D. Recycled PET nanofibers for water filtration applications. *Materials*. 2016;9(4):247:1–247:10.
293. Kastner JR, Ganagavaram R, Kolar P, Teja A, Xu C. Catalytic ozonation of propanal using wood fly ash and metal oxide nanoparticle impregnated carbon. *Environmental Science & Technology*. 2008;42(2):556–562.
294. Gheorghii V, Katerina Z. Nanodispersed oxides-plasma-chemical synthesis and properties. *Plasma Science and Technology*. 2007;9(5):603–610.
295. Hayashi H, Hakuta Y. Hydrothermal synthesis of metal oxide nanoparticles in supercritical water. *Materials*. 2010;3(7):3794–3817.
296. Chu W, Xu J, Hong J, Lin T, Khodakov A. Design of efficient Fischer Tropsch cobalt catalysts via plasma enhancement: Reducibility and performance (Review). *Catalysis Today*. 2015;256(Part 1):41–48.
297. Bansal V, Bharde A, Ramanathan R, Bhargava SK. Inorganic materials using ‘unusual’ microorganisms. *Advances in Colloid and Interface Science*. 2012;179–182:150–168.
298. Sōmiya S, Roy R. Hydrothermal synthesis of fine oxide powders. *Bulletin of Materials Science*. 2000;23(6):453–460.

299. Arafat MM, Dinan B, Akbar SA, Haseeb ASMA. Gas sensors based on one dimensional nanostructured metal-oxides: a review. *Sensors*. 2012;12(6):7207.
300. Pang YL, Lim S, Ong HC, Chong WT. Research progress on iron oxide-based magnetic materials: Synthesis techniques and photocatalytic applications. *Ceramics International*. 2016;42(1, Part A):9–34.
301. Bozbag SE, Sanli D, Erkey C. Synthesis of nanostructured materials using supercritical CO₂: part II. Chemical transformations. *Journal of Materials Science*. 2011;47(8):3469–3492.
302. Dowson M, Grogan M, Birks T, Harrison D, Craig S. Streamlined life cycle assessment of transparent silica aerogel made by supercritical drying. *Applied Energy*. 2012;97:396–404.
303. Rao KJ, Vaidhyanathan B, Ganguli M, Ramakrishnan PA. Synthesis of inorganic solids using microwaves. *Chemistry of Materials*. 1999;11(4):882–895.
304. Conrads H, Schmidt M. Plasma generation and plasma sources. *Plasma Sources Science and Technology*. 2000;9(4):441–454.
305. Brooks DJ, Douthwaite RE. Microwave-induced plasma reactor based on a domestic microwave oven for bulk solid state chemistry. *Review of Scientific Instruments*. 2004;75(12):5277–5279.
306. Kuśtrowski P, Chmielarz L, Dziembaj R, Cool P, Vansant EF. Modification of MCM-48-, SBA-15-, MCF-, and MSU-type mesoporous silicas with transition metal oxides using the molecular designed dispersion method. *The Journal of Physical Chemistry B*. 2005;109(23):11552–11558.
307. Kuśtrowski P, Chmielarz L, Surman J, Bidzińska E, Dziembaj R, Cool P, Vansant EF. Catalytic Activity of MCM-48-, SBA-15-, MCF-, and MSU-Type mesoporous silicas modified with Fe³⁺ species in the oxidative dehydrogenation of ethylbenzene in the presence of N₂O. *Journal of Physical Chemistry A*. 2005;109(43):9808–9815.
308. Chmielarz L, Kuśtrowski P, Dziembaj R, Cool P, Vansant EF. SBA-15 mesoporous silica modified with metal oxides by MDD method in the role of DeNO_x catalysts. *Microporous and Mesoporous Materials*. 2010;127(1–2):133–141.

309. Chmielarz L, Kuśtrowski P, Drozdek M, Rutkowska M, Dziembaj R, Michalik M, Cool P, Vansant EF. SBA-15 mesoporous silica modified with rhodium by MDD method and its catalytic role for N₂O decomposition reaction. *Journal of Porous Materials*. 2010;18(4):483–491.
310. Bérubé F, Khadraoui A, Florek J, Kaliaguine S, Kleitz F. A generalized method toward high dispersion of transition metals in large pore mesoporous metal oxide/silica hybrids. *Journal of Colloid and Interface Science*. 2015;449:102–114.
311. Dedushenko SK, Zhizhin MG, Perfiliev YD. X-ray and Mössbauer study of structural changes in K₃Na(FeO₄)₂. *Hyperfine Interactions*. 2006;166(1):367–371.
312. Shi J. On the synergetic catalytic effect in heterogeneous nanocomposite catalysts. *Chemical Reviews*. 2013;113(3):2139–2181.
313. Sellitto VM, Fernandes RBA, Barrón V, Colombo C. Comparing two different spectroscopic techniques for the characterization of soil iron oxides: Diffuse versus bi-directional reflectance. *Geoderma*. 2009;149(1–2):2–9.
314. Hegde MS, Bera P. Noble metal ion substituted CeO₂ catalysts: electronic interaction between noble metal ions and CeO₂ lattice. *Catalysis Today*. 2015;253:40–50.
315. Yu X, Licht S. Recent advances in synthesis and analysis of Fe(VI) cathodes: solution phase and solid-state Fe(VI) syntheses, reversible thin-film Fe(VI) synthesis, coating-stabilized Fe(VI) synthesis, and Fe(VI) analytical methodologies. *Journal of Solid State Electrochemistry*. 2008;12(12):1523–1540.
316. Ingham B. X-ray scattering characterisation of nanoparticles. *Crystallography Reviews*. 2015;21(4):229–303.
317. Bing J, Hu C, Nie Y, Yang M, Qu J. Mechanism of catalytic ozonation in Fe₂O₃/Al₂O₃@SBA-15 aqueous suspension for destruction of ibuprofen. *Environmental Science & Technology*. 2015;49(3):1690–1697.
318. Li J, Chen C, Zhang R, Wang X. Nanoscale zero-valent iron particles supported on reduced graphene oxides by using a plasma technique and their application for removal of heavy-metal ions. *Chemistry – An Asian Journal*. 2015;10(6):1410–1417.

List of Symbols, Abbreviations, and Acronyms

1-D	1-dimensional
2-D	2-dimensional
3-D	3-dimensional
Ag	silver
Al	aluminum
Al ₂ O ₃	alumina
AOII	acid orange II
As	arsenic
ATL	Atenolol
BPA	bisphenol A
BrO ₃	bromate
BT	benzotriazole
Ca	calcium
CBZ	carbamazepine
Cd	cadmium
Ce	cesium
Ce(SO ₄) ₂	cerium sulfate
CeO _x	ceria
cip	ciprofloxacin
Cl	chlorine
Cl ₂	chlorine gas
ClO ₂	chlorine dioxide
CNTs	carbon nanotubes
Co	cobalt
COD	chemical oxygen demand

Cr	chromium
CSAC	coconut shell activated carbon
Cu	copper
CVD	chemical vapor deposition
DRS	diffuse reflectance spectroscopy
EDCs	endocrine-disrupting compounds
EDX	energy-dispersive X-ray spectroscopy
EE2	17 α -ethinylestradiol
EISA	evaporation-induced self-assembly
Fe	iron
Fe ₃ O ₄	iron oxide
GE	graphene
GNs	graphene nanosheets
GO	graphene oxide
H ₂ O ₂	hydrogen peroxide
HCl	hydrogen chloride
HF	hydrogen fluoride
HFeO ₄ ⁻	ferrate (V)
Hg	mercury
HOCl	hypochlorous acid
HR	high resolution
HTS	hydrothermal
IDA	iminodiacetic acid
K ₂ FeO ₄	potassium ferrate
K _d	distribution coefficient
KMnO ₄	potassium permanganate
LBL	layer-by-layer

LCA	life-cycle -assessment
LMCTs	ligand-to-metal-charge-transitions
MDD	molecular designed dispersion
MgO	magnesium oxide
Mn	manganese
MnO ₂	manganese oxide
MnO _x	manganese oxides
MWCNTs	multi-wall CNTs
NaCl	sodium chloride
NaOH	sodium hydroxide
NDMA	n-nitrosodimethylamine
NO ₃ ⁻	nitrate
NTA	nitrilotriacetic acid
nZVI	nano-zero-valent iron
OCl	hypochrite anion
Pb	lead
<i>p</i> CBA	<i>para</i> -chlorobenzonate
PCPs	personal care products
PMMA	poly(methyl methacrylate),
PSD	pore size distribution
PZC	point-of-zero charge
rGO	reduced graphene
ROS	reactive oxygen species
Ru	ruthenium
S	sulfur
SAED	selected area (electron) diffraction
SEM	scanning electron microscopy

SMX	sulfamethoxazole
SOZ	sulfisoxazole
TEM	transmission electron microscopy
TiO ₂	titanium oxide
TOF	turn-over-frequency
TPD	temperature-programmed desorption
TPO	temperature-programmed oxidation
TPR	temperature-programmed reduction
UV	ultraviolet
Vis	visible
XPS	X-ray photoelectron spectroscopy
XRD	X-ray diffraction
Zn	zinc
ZnO	zinc oxide

1 DEFENSE TECHNICAL
(PDF) INFORMATION CTR
DTIC OCA

2 DIR ARL
(PDF) IMAL HRA
RECORDS MGMT
RDRL DCL
TECH LIB

1 GOVT PRINTG OFC
(PDF) A MALHOTRA

1 ARL
(PDF) RDRL SED E
I LEE